ELASTIC NETWORK MODELS OF PROTEINS

Uncovering the Internal Mechanics of Actin and Myosin

vorgelegt von

Diplom-Physiker

Markus Düttmann

geboren in Haselünne

Von der Fakultät II - Mathematik und Naturwissenschaften

der Technischen Universität Berlin zur Erlangung des akademischen Grades

Doktor der Naturwissenschaften

– Dr.rer.nat. –

---

genehmigte Dissertation

Promotionsausschuss:

Vorsitzender: Prof. Dr. Dieter Breitschwerdt

Gutachter: Prof. Dr. Alexander S. Mikhailov

Gutachter: Prof. Dr. Harald Engel

Tag der wissenschaftlichen Aussprache: 21. November 2012

Berlin 2012

D 83

ABSTRACT

Throughout the course of evolution, proteins have obtained the ability to perform a variety of tasks within the cell. Two important examples are the structural protein actin and the molecular motor myosin. They are so-called ATPases, i.e. binding and subsequent hydrolysis of an ATP molecule provide energy fueling these molecular machines. Here, an elastic-network (EN) approximation will be employed to study ATP induced conformational changes of actin, internal communication mechanisms of myosin and the interaction of these two molecules. We found that they essentially behave like strain sensors, both responding by well-defined domain motions to mechanical perturbations.

To describe the actin monomer, we extended the EN model by introducing a set of breakable links. These become effective only when two domains approach one another. In this framework, actin possesses a metastable state corresponding to a closed conformation and appropriate perturbations in the nucleotide-binding pocket (NBP) can induce a transition to this state. Furthermore, a coarse-grained ligand model was introduced. Our analysis suggests that the presence of ATP stabilizes a closed conformation. This may play an important role in the explanation why the polymerization process is highly accelerated in the presence of ATP. Next, we explore the sensitivity of myosin to external forces. Conformational responses of the motor protein to the application of forces to individual residues in its principal functional regions were systematically investigated. In this way, a detailed sensitivity map of myosin-V could be obtained. The results suggested that the intrinsic operation of this molecular motor is regulated by its strain-sensor behavior. In agreement with experiments, we find that such forces invoke conformational changes that should affect filament binding and nucleotide release. Finally, interactions between the filament and actin or myosin have been investigated. Electrostatic interactions were seen to guide proteins toward specific binding sites. Here, strong binding occurs due to directly interacting residues which form stable bonds if they come close to each other.

ZUSAMMENFASSUNG

Im Laufe der Evolution haben Proteine zahlreiche Fähigkeiten entwickelt und regulieren so gut wie jeden Prozess in der Zelle. Wichtige Beispiele sind das Strukturprotein Aktin und der molekulare Motor Myosin. Sie gehören zu der Gruppe der ATPasen, d.h. sie werden durch eine chemische Reaktion mit diesem Nukleotid angetrieben. In dieser Arbeit werden ATP-induzierte Konformationsänderungen von Aktin, interne Kommunikationsmechanismen von Myosin und die Wechselwirkung beider Moleküle im Rahmen eines elastischen Netzwerksmodells untersucht. Wir haben herausgefunden, dass Aktin und Myosin sich wie Kraftsensoren verhalten; beide reagieren mit wohldefinierten Domänenbewegungen auf mechanische Störungen.

Um den Aktin-Monomer zu beschreiben, haben wir das Netzwerkmodell durch Einführung von neuen Bindungen erweitert. Diese entstehen, wenn sich Domänen nahe genug annähern. Dadurch besitzt Aktin einen metastabilen, geschlossenen Zustand. Geeignete Störungen in dem Bereich in dem Liganden binden können einen Übergang dorthin bewirken. Weiterhin entwickelten wir ein Liganden-Modell und konnten zeigen, dass ein so modelliertes ATP den geschlossenen Zustand stabilisiert. Dies könnte eine Rolle bei der Erklärung spielen, warum in Anwesenheit von ATP die Aktin-Polymerisierung beschleunigt wird. Außerdem untersuchten wir den Einfluss externer Kräfte auf Myosin. Indem wir systematisch Kräfte auf einzelne Residuen in den wichtigen Bereichen des Moleküls wirken ließen und deren Effekte quantifizierten, konnten wir die Empfindlichkeiten einzelner Bereiche charakterisieren. Unsere Ergebnisse deuten darauf hin, dass intrinsische Mechanismen durch äußere Kräfte reguliert werden. In Übereinstimmung mit experimentellen Daten konnten wir zeigen, dass äußere Kräfte Konformationsänderung induzieren, die das Binden von Filamenten und Nukleotiden beeinflussen können. Abschließend untersuchten wir die Wechselwirkung zwischen Aktin und Myosin auf der einen und dem Filament auf der anderen Seite. Wir zeigten, dass elektrostatische Wechselwirkungen dafür sorgen, dass die beiden Proteine sich die gewissen Bindungsstellen im Filament nähern. Dort gehen sie stabile Bindungen ein, die für eine starke Wechselwirkung zwischen Filament und Protein sorgen.

PUBLICATIONS

The main results of this work have appeared previously in the following publications:

Düttmann M, Togashi Y, Yanagida T, Mikhailov AS (2012) Myosin-V as a Mechanical Sensor: An Elastic Network Study. Biophysical Journal. 102: 541–555.

Düttmann M, Mittnenzweig M, Togashi Y, Yanagida T, Mikhailov AS (2012) Complex Intramolecular Mechanics of G-actin – an Elastic Network Study. PLoS ONE. e45859.

ACKNOWLEDGMENTS

I am truly indebted and grateful to my advisor, Prof. Alexander Mikhailov, for the support he showed me throughout the past three years. I am sure this thesis would have not been possible without his help. Besides I would like to thank my colleagues and coworkers for fruitful discussions and a pleasant working atmosphere. I would also like to show my gratitude to Prof. Yuichi Togashi and Prof. Toshio Yanagida who heartily hosted me in their research groups. Finally, I acknowledge financial support from the Deutsche Forschungsgemeinschaft through the Research Training Group 1558 "Nonequilibrium Collective Dynamics in Condensed Matter and Biological Systems".

CONTENTS

1 INTRODUCTION 1

2 BACKGROUND 7
- 2.1 Proteins . . . 7
  - 2.1.1 Actin . . . 9
  - 2.1.2 Myosin . . . 10
  - 2.1.3 Actomyosin Complex . . . 13
- 2.2 Experimental Methods . . . 15
- 2.3 Modeling of Protein Dynamics . . . 19
  - 2.3.1 Molecular Dynamics . . . 19
  - 2.3.2 Reduced Descriptions and Coarse-Graining 21
  - 2.3.3 Elastic-Network Models . . . 23

3 MATHEMATICAL METHODS 27
- 3.1 The Elastic Network Model . . . 27
- 3.2 Linearized Equations of Motion . . . 30
- 3.3 Immobilization Procedure . . . 31
- 3.4 Extensions of the Model . . . 33
  - 3.4.1 Breakable Links . . . 33
  - 3.4.2 Thermal Fluctuations . . . 35
- 3.5 Protein-Protein Interactions . . . 36
  - 3.5.1 Electrostatic Interactions . . . 36
  - 3.5.2 Soft sphere potentials . . . 37
  - 3.5.3 Protein Binding . . . 37

4 INTRAMOLECULAR MECHANICS OF G-ACTIN 39
- 4.1 G-actin Model . . . 39
- 4.2 Domain Motions and Metastable States . . . 41
- 4.3 Responses to Perturbations in the Nucleotide-Binding Pocket . . . 46
- 4.4 Ligand-Induced Conformational Changes . . . 49
  - 4.4.1 Ligand Model . . . 50
  - 4.4.2 Effects of Thermal Fluctuations . . . 54
- 4.5 Discussion . . . 55

5 MYOSIN-V AS A MECHANICAL SENSOR 59
- 5.1 Myosin-V Model . . . 59
- 5.2 Forces Acting on the Tail . . . 62
- 5.3 Forces in the Nucleotide-Binding Pocket . . . 65

5.4 Forces in the Actin-Cleft Region 68
5.5 Discussion 70

6 INTERACTIONS WITH THE FILAMENT 75
6.1 Actin Monomer and Filament Models 75
6.2 Actin-Actin and Actin-Myosin Binding Sites . . . 78
6.3 Guided by Electrostatic Interactions 80
6.3.1 Interaction of Actin Monomer with the Filament 81
6.3.2 Interaction of Myosin with the Filament . . 83
6.4 Ligand Binding facilitates Docking 86
6.4.1 Toy Model 86
6.4.2 Nucleotide-Dependent Dynamics 88
6.5 Discussion 90

7 SUMMARY AND OUTLOOK 93

A APPENDIX 99
A.1 Ligand Model for Actin Monomer 99
A.2 Myosin Directions 100
A.3 Myosin Sensitivity Tables 101
A.3.1 Forces in the Nucleotide-Binding Region . 102
A.3.2 Forces in the Actin-Cleft Region 103
A.4 Comparison to the Linearized Model 104
A.5 Actin-Actin Binding Sites 107
A.6 Tables 108

BIBLIOGRAPHY 111

LIST OF FIGURES

Figure 1 ATP hydrolysis . . . 9
Figure 2 Treadmilling . . . 10
Figure 3 Actin filament mesh . . . 11
Figure 4 Schematic view of sarcomere and two-headed myosin . . . 12
Figure 5 Schematic view of sarcomere and two-headed myosin . . . 13
Figure 6 Lymn-Taylor cycle . . . 14
Figure 7 Example of X-ray diffraction . . . 16
Figure 8 Cryo-electron microscopy picture of actin filaments . . . 17
Figure 9 Experimental set-up of a single molecule strain experiment . . . 18
Figure 10 Illustration of Harmonic Links . . . 29
Figure 11 Immobilization . . . 32
Figure 12 Truncated Lennard-Jones potential . . . 34
Figure 13 Actin and its elastic network . . . 40
Figure 14 Subdomain distances and dihedral angle . 41
Figure 15 Responses to global perturbations . . . 42
Figure 16 Responses to global and local perturbaions 43
Figure 17 Residues in the nucleotide-binding pocket 47
Figure 18 Simple modeling of ligands . . . 50
Figure 19 Snapshots of ligand-induced conformational motions . . . 51
Figure 20 The pattern of relaxation trajectories for the ligand-network complex. . . . 52
Figure 21 Statistical distributions of interdomain distance L_{24} . . . 55
Figure 22 Myosin-V and its elastic network . . . 60
Figure 23 Residues probed and labels/order parameters . . . 61
Figure 24 Responses to forces applied to the tail . . . 63
Figure 25 Sensitivity of residues in the nucleotide-binding region . . . 67
Figure 26 Opening of actin cleft if forces act on tail . 69
Figure 27 Responses induced by the application of forces to the residues in the actin binding cleft region . . . 70

Figure 28 G-actin vs. F-actin 76
Figure 29 G-actin with open loop 77
Figure 30 Charged residues 81
Figure 31 Actin subunit guided by electrostatic interactions 82
Figure 32 Actin subunit binding to filament 83
Figure 33 Myosin guided by electrostatic interaction with filament 84
Figure 34 Myosin binding to filament 85
Figure 35 Actin trimer 87
Figure 36 Actin trimer – ligand induced conformational changes 88
Figure 37 Distance between actin and filament 89
Figure 38 Myosin-V modeled on actin filament 101
Figure 39 Network responses to the application of a static force to the tail 106
Figure 40 Actin-actin binding sites 107

LIST OF TABLES

Table 1 Sensitivity of selected residues in the nucleotide-binding pocket (NBP) region. 48
Table 2 Links between myosin and actin monomers in the filament 79
Table 3 Maximal distance changes (Å) observed when forces are applied to different residues in the nucleotide-binding pocket 108
Table 4 Maximal distance changes (Å) observed when forces are applied to different residues in the actin-binding pocket 109

ACRONYMS

ATP adenosine triphosphate

ADP adenosine diphosphate

P_i	γ-phosphate
EN	elastic network
NBP	nucleotide-binding pocket
ABP	actin binding protein
FRET	fluorescence resonance energy transfer
MD	molecular dynamics
HCM	hypertrophic cardiomyopathy
AFM	atomic force microscopy
DB	DNase-I binding
NMR	nuclear magnetic resonance
BPTI	bovine pancreatic trypsin inhibitor
GNM	Gaussian network model
ANM	anisotropic network model

1

INTRODUCTION

Proteins are the machinery of life and their complex interactions regulate virtually every process in the cell [2, 170]. They are macromolecules assembled out of only 20 standard parts, the amino acids. These molecular compounds have proven to be a formidable construction kit for nature and, although being created out of only these few ingredients, proteins have achieved a remarkable functional diversity throughout the course of evolution [2, 30, 104].

An important class of proteins are the enzymes, molecules that catalyze chemical reactions [13, 170]. Two very prominent examples are the structural protein actin and the molecular motor myosin. Both are molecular machines that gain energy by binding and subsequent decomposition of adenosine triphosphate (ATP) into its products adenosine diphosphate (ADP) and a so-called γ-phosphate (P_i). This chemical reaction fuels the machine cycles of the two macromolecules. Actin, e.g., uses the gained energy in a process called treadmilling to polymerize into long filaments and myosin is able to perform directed motion or exert forces. Despite decades of research, important aspects of their working mechanisms remain to be uncovered [42, 168].

In the beginning of protein research, the field has been mainly observation-driven. On the basis of experimental results, first ideas about the internal working mechanisms have been developed [76, 173]. First successful theoretical descriptions of protein dynamics have been in the form of kinetic rate equations. An outstanding example is the so-called Lymn-Taylor cycle, which for the first time provided a complete model of the interaction of actin and myosin within the muscle [58, 108, 155]. In such models, the machine cycle is characterized in terms of states and corresponding transition rates. In combination with experimental data, kinetic models can qualitatively describe the behavior of certain proteins and even make predictions about local structural mechanisms [14]. In general, however, these results lack the resolution to explain structural details and, accordingly, no complete model of protein dynamics is to be expected.

In recent years, molecular dynamics (MD) simulation methods have been applied to study proteins [87]. Such models incorporate the interactions between all atoms and, thus, provide high-resolution results. A major drawback of this approach is the enormous computational complexity involved. Despite today's growing computational power and the development of a variety of acceleration methods aiming to overcome such limitations, it remains currently unfeasible to follow the slow conformational dynamics that define the actions of many biomolecules [88].

A solution is offered by approximate methods of intermediate complexity [165]. By appropriate coarse-graining of the protein structure and interactions between atoms, such models can reduce the high computational costs of MD approaches while avoiding the lack of resolution of kinetic models. In this thesis, we will employ an elastic network (EN) approximation to model protein dynamics. This approach has initially been developed to describe thermal motions of residues and has continually been extended and advanced [9, 63, 69, 36, 161]. Here, we expand the standard EN model to account for effects of external forces, protein-protein interactions and ligand binding.

The study of two major players in the cell – actin and myosin – is a challenging subject. A broad community of researchers is dedicated to studying the underlying working principles of these macromolecules and many experimental techniques and theoretical tools have been developed accordingly. Nonetheless, a final understanding of the working mechanisms of the two proteins has not been reached. The vast amount of existing data, however, provides a useful benchmark for our modeling.

Actin is one of the most versatile and, thus, most studied proteins. In the cell, it interacts with a large number of actin-binding proteins (ABPs) [41, 42]. Many detailed studies have been performed and experiments have been developed to shed light on such interactions, which are, e.g., responsible for regulating the treadmilling process [133, 142, 160, 172]. Interestingly, actin is only known to be functional in its filamentous form [42] and the minimal requirements to enable polymerization have been determined in experiments: along with a sufficient amount of actin monomers, the presence of ATP molecules is needed to provide the energy for treadmilling [95]. Thus, we will go right to the core of this process and study the influence of ligand-binding on the macromolecule.

In complex with actin, the molecular motor myosin is known for its role in muscle contraction [2]. However, even outside of muscle cells, myosins have vital functions transporting loads inside the cell. Hence, this class of biomolecules is one of the most important members of the protein family. Due to its significance, all aspects of myosin have been investigated. The fundamental question arising is how the energy, also provided in form of ATP molecules, is converted into directed motion. Inspired by recent experiments [80], we investigate the role of strain and external forces in the motor mechanism to understand how myosin molecules regulate processivity.

The overall aim of this study is to shed light on the working principles of the two proteins actin and myosin. More specifically, we want to identify internal communication and regulation mechanisms.

Chapter 2 provides background information of properties of proteins in general. An overview of enzymes and more specifically of the myosin motor and the structural protein actin will be given. Throughout the years, many experimental and theoretical approaches have been developed within the field of protein research. Different methods investigating various aspects of biomolecules will be reviewed.

The methodology followed in this study will be introduced in **Chapter** 3. In order to investigate slow conformational motions, a coarse-grained method, the EN model, will be applied. Despite their high degree of simplification, EN models have turned out to be remarkably efficient and, therefore, provide a suitable compromise retaining single residue resolution while avoiding the numerical complexity of all-atom simulations. General aspects of this method will be discussed and, moreover, several expansions of the EN model will be presented.

Our aim in **Chapter** 4 is to investigate complex intramolecular communication within the actin protein. In order to understand the internal organization of its dynamics, mechanical responses of the macromolecule are systematically probed. We find that two mobile actin domains are able to perform well-defined large-scale motions. They can approach each other so that additional interactions between the residues from different domains develop; thus the actin can get locked in a metastable closed state. Furthermore, our detailed study of mechanical sensitivity of the molecule to application of various perturbations in the nucleotide-binding region reveals that the characteristic

global domain motions can also be easily induced by the application of only local perturbations to some selected residues in the NBP.

Binding of nucleotides and the hydrolysis reaction lead to local mechanical perturbations in the NBP. In this way, characteristic large-magnitude motions of mobile domains are induced. This can result in a transition to a locked closed state. In this thesis we want to demonstrate, in a strongly simplified way, that characteristic global responses to small local structural changes in the NBP region are feasible. This is done by placing into the actual nucleotide-binding region a fictitious ligand dimer and introducing elastic links between the ligand and the nearest residues in the pocket. We find that the binding of a model ligand, imitating the ATP, can stabilize the closed state of actin and induce a transition to this state from the equilibrium open state of the molecule.

In **Chapter** 5, our investigations will focus on the myosin motor protein. It is known that a single macromolecule of myosin naturally exhibits coordinated movements of its parts which would have required complicated machinery in a comparable macroscopic device. In this chapter, an elastic network will be used as a model of the myosin-V molecule. We will study how the protein responds to the application of an external force of arbitrary orientation to each single residue in important functional regions. The goal of this study is to identify those residues which are particularly sensitive to strains, so that their perturbation invokes strong conformational responses. In this way, a detailed pattern of intrinsic intramolecular communication can be obtained.

ATP binding and hydrolysis, followed by product release, are localized near the ATP-binding site in the region comprising the so-called front and back doors [71, 100]. It will be shown that the application of static forces to the myosin tail induces opening and closing of the front door and in this way provides an effective control mechanism for nucleotide release. Moreover, backward strain in the tail region leads to conformational changes in the actin cleft which are suited to facilitate binding to the filament. We will see that the nucleotide-binding region is divided into two functional parts: the application of forces in the front-door region, where the adenylate ring of ADP binds, leads to a movement of the tail, whereas forces in the back-door region, where phosphate is trapped after hydrolysis, induce conformational changes in the actin-binding cleft. We monitor

the effects of perturbations in the actin-binding region and observe communication between the hypertrophic cardiomyopathy (HCM) loop and the tail, indicating a connection between the binding to the filament and a motion of the tail. Thus, a complex pattern of intramolecular communication, based on elastic deformations and strain-sensor behavior, is revealed in myosin-V.

Interaction of actin-binding proteins with the filament will be studied in **Chapter** 6. More specifically, we will study how the actin-binding protein myosin and actin monomers themselves can attach to the filament. To this end, a model filament will be constructed out of single actin monomers. Different subunits can interact via their Coulomb interaction between charged residues and, if the residues are close enough, by soft sphere potentials. Most importantly, specific binding sites between proteins are modeled by breakable Lennard-Jones bonds.

Firstly, electrostatic interactions which guide either actin or myosin to their specific binding sites in the filament are investigated. Here, the proteins strongly interact with the filament via breakable bonds and may form stable complexes. Moreover, this chapter will show that binding of the ligand indeed induces conformational changes that make the actin monomer more likely to attach, i.e. it facilitates the docking to the filament. This is achieved by constructing a toy model and monitoring the ligand-induced conformational changes with respect to the filament.

The final **Chapter** 7 will conclude this thesis. The results of this work are briefly summarized and an outlook is provided.

2

BACKGROUND

This chapter serves as an introduction and gives a brief overview of the field of protein research. First, general aspects of proteins will be considered, i.e. structures and specific features of these biomolecules will be presented. Afterwards, we will discuss the two proteins which form the main focus of this thesis, actin and myosin, and their functions and modes of action will be elucidated. Furthermore, the reader will get a review of the most important experimental techniques and theoretical approaches used in such studies.

2.1 PROTEINS

The cell is the building block of life and is organized in a very complex manner. It may be seen as a factory comprised of many specialized machines that work together in a highly coordinated fashion. The machinery of this factory are the proteins. They are the workhorses of the cell and involved in virtually each intracellular process [2]. Through evolutionary pressure proteins have developed an impressive variety of functions. Enzymes, e.g., catalyze chemical reactions, transmembrane proteins act as gateways in the cell membrane and motor proteins are responsible for intracellular transport [2, 170]. For each of the innumerable tasks in the cell there exists a specifically adapted protein ready to complete it.

Although the functional diversity of proteins is extremely large, their construction principle is rather simple – all proteins are built out of only 20 *standard* amino acids [170]. These molecular compounds are called α-amino acids and they are simple molecules made out of an amino group, a carboxylic group and a side-chain specific for each amino acid [170]. The blueprint of a protein is stored in genes, which are the basis for biosynthesis of proteins or gene expression [2, 170].

All amino acids can bind to each other and, in this way, they provide a formidable construction kit for nature. Every protein is initially constructed as a polymer of these monomeric

units and obtains its structure and function in a process called folding [33]. Minimizing its energy, the amino acid polymer reaches its characteristic equilibrium conformation, the native state [11, 39, 174]. The native conformation corresponds to the most thermodynamically stable shape of a protein [40]. It is only in this state that the protein is able to perform work.

Proteins can fold efficiently on the time scale of milliseconds and faster [97], whereas a stochastic search through all possible conformations would have been unfeasible (see the Levinthal paradox [86, 101]). Therefore, folding pathways need to proceed along a definite pathway on a complex but very specific energy surface [11, 39, 86, 174]. In this energy landscape, metastable conformations with different basins of attraction exist and ensure the existence of a robust path leading toward the equilibrium conformation [61]. In this view, protein folding can be described as a series of hopping events between such metastable states. Moreover, such states are responsible for the separation of time scales between slow folding kinetics and fast dynamical motions of individual atoms in the protein [147].

An important group of proteins are enzymes which catalyze chemical reactions [2, 170]. *In vivo* enzymes are involved in most biological reactions. Common examples are the extraction of energy by the cell from food or the conversion of CO_2 into sugars during photosynthesis in plants. Also well known are the enzymes tubulin and actin which self-assemble into the filaments making up the cytoskeleton. Moreover, motor proteins are enzymes that catalyze the decomposition of ATP molecules and convert the energy gained in this process into directed motion [2, 175].

The mathematical description used to model enzymatic reactions in a simple way is the so-called Michaelis-Menten kinetics [2, 114, 170]. The enzyme E binds to a substrate S. Within the enzyme-substrate complex ES the substrate S is converted into the product P. Schematically, this process is written as

$$E + S \underset{k_{-1}}{\overset{k_1}{\rightleftarrows}} ES \overset{k_{\text{cat}}}{\rightarrow} E + P \tag{2.1}$$

with the phenomenological rate constants k_1, k_{-1} and k_{cat}. Here it was assumed that the back reaction in which the enzyme and the product recombine to form the ES complex can be neglected.

Prominent members of the enzyme family are ATPases. An ATPase catalyzes the decomposition of adenine triphosphate

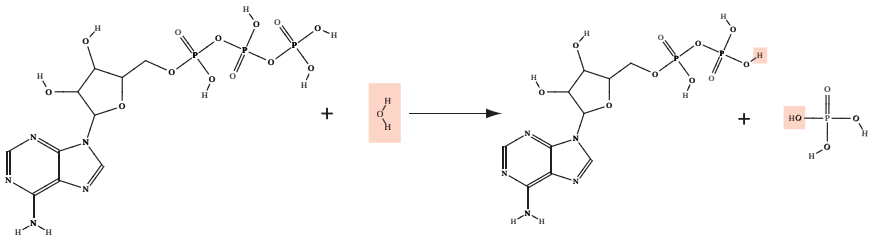

Figure 1: ATP hydrolysis: $ATP + H_2O \rightarrow ADP + P_i$

(ATP) into its products adenine diphosphate (ADP) and a phosphate (P_i). In this process called hydrolysation energy is released that the cell can use in various ways. The chemical hydrolysis reaction is displayed in Fig. 1. ATP is used as a source of energy in a wide range of processes within the cell. Because ATP stores and transports energy, it may be understood as an energy currency within the cell. This thesis mainly deals with the two ATPases – actin and myosin.

2.1.1 *Actin*

Actin is one of the most abundant proteins. In eukaryotic cells between 1% and 5% of all proteins are actin molecules [104]. The importance of actin is further highlighted by the fact that it is involved in more protein-protein interactions than any other known protein [42]. Close to a hundred proteins can regulate the actin dynamics. Moreover, the actin molecule has been highly conserved during evolution [133].

An important feature of the actin macromolecule is its ability to form long and stable filaments. Such filaments are an integral part of the cytoskeleton [2, 170]. It is noteworthy that actin is functional in its filamentous form only, i.e. no function of globular actin is up-to-date known [42].

Filaments polymerize in the dynamical process called treadmilling (see Fig. 2). While actin proteins on one side of the filament preferentially attach, they tend to dissociate on the other. This is sometimes described as the polarity of the filament; the plus end grows faster than the minus end [2]. The process of treadmilling is the basis of cell motility, i.e. the ability of a cell to move autonomously. Such a behavior is seen, e.g., in *E. coli* bacteria or the vaccinia virus [19, 116, 118].

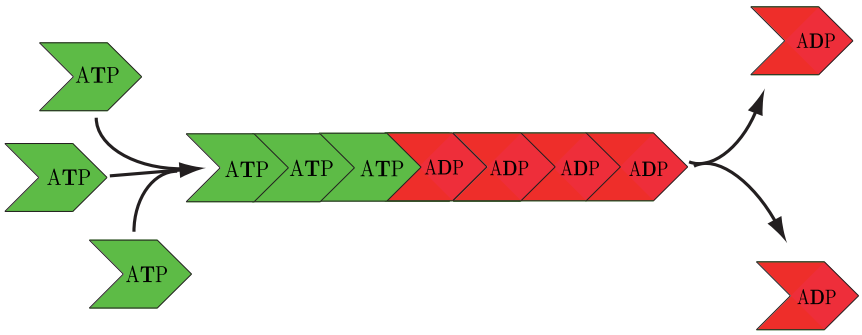

Figure 2: Treadmilling. Actin monomers tend to attach on one side of the filament and detach on the other. Treadmilling strongly depends on the nucleotide state of actin.

Polymerization strongly depends on the nucleotide state of actin [95, 131]. The binding affinity of ATP-bound actin at the growing end of the filament is much higher than the binding affinity of the ADP-actin complex. At the other end of the filament, the situations is contrary (see Fig. 2).

Actin filaments are an essential basis for muscle contraction [2] and, furthermore, form meshes which give structure and stability to the cell. An electron micrograph of such structures from Svitkina *et al.* [154] is shown in Fig. 3. The actin meshes can be seen as a complex highway system through the cell. Motor proteins like myosin move along actin tracks, e.g. to transport vesicles into or out of the cell.

2.1.2 *Myosin*

Myosins comprise a family of actin-based motor proteins [70]. Its members share the same general features, but exhibit minor structural differences [145]. All myosins, however, have in common that, attached to actin filaments, they can generate forces which allows them to move processively. Such a directed motion is fueled by the hydrolysis of ATP [2, 170].

Myosin was first discovered in muscle fibres and, therefore, muscle myosin is sometimes called conventional whereas all other myosins have been named unconventional. A more concise characterization has been done in form of classes. Class-I myosin (abbreviated myosin-I) is, e.g., responsible for vesicle transport inside the cell, whereas the muscle myosin belongs

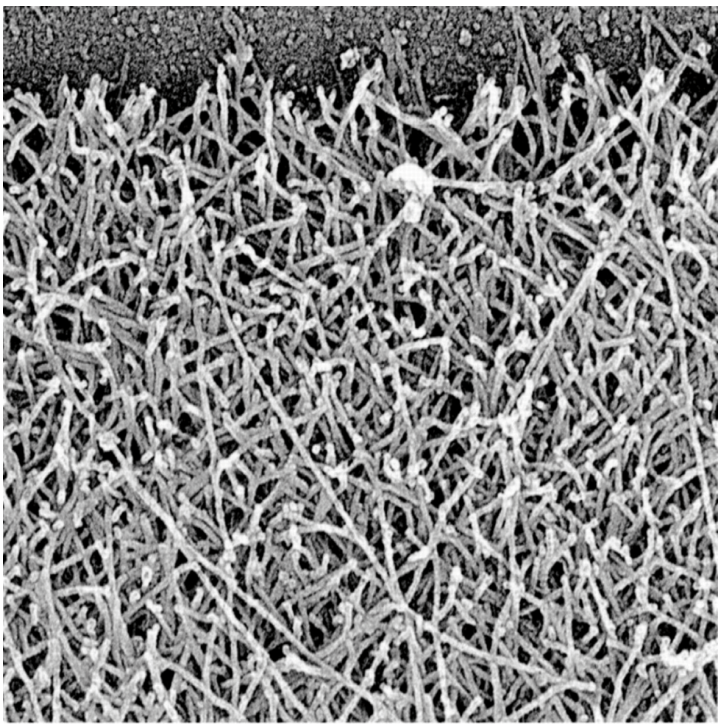

Figure 3: Actin filaments form meshes (electron micrograph, modified from [154])

to class II. Other myosins are consecutively numbered (III, IV, V, ...) according to the date of their discovery and, currently, eighteen different classes of myosin are known [57, 146]

Generally, the myosin motor protein consists of two main domains: the motor domain and the tail. Within the motor domain, the nucleotide-binding pocket (NBP) is located [21, 170]. Here the chemical reactions that fuel the motor mechanism, i.e. the binding of ATP, subsequent hydrolysis and product release, take place. The motor domain also interacts with the actin filament. Nucleotide or strain induced conformational changes in the actin-binding region control the binding affinity to the filament [80]. Likewise, the tail region plays an important role for force generating within the myosin machine cycle [2, 146]. This role, however, is not entirely clarified [151].

Myosins can exist both as single monomers (e.g. myosin-I) or as dimers (e.g. myosin-II, myosin-V). In the case of a dimeric molecule, myosin heads are connected via their tails [78]. This region also binds cargo that is transported through the cell. In Fig. 4 the two-headed myosin-V is depicted pulling a cargo along an actin filament.

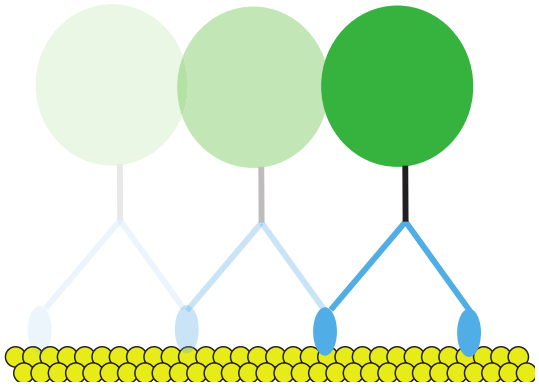

Figure 4: Schematic view of a two-headed myosin motor transporting a load along the actin filament.

The complex of actin and myosin, also called actomyosin, is best known for its role in muscle contraction [139]. The muscle consists of muscle fibers which, in turn, consist of sarcomeres. These cells have the ability to contract [2, 146, 170]. The muscle contraction is realized by a large number of myosin molecules interacting with actin filaments. A schematic illustration of a sarcomere is shown in Fig. 5. The functional basis of the sarcomere are thick bundles of muscle myosin (myosin-II) and actin filaments connected to the walls of the sarcomere (Z-discs). Myosin heads randomly attach to the filament and, in this way, pull the Z-discs toward each other [111]. This results in contraction of the sarcomere. The binding rate of the myosin heads, i.e. the strength of contraction, depends on the ATP concentration in the muscle cell [12, 29].

A different myosin protein is myosin-V. It is involved in the transport of vesicles and organelles along actin filaments in a specific direction. A schematic drawing of the two-headed motor is shown in Fig. 4. Myosin-V moves in a hand-over-hand fashion in 36nm steps along actin filaments [141, 166]. An interesting cousin of myosin-V is the class-VI myosin. It is also two-headed and involved in the transport of vesicles, but moves with a smaller step size into the opposite direction. The structural differences between these two proteins are subtle and, thus, they have challenged how people think about the motor mechanism [80, 151].

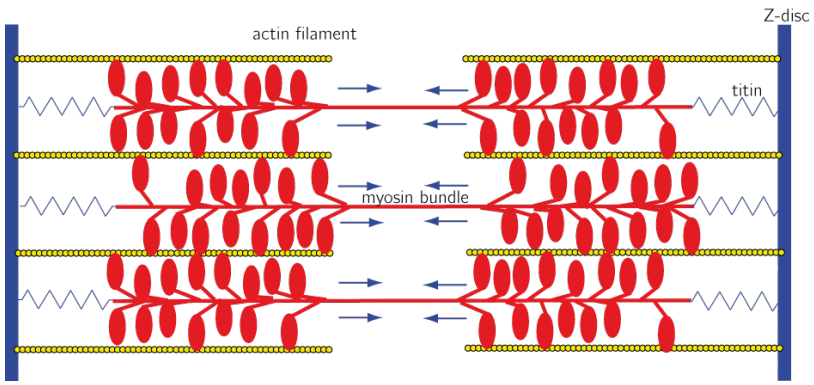

Figure 5: Schematic view of a sarcomere.

2.1.3 *Actomyosin Complex*

In 1971 the two biophysicists Richard W. Lymn and Edwin W. Taylor have considered the mechanism of the myosin motor operation [108]. Their model is commonly referred to as the Lymn-Taylor cycle [58, 155]. In Fig. 6 the mechano-chemical cycle is schematically shown for myosin-V moving along actin.

The starting point to describe the machine cycle of the two-headed dimer is the state where both heads are attached to the filament. Due to the periodicity of the actin filament, a myosin head can only bind to the filament at specific binding sites (e.g. every 36nm for myosin-V). In the initial step, the rear head is nucleotide-free, whereas in the leading head ADP is bound. Then, ATP attaches to the rear head and, in this way, leads to a dissociation of myosin from the filament [59]. The now following step in the myosin motor cycle is the so-called force-generating step. This part of the Lymn-Taylor cycle still remains unclear [151] and the discussion in the research community focuses on two alternatives.

The majority of scientists think that the force is generated by the so-called power stroke [28, 72, 75, 134, 148]. The release of a nucleotide in the leading head is assumed here to lead to a lever arm swing. After that, the head finds a possible binding site through rotational diffusion. Note that in this view, there is a unique binding site in the filament where the free myosin head eventually binds.

In the opposing explanation, force is generated by a Brownian search-and-catch mechanism [158, 49, 80]. In this model, the tail is assumed to be very flexible. The rear, detached head moves by thermal fluctuations. The molecule finds the filament

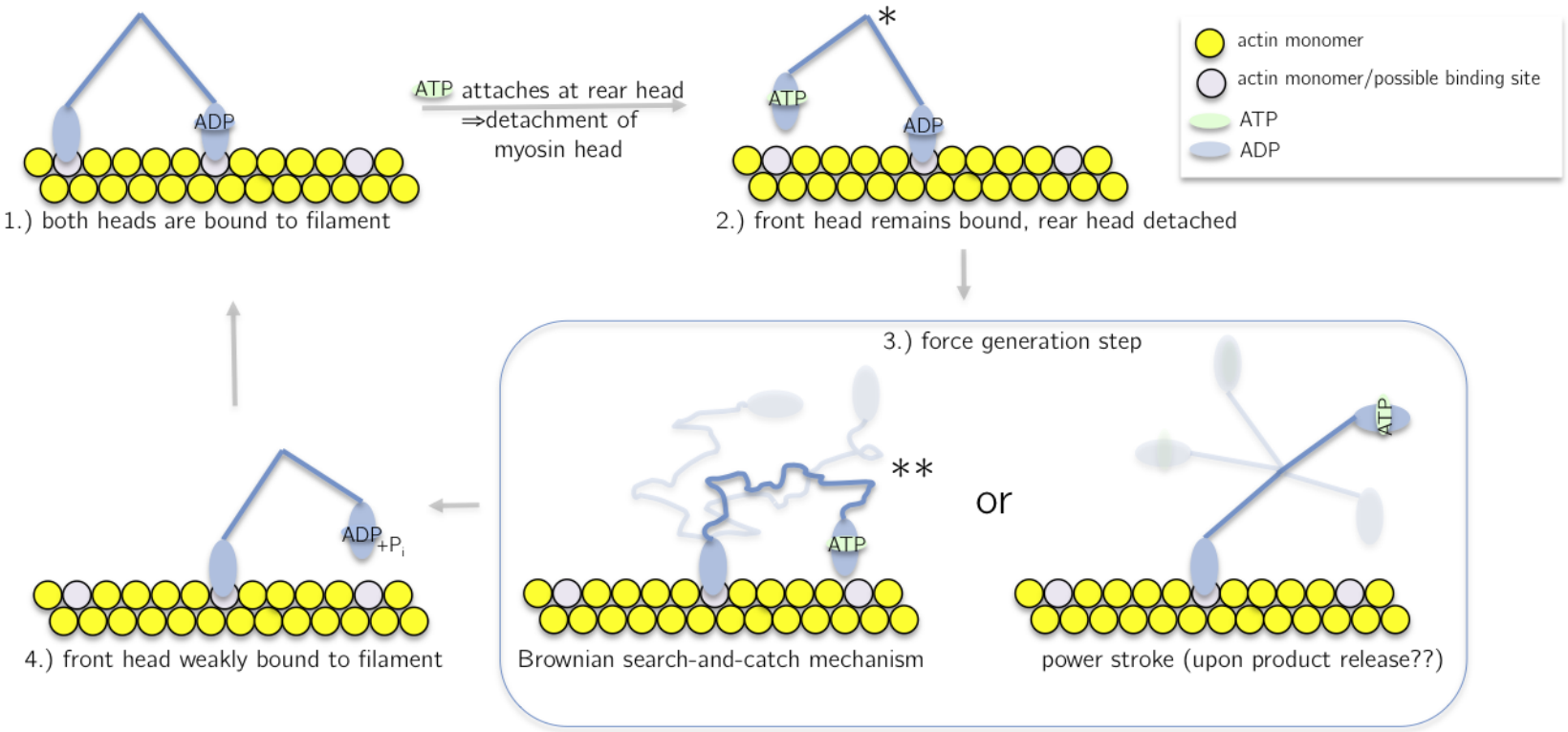

Figure 6: Lymn-Taylor cycle. Actin monomers are shown as yellow circles, pink circles show the possible binding sites for myosin. Myosin is shown in blue. The oval structures are the myosin heads connected via their tails.

binding site in front of the other head by some biasing mechanism. The important difference to the swinging lever-arm hypothesis is that, in the latter case, myosin has the possibility to attach to two different sites on the filament. The Brownian motion, however, is biased, and thus the myosin head is able to perform directed motion. Such a mechanism is possible, because ATP acts as a source of energy, and therefore the actin-myosin system is far from thermal equilibrium.

After the force generation step, however, both models are again found in the same state. ATP is hydrolyzed in the new leading head and this leads to a strong binding to the filament.

It is to note that communication between the two myosins is essential to ensure processive motion. First, it is important in the second step of the mechano-chemical cycle that the rear head detaches from the filament while the leading head is still attached to the filament. Otherwise, the dimer would have either stepped backward or fallen of the filament. Moreover, if myosin generates force by means of a Brownian search-and-catch mechanism, there has to be a bias to direct the motion. This can be achieved in two ways: either the two myosin heads communicate via the actin filament or via their tails, their only physical connections.

2.2 EXPERIMENTAL METHODS

Proteins are functional in their folded state only. Thus, the structure of the protein is essential to understand protein dynamics and many experimental methods have been developed for high-resolution structure determination. A standard technique to resolve protein structures with atomic resolution is X-ray crystallography [2, 44, 99]. The first crystal structure of a protein was that of the iron- and oxygen-binding protein myoglobin and it was obtained by Perutz and Kendrew. For this work they were awarded the Nobel Prize in Chemistry in 1962 [89, 90]. An example of an X-ray diffraction pattern for the actin filament is shown in Fig. 7.

The main technical hindrance in using X-ray diffraction is the necessity to grow protein crystals [44]. While being a complex procedure in itself, crystallization of proteins may also introduce physical perturbations which lead to erroneous structural data [109].

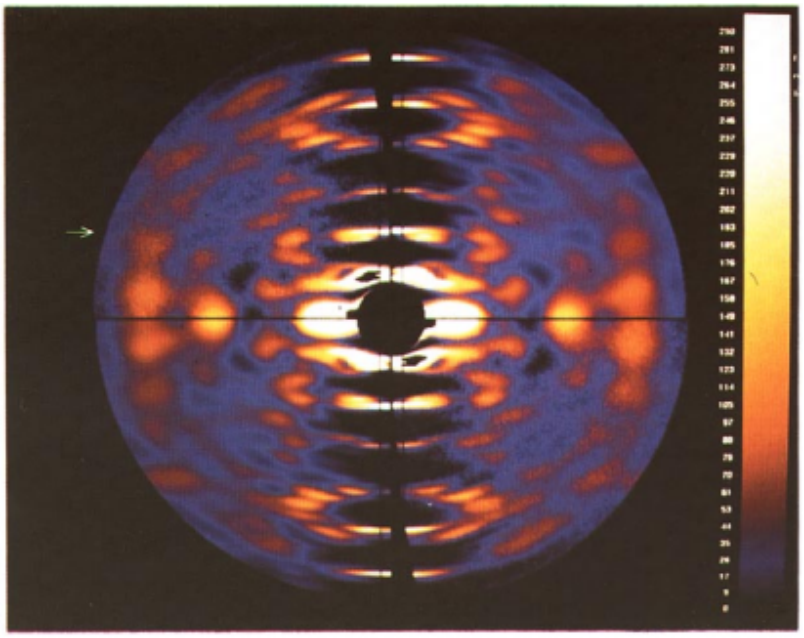

Figure 7: X-ray diffraction pattern of the actin filament. The upper left and the lower right quadrants show the experimental data, the other quadrants display the calculated values [106].

A powerful alternative to X-ray crystallography is nuclear magnetic resonance (NMR) spectroscopy [20, 143]. This method has been pioneered by Richard R. Ernst, who was awarded the Nobel Prize in Chemistry in 1991 for *"for his contributions to the development of the methodology of high resolution nuclear magnetic resonance (NMR) spectroscopy"*[2] and by Kurt Wüthrich, awarded the Nobel Prize in chemistry in 2002 for *"for the development of methods for identification and structure analyses of biological macromolecules"*[2] [98, 125, 176, 177].The advantage of NMR spectroscopy is its ability to determine the structure of a protein in solution with atomic resolution.

A different approach to obtain protein structure information is cryo-electron microscopy [56, 167, 182]. With this approach, biological specimens can be monitored in their biological environment and, similar to the NMR method, no crystallization is needed. To use cryo-electron microscopy, the bio-material is rapidly frozen and subsequently introduced into a high-vacuum electron microscope. High resolution structures can be obtained by averaging many electron microscopy images. Fig. 8 shows cryo-EM images of actin filaments [56].

2 http://www.nobelprize.org/

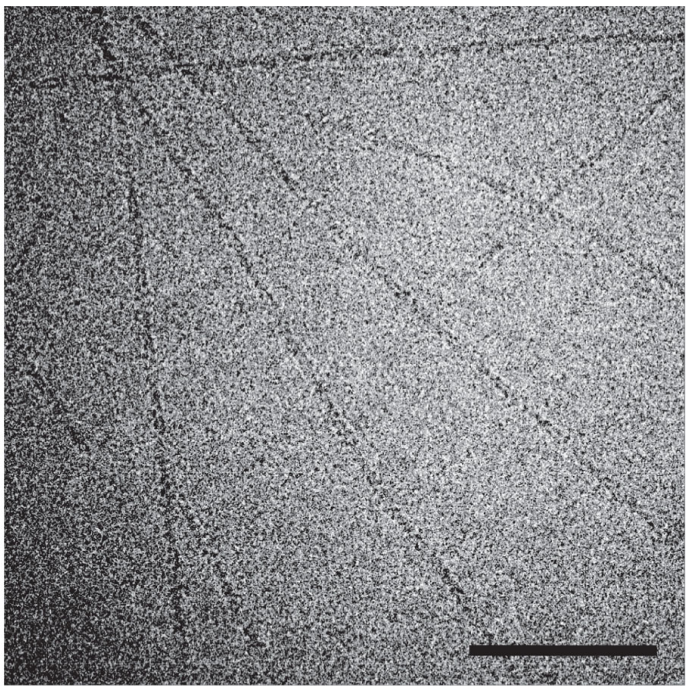

Figure 8: Cryo-electron microscopy picture of actin filaments. Scale bar, 100nm.[56]

Throughout the years, a large number of proteins has been resolved using various methods. Such experimental data has been collected and made available in an openly accessible online repository. Accordingly, structural data of a large number of biomolecules can be found in the Protein Data Bank[3].

Apart from 3-D structural data, researchers are interested in dynamic properties of protein. In recent experiments [80, 122, 123], proteins have been probed by applying external forces. Figure 9 schematically shows the experimental set-up used by Iwaki *et al.* [80]. In this experiment, a gold bead was attached to the tail of a myosin monomer. By means of an optical tweezer, the molecule was dragged along the actin filament in two opposite directions. The transition from strong to weak binding to the filament was seen to strongly depend on the direction of the applied force. It was found that the probability of strong binding increases when forces are applied in the direction opposite to that of the intrinsic processive motion. Thus, the myosin molecule operates as a strain sensor, with well-defined responses

3 http://www.rcsb.org/pdb/home/home.do

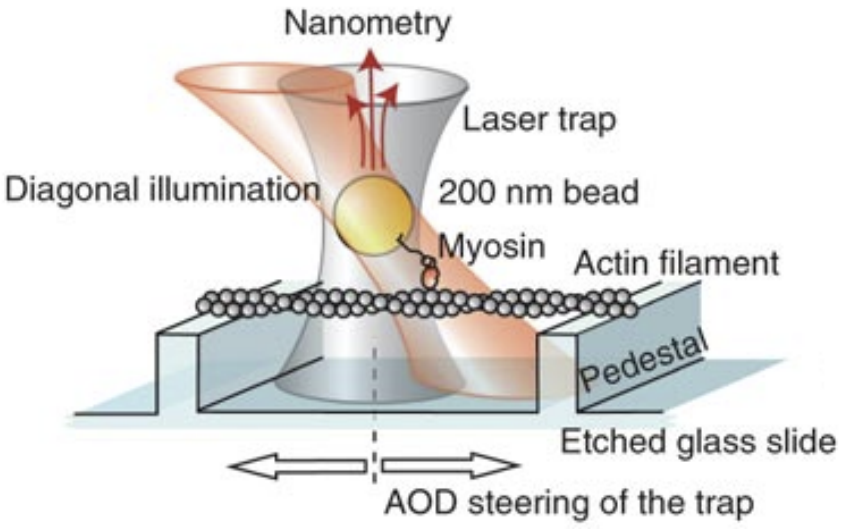

Figure 9: Experimental set-up of a single molecule experiment. A gold attached to a myosin tail is caught by an optical tweezer. In this way, myosin can be moved along the actin filament and forces can be applied [80].

in its different parts induced by specific mechanical perturbations.

A frequently used method allowing to monitor conformational motions directly is fluorescence resonance energy transfer (FRET), also called Förster resonance energy transfer [55]. Despite its low accuracy, distance changes in the range of 1-10 nm can be resolved in FRET experiments [83]. In this method, a protein is labeled by a fluorophore, serving as a donor, and a corresponding acceptor. Because of long-range dipole-dipole coupling, energy is transferred between the two marker molecules. The transfer rate depends strongly on the donor-acceptor separation and, hence, distance changes on the order of Å can be followed dynamically [62, 83]. The possibility to follow distance changes between acceptor and donor over time is the main advantage of the FRET technique.

2.3 MODELING OF PROTEIN DYNAMICS

Proteins have been the subject of many theoretical studies. The straightforward way to investigate protein dynamics is, of course, to include all particles and all interactions between them. With growing computational power, such molecular dynamics (MD) simulations have become a standard tool in this research field. Such descriptions, however, involve large systems of equations and suffer from high computational costs. To overcome such limitations, a wide range of simplified and coarse-grained approximations have been developed to tackle the open questions of protein research.

2.3.1 *Molecular Dynamics*

In the standard MD simulation method, Newton's equations of motion are numerically integrated. Here, the interatomic potentials are usually separated into bonded and non-bonded interactions. The bonded interactions are characterized by the bond length r_i, the bond angles θ_i and the dihedral angle ϕ_i. Non-bonded interactions can, e.g., be Coulomb interactions for charged atoms or Lennard-Jones-type potentials to model van-der-Waals bonds. In this case, the interatomic potential is

$$\begin{aligned} U_{ij} = & \sum_{\text{bonds}} k_i^{bond}(r_i - r_0)^2 + \sum_{\text{angles}} k_i^{angle}(\theta_i - \theta_0)^2 \\ & + \sum_{\text{dihedrals}} k_i^{dihedral}[1 + \cos(n_i\phi_i + \delta_i)] \\ & + \sum_i \sum_{j \neq i} 4\epsilon_{ij} \left[\left(\frac{\sigma_{ij}}{r_{ij}} \right)^{12} - \left(\frac{\sigma_{ij}}{r_{ij}} \right)^{6} \right] \\ & + \sum_i \sum_{j \neq i} \frac{q_i q_j}{\epsilon r_{ij}} . \end{aligned} \tag{2.2}$$

While the charges q_i are generally known, the parameters k_i^{bond}, k_i^{angle}, $k_i^{dihedral}$, n_i, δ_i, ϵ_i and σ_{ij} have to be obtained from experimental data. Approximate values of these parameters have been collected and are stored in force field parameter databases. Popular for protein simulations are the CHARMM or GROMACS force fields maintained at Harvard and Groningen University, respectively [15, 103].

The method of MD simulations has been first applied as early as 1957 in the field of statistical physics. The two scientists

Bernie Alder and Thomas Wainwright used it to describe simple liquids [3, 4]. The method was advanced by Rahman who used such simulations to describe liquid argon [137]. About ten years later, a realistic system was investigated by Rahman and Stillinger who studied properties of liquid water [152]. Finally, MD simulations found their way into the field of protein research in the late 1970s and have since then prospered. Indeed, they have become one of the principal tools of theoretical biophysics.

The first protein investigated was bovine pancreatic trypsin inhibitor (BPTI) [112]. Because BPTI is small and stable, it has been used as a guinea pig system to test both experimental and theoretical methods. With growing computational power MD simulations have become widespread. Initially only used to refine the experimental data obtained by X-ray diffraction or NMR [18, 88], various MD studies investigating many different aspects of proteins are available today. They can be used, for instance, to understand the role of the solvent in protein functions or to investigate the mechanisms of protein folding [87].

All-atom MD methods are also used to study mechanochemical conformational motions in proteins. Although such simulations have been successfully used to describe atomic fluctuations on the order of nano-seconds, tracing the slow large-scale collective motions is prevented by the excessive computational costs [66]. Such motions are typically on the scale of milliseconds or longer, whereas, in full MD simulations, generally only the dynamics on much shorter time scales up to a microsecond can be resolved

To overcome such computational limitations, various acceleration methods have been proposed. A typical example of such a method is provided by steered MD simulations, which were first developed to study the unbinding of avidin and biotin [81, 107, 79]. In such simulations, external harmonical forces are applied to lower energy barriers and, in this way, speed up rare events. Another method to accelerate MD simulations is the Replica-exchange method [21, 23, 138]. Here, several copies (replicas) of the investigated system with different temperatures are evolved independently in time using conventional MD simulations. After some time interval t_{swap} the states with neighboring temperatures are swapped by velocity rescaling with a certain probability $p_{\text{swap}}(\Delta E)$, which depends on the energy difference between the two states. This method has been applied, for example, to the myosin NBP to identify possible exit pathways of

P_i after hydrolysis [21]. Moreover, specialized hardware for efficient MD simulations is being developed [52, 120, 147]. By using it., the native-state dynamics of the small protein BPTI could be followed over a time scale of one millisecond, the longest published all-atom MD simulation of a protein up-to-date [147].

A large number of studies using accelerated methods have been performed for myosin and actin. For instance, conformational dynamics of actin monomers have been investigated in this way and responses due to interaction with ATP and other ligands have been analyzed. Moreover, nucleotide-dependent folding of the flexible DNase-I binding (DB) loop could be observed [128, 185]. It was demonstrated that the nucleotides induce significant local deformations in the region of the ATP binding pocket, which can partially close [128]. Slow large-scale ligand-induced motions of principal actin domains, however, could not be traced. For the myosin macromolecule, mechanical coupling has been theoretically studied. By means of guided MD simulations, i.e. molecular dynamics with an external restraining potential, it was demonstrated that significant conformational changes in the converter and actin-binding cleft could be induced by imposing a local perturbation of the protein configuration in the region of the ATP-binding pocket [127].

2.3.2 *Reduced Descriptions and Coarse-Graining*

As general experience in dealing with complex systems reveals (see, e.g. [115]), the very existence of robust ordered collective motions often implies that some reduced dynamical descriptions should be possible. Thermodynamic approaches, for instance, have been used to describe protein systems [5, 16, 111]. Even after considerable simplifications that may involve the loss of all structural information, important insights can be gained by such models.

An example of a greatly simplified approach is the Brownian ratchet models for motor proteins [1, 6, 111]. Brownian motion is the thermally induced motion of small particles suspended in liquid. This behavior is named after the the botanist Robert Brown [17] and theoretically considered by Einstein and Smoluchowski [48, 149]. The term Brownian ratchet refers to a thought experiment by Smoluchowski, which Feynman made popular in his famous lectures at the California Institute of Technology [51].

Today, some proteins are thought to make use of thermal fluctuations to perform their functions [179]. Particularly this refers to the processive motion of motor proteins along actin filaments and microtubules. Experiments suggest that motor stepping may be based on a Brownian-search mechanism [35, 80] and corresponding kinetic models have been developed [6, 14]. The basic idea is that the motor makes use of thermal fluctuations to efficiently and robustly perform its task. The motor proteins may have developed the mechanisms to bias the fluctuations, so that the motor preferentially moves into one direction. The bias is possible because, due to binding and hydrolysis of ATP, such molecular systems are far from its thermal equilibrium.

Kinetic models by Bierbaum and Lipowsky [14] have shown that, for the myosin-V motor, the chemical transition rates for binding of ATP and ADP have to be force dependent. While this dependence provides a qualitative understanding of a possible bias mechanism, its structural nature cannot be resolved by such models. The chemical activity of proteins, however, is to a large extent regulated by microscopic changes of its conformation [22, 140]. To resolve these effects, it is necessary to use high-resolution methods. In order to avoid the computational complexity of all-atom MD simulations, appropriate approximation techniques have to be developed.

Various coarse-grained descriptions have been proposed (see a review in Ref. [165]) and the Gō-models [10, 60, 93, 157] deserve to be particularly mentioned. In their original formulation, a residue is described as a bead and neighboring backbone residues are connected via harmonic potentials. Interactions between the neighbors within the native conformation of a protein are usually described with a phenomenological Lennard-Jones type potentials [68, 153]. Hence the equations of motion look identical to (2.2). In the case of Gō-models, however, the particles are not atoms, but represent residues. Usually a point particle at the C_α position of the amino acid is taken as a representative for the whole residue. The parameters are chosen in a way that the native state of the protein is the equilibrium conformation. Gō-models have been developed to study the problem of protein folding and have successfully described folding pathways and corresponding energy landscapes of various protein structures [27, 64, 85, 119, 157]. Moreover, Gō-models have recently been applied to investigate large-scale conformational motions of proteins [124].

A simplification of standard Gō-models is the EN approximation. Such models have gained an increasing popularity in the last years [9, 63, 69, 36, 161]. In the EN approach, the phenomenological Lennard-Jones type potentials are replaced by harmonic potentials. Instead of differentiating between native and non-native bonds, all neighboring residues, irrespective of whether they are interacting over the backbone or over their sidechains, are connected by elastic links. The EN model can thus be pictured as a network of residues where all residues, that are within a certain range, are connected by elastic links.

2.3.3 *Elastic-Network Models*

We see that the construction of EN models is very straightforward. Amino acids are replaced by identical point particles, which typically correspond to a residue, and the interactions between residues are approximated by introducing elastic links between neighboring particles. The links have different natural lengths, but, as often assumed, the same stiffness. The architecture of the elastic network, i.e. the pattern of connections between its nodes, is constructed on the basis of experimentally known equilibrium conformation of a protein in a way that its lowest energy state coincides with the known equilibrium conformation of a protein. The exact formulations will be given below in the next chapter.

An EN model was first used by Tirion in 1996 to describe the thermal fluctuations (B-factors) in several proteins using an all-atom description [161] and nowadays several variants of the EN approach exist. The work of Tirion laid the foundation for the development of the so-called Gaussian network model (GNM) [9, 63]. This approach considers protein networks on the level of amino acids and it has been very useful to understand vibrational dynamics, i.e. mean-square fluctuations and correlations between fluctuations of pairs of residues [136]. Inspired by such results, the anisotropic network model (ANM) was put forward in 2000 [7, 43]. In this description, the directional dependence of deformations was additionally included. The ANM will be used to model actin and myosin proteins in the course of this thesis.

Despite their high degree of simplification, EN models have turned out to be remarkably efficient. Investigations revealed that such models, apart from describing the B-factors in many

proteins, can also predict ligand-induced conformational changes [36, 159, 102, 24, 180]. Much attention has been paid to the normal-mode analysis corresponding to linearized EN models. However, full nonlinear equations of relaxational EN dynamics were also explored [46, 53, 54, 65, 129, 163, 164]. It was even shown that EN models can be extended to include the possibility of partial unfolding and refolding of proteins [67, 91, 110, 117].

Nonlinear EN models have been the focus of our research group at the Fritz Haber Institute of the Max Planck Society. It has been, for example, shown that motor proteins respond by well-defined motions to external perturbations. On the basis of such results, a design principle for protein machines was suggested and, in an evolutionary process, artificial machines have been constructed [163]. Furthermore, Togashi *et al.* [164] have examined the validity of the assumption of linearity which underlies the normal-mode analysis of proteins and, thus, represents the basis for a wide range of works. They have shown that the protein kinesin KIF1A behaves strongly nonlinear and conformational motions of this macromolecule follow trajectories much different from the ones expected in the linearized EN approximation.

Additionally, nonlinear EN models have been used to study helicases. Entire operation cycles of the molecular motor hepatitis C helicase were described using a simple coarse-grained ligand model [53]. In the same framework, operation mechanism of different helicases could be understood by modeling them as elastic networks [54]. Moreover, effects of hydrodynamic interactions with the solvent were incorporated into EN models [47, 34] and thermal fluctuations could also be considered in the framework of this approach. In this way, the machine cycles of the enzyme adenylate kinase [47] interacting with solvent were reproduced by EN simulations.

There is one property of elastic-network models which makes them particularly appealing. Since all residues are pictured as identical point particles, irrespective of their actual chemical structure, and because interactions between the particles do not depend on the chemical nature of the corresponding residues, EN models turn out to be stripped of almost all chemical details. In this rough approximation, a protein is viewed as a mechanical object, i.e. as a complex elastic network. Therefore, by studying such models, one can investigate purely mechanical

aspects of conformational protein dynamics, distinct from the chemical aspects.

3

MATHEMATICAL METHODS

The dynamics of actin monomers, the molecular motor myosin and the complex of the two proteins are investigated in this thesis from a theoretical point of view. This chapter is a complete collection of the mathematical tools used in our study. Both actin and myosin are molecular machines and they perform certain tasks characterized by collective domain motions. Such collective motions can be slow, even up to 1s. Accordingly, all-atom MD simulations, the standard approach to describe conformational dynamics of proteins numerically, are currently unfeasible due to the high computational costs involved. To overcome these limits, the so-called anisotropic network model or simply elastic-network (EN) model [7, 43] is used to approximatethe proteins.

Below, the general EN approach is introduced. Furthermore, we discuss linearization of the corresponding equations of motion. We also show how to extend such an approximation in order to be able to describe protein-specific features. Throughout this thesis, figures of proteins and networks will be found. For visualization we used the VMD software, developed and advanced in the Theoretical and Computational Biophysics Group at the University of Illinois [74].

3.1 THE ELASTIC NETWORK MODEL

To approximate proteins, a structural coarse-graining takes place. An elastic network is formed by N identical point particles (nodes) which are connected by identical elastic links. The network architecture is defined by the experimentally known equilibrium positions $\mathbf{R}_i^{(0)}$ of all residues i in the protein. For this purpose, the positions of α-carbon atoms are taken. Note that such an approach neglects the chemical character of each amino acid – they are treated as identical objects – and, thus, strips the protein of all chemical details. Having done so, it is necessary to introduce interactions between residues in a suitable way.

In the EN model, only residues that are located in the neighborhood of each other in the folded conformational state can interact. Interaction is modeled in a simple approximation. An elastic link is introduced between two nodes i and j if the equilibrium distance $d_{ij}^{(0)} = |\mathbf{R}_i^{(0)} - \mathbf{R}_j^{(0)}|$, i.e. the distance between the α-carbons in the experimentally obtained conformation used as a reference, is smaller than some cutoff l_0. The natural length of the link is chosen equal to the respective equilibrium distance $d_{ij}^{(0)}$. Hence, in the EN approximation, the experimentally found equilibrium state is by definition the state with the lowest elastic energy $E = 0$.

The total elastic energy of the network is given by the sum of the energy stored in its elastic links

$$E_{\mathrm{el}} = \frac{1}{2}\kappa \sum_{i,j} \mathrm{A}_{ij} \left(d_{ij} - d_{ij}^{(0)} \right)^2 \tag{3.1}$$

where $d_{ij} = |\mathbf{R}_i - \mathbf{R}_j|$ is the distance between two particles i and j and the elements of the adjacency matrix $\mathbf{A}$ are $\mathrm{A}_{ij} = 1$, if $d_{ij}^{(0)} < l_0$, and $\mathrm{A}_{ij} = 0$ otherwise. The elastic constant κ is the same for all nodes. If external forces $\mathbf{F}_i$ are applied to the network, its energy is $E = E_{\mathrm{el}} - \sum_i \mathbf{F}_i \cdot \mathbf{R}_i$. The different quantities used in equations (3.1) are illustrated in Fig. 10.

In our study, the cutoff length in the anisotropic EN has been determined by following the arguments by Atilgan et al. [8]. They constructed a sequence of EN models with gradually increasing values of the cutoff length and, for each cutoff length, computed the eigenvalues of the linearization matrix (see below). If the cutoff length was too small, the network was falling into disconnected components or free rotations inside it were possible, as evidenced by the fact that more than six zero eigenvalues of the linearization matrix were found. The cutoff length of 8.5Å for G-actin and 10Å for myosin-V, used in our numerical investigations, was chosen as the first cutoff length at which only six zero eigenvalues were present. Note that, in the study [8], a cutoff length of 9.5Å was found to hold in the anisotropic network approximation for a large group of proteins (but actin and myosin were both not considered there).

On the considered time scale of milliseconds, inertial effects are negligible and conformational dynamics is purely dissipative [92]. In our present study, hydrodynamical interactions between particles will be neglected. In the overdamped limit, par-

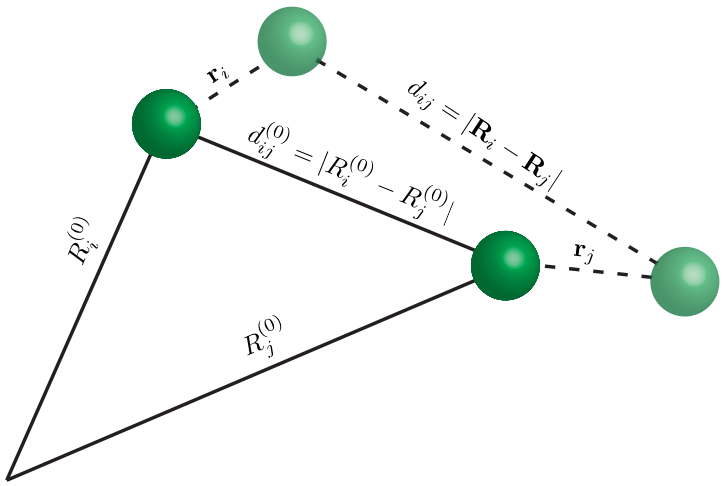

Figure 10: Illustration of the EN model. Two residues i and j are connected via an elastic link. Deformation from the equilibrium position leads to a force proportional to the distance change $d_{ij} - d_{ij}^{(0)}$

ticle velocities are proportional to the forces acting on it and the equations of motion are

$$\gamma \dot{\mathbf{R}}_i = \mathbf{F}_i - \frac{\partial E_{\text{el}}}{\partial \mathbf{R}_i} \,. \tag{3.2}$$

Within the coarse-grained EN approximation, we assume that the friction coefficient γ is equal for all particles. After an appropriate rescaling of time, the parameters κ and γ can therefore be removed from these equations and they take the form

$$\dot{\mathbf{R}}_i = \mathbf{F}_i - \sum_{j=1}^{N} \mathrm{A}_{ij} \left(d_{ij} - d_{ij}^{(0)} \right) \frac{\mathbf{R}_i - \mathbf{R}_j}{d_{ij}}. \tag{3.3}$$

Note that, in the new units employed, the force $\mathbf{F}$ is measured in Å. A force of $F = 1$Å is stretching a single elastic link by 1Å. An important property of equations (3.3) is that they are generally nonlinear in terms of the coordinates $\mathbf{R}_i = (X_i, Y_i, Z_i)$ because of the nonlinear dependence of the distances $d_{ij} = \sqrt{(X_i - X_j)^2 + (Y_i - Y_j)^2 + (Z_i - Z_j)^2}$. Such a dependence can give rise to interesting nonlinearities [164].

The dynamics of the EN is followed by integrating equations (3.3) using the explicit Euler method with the time step $dt = 0.1$. Although this integration scheme sometimes suffers from stability problems and may produce large errors, it can be used

in the dissipative systems investigated. On the example of an actin EN, we have studied the effect of different values dt. By repeating integrations for some relaxation trajectories with a smaller time step of $dt = 0.01$, we have checked that this does not lead to significant changes. To test this, we have compared the two stationary states in the presence of external forces that were obtained by integrating the equations of motion (3.3) with two different time steps of 0.1 and 0.01. The time evolution of the sum of distances between all residues in the network were followed in both simulations and were found to be below 0.001Å. Thus, the decrease of the time step did not lead to an accuracy improvement and the choice of the time step as $dt = 0.1$ was sufficient for our analysis.

Integration of the equations of motion (3.3) has been continued until a stationary state was reached. The numerical criterion was that the sum of the corresponding order parameters (see the following chapters for exact definition of the order parameters) has ceased to change by more than 10^{-14}Å.

3.2 LINEARIZED EQUATIONS OF MOTION

The equations of motions (3.3) of the EN model are nonlinear because distances are nonlinear functions of the coordinates. EN models are often used for the normal-mode analysis [7, 9, 24, 36, 43, 63, 102, 159, 180]. Then, only small displacements of particles from their equilibrium position are considered and, thus, a linear approximation of the equations (3.3) can suffice. The linearized equations are

$$\dot{\mathbf{r}}_i = -\sum_{j=1}^{N} \mathrm{A}_{ij} \frac{\mathbf{R}_i^{(0)} - \mathbf{R}_j^{(0)}}{\left[d_{ij}^{(0)}\right]^2} \left[\left(\mathbf{R}_i^{(0)} - \mathbf{R}_j^{(0)}\right) \cdot \left(\mathbf{r}_i - \mathbf{r}_j\right)\right] . \quad (3.4)$$

They hold for small deviations $\mathbf{r}_i = \mathbf{R}_i - \mathbf{R}_i^{(0)}$ from the equilibrium. Equations (3.4) can also be written in the matrix form $\dot{\mathbf{r}}_i = -\Lambda_{ij}\mathbf{r}_j$, with a $3N \times 3N$ matrix Λ. Such dynamical equations can be solved analytically in terms of the normal modes of the linearization matrix Λ. In terms of the eigenvalues λ_α and the eigenvectors $\mathbf{e}_i^{(\alpha)}$ the general solution is

$$\mathbf{r}_i(t) = \sum_\alpha k_\alpha \exp(-\lambda_\alpha t)\mathbf{e}_i^{(\alpha)} , \quad (3.5)$$

where coefficients k_α are determined by the initial conditions. Thus, the eigenvalues determine the relaxation rate constants of the respective normal modes. The slowest relaxation processes are controlled by the normal modes with the lowest eigenvalues. Characteristic normal motions that occur on different time scales are separated by a gap in the eigenvalue spectrum.

Assuming that only one of the normal modes is excited, the motions of network particles are given by equations (3.4) where only one term, corresponding to a particular mode, is present. Thus, characteristic network motions in a specific normal mode can be determined and visualized.

The equations of motion (3.3) depend only on relative distance changes. Therefore, they are always invariant against rigid translations and rotations of the entire elastic network. This implies that the linearization matrix Λ should always have six zero eigenvalues. On the other hand, if more than six zero eigenvalues are found, this indicates that the network breaks down into disconnected components or that free internal rotations of some residue groups are possible. This property can be used in the selection of the cutoff length, as explained above.

3.3 IMMOBILIZATION PROCEDURE

If a force acts on a single node of an elastic network, it induces not only internal deformations in the network, but also rigid translations and rotations of the entire object. If the network is pinned, e.g. by immobilizing one of its nodes, this can introduce additional internal deformations and the results of the study would depend on the location of the pinned node. To avoid such effects in our simulations, we have employed a special immobilization procedure. Compensating forces were applied to all network nodes in such a way that they could only lead themselves to a rigid translation or rotation. The magnitudes of the additional forces were determined by the condition that prevented translational and rotational motions induced by the external force. The computation of compensating forces was performed at each next integration step, so that they were automatically adjusted to the conformational changes. An illustration of the immobilization procedure is shown in Fig. 11.

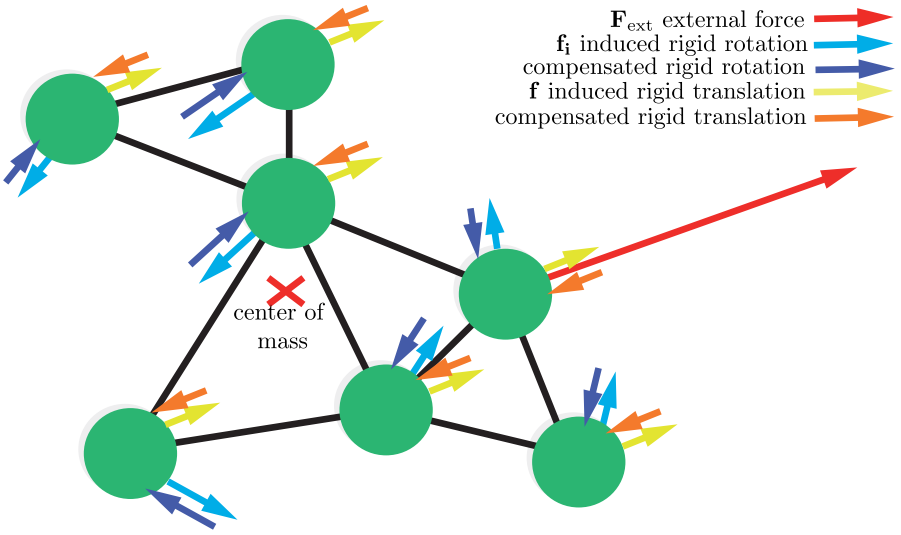

Figure 11: Illustration of the immobilization procedure. An external force $\mathbf{F}_{\text{ext}}$ is applied to a single residues of an elastic network. Induced rotation and translation described in terms of the forces $\mathbf{f}$ and $\mathbf{f}_i$, respectively, are shown. The corresponding compensating forces are indicated by arrows.

To construct compensating forces, we first note that, if the same force $\mathbf{f}$ is applied to each particle, it would lead to a rigid translation of the entire network. Moreover, if forces

$$\mathbf{f}_i = \boldsymbol{\omega} \times \mathbf{R}_i \tag{3.6}$$

with an arbitrary vector $\boldsymbol{\omega}$ are applied to the particles with coordinates $\mathbf{R}_i$, they can induce only rigid rotation.

Without loss of generality, the coordinates $\mathbf{R}_i$ can always be chosen in the coordinate frame whose origin coincides with the center of mass of the network. Suppose that an external force $\mathbf{F}_{\text{ext}}$ acts on a particle with coordinates $\mathbf{R}_0$. Then, it generates an external torque $\mathbf{R}_0 \times \mathbf{F}_{\text{ext}}$ that should be balanced by some compensating forces $\mathbf{f}_i$. Because the coordinates $\mathbf{R}_i$ of all network nodes are known, the compensating forces are completely determined by the constant angular velocity $\boldsymbol{\omega}$. It describes the rigid rotation that would be induced by external forces.

The additional compensating forces should satisfy the balance equation

$$\mathbf{R}_0 \times \mathbf{F}_{\text{ext}} + \sum_{i=1}^{N} \mathbf{R}_i \times \mathbf{f}_i = 0\,, \tag{3.7}$$

which can be rewritten as

$$-\mathbf{M}\boldsymbol{\omega} = \mathbf{R}_0 \times \mathbf{F}_{\text{ext}} \tag{3.8}$$

with the matrix

$$\mathbf{M}=\sum_{i=1}^{N}\begin{pmatrix} |\mathbf{R}_i|^2 - X_i^2 & -X_iY_i & -X_iZ_i \\ -X_iY_i & |\mathbf{R}_i|^2 - Y_i^2 & -Y_iZ_i \\ -X_iZ_i & -Y_iZ_i & |\mathbf{R}_i|^2 - Z_i^2 \end{pmatrix}. \tag{3.9}$$

Thus, to prevent rigid rotation, additional forces

$$\mathbf{f}_i = -\left[\mathbf{M}^{-1}\left(\mathbf{R}_0 \times \mathbf{F}_{\text{ext}}\right)\right] \times \mathbf{R}_i \tag{3.10}$$

should be supplied. Note that, as can be easily checked, $\sum_i \mathbf{f}_i = 0$ and, hence, such compensating forces do not induce translational motion of the network. To prevent rigid translation induced by the external force, the compensating force $\mathbf{f} = -\mathbf{F}_{\text{ext}}/N$ should be additionally applied to each network node.

Thus, if compensating forces $\mathbf{f} + \mathbf{f}_i$ are applied to all nodes at every integration step, both translation and rotation induced by the external force can be balanced out in a noninvasive manner.

3.4 EXTENSIONS OF THE MODEL

In the EN approximation, residues within a cutoff l_0 should be connected by elastic links. A problem arises if some residues that are not neighbors in the equilibrium conformation of a protein come too close to each other. This, for instance, can occur in the case of the actin monomer. Following the logic of the EN model, residues within the cutoff range should interact. Thus, we allow breakable links to be established between such nodes that are known to approach each other considerably. With a reasonable choice of parameters, these additional bonds may lead to a metastable conformational state. If such a metastable states exists, its stability is tested with and without thermal fluctuations. The general EN approach is extended as follows.

3.4.1 *Breakable Links*

We may include breakable links between residues not connected by elastic links. In contrast to other intramolecular interactions,

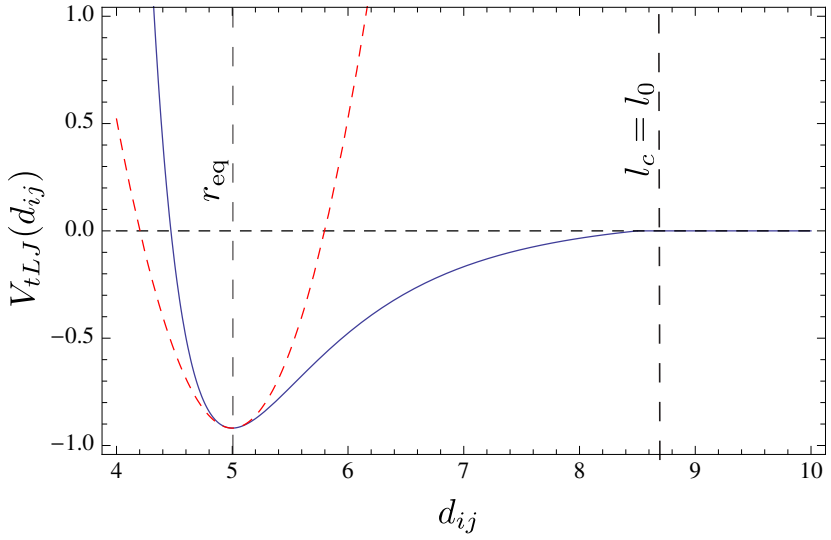

Figure 12: The truncated Lennard-Jones potentials with parameters $l_c = 8.5$Å, $r_{eq} = 5$Åand $D = 1$Å^2 is shown. The red dashed curve shows the approximation near the equilibrium by a harmonic potential.

breakable links are described by the truncated Lennard-Jones potentials

$$V_{\mathrm{tLJ}}(d_{ij}) = \begin{cases} V_{\mathrm{LJ}}(d_{ij}) - V_{\mathrm{LJ}}(l_c) & d_{ij} < l_c \\ 0 & \text{otherwise} \end{cases} \tag{3.11}$$

with the function

$$V_{\mathrm{LJ}}(d_{ij}) = B_{ij} D \left[\left(\frac{r_{\mathrm{eq}}}{d_{ij}} \right)^{12} - 2 \left(\frac{r_{\mathrm{eq}}}{d_{ij}} \right)^{6} \right] . \tag{3.12}$$

The interaction parameters are the equilibrium distance r_{eq} and the strength of the potential D. The matrix elements are $B_{ij} = 1$, if a breakable link between residues i and j exists, and $B_{ij} = 0$, otherwise. The cutoff length of the potential l_c is set to be equal to the cutoff length l_0 of the EN model. This reflects the fact that links that are too far away from each other should be broken. Additional links are effective only when the distances between the two residues are below the truncation length l_c.

When breakable bonds are added between residues that come close to each other, the equations of motion (3.3) should be modified by including additional forces

$$\mathbf{F}_i^{\text{add}} = -\sum_j \frac{\partial V_{\text{tLJ}}(d_{ij})}{\partial \mathbf{R}_i}, \tag{3.13}$$

where the summation is performed over all nodes j.

The choice of the interaction parameters for breakable links should be based on the requirements that (i) this potential becomes flat when distances between the residues exceed the cutoff length used in the construction of the elastic network from the experimental data, (ii) the minimum of the interaction potential is found at the distance which lies between the minimum and the maximum values of the natural lengths $d_{ij}^{(0)}$ of elastic links, as deduced from the experimental data, and (iii) near its minimum the potential (3.12) can be approximated by a parabolic potential with a strength of the same order of magnitude as that of the elastic potential of the regular links.

A reasonable parameter choice is $r_{\text{eq}} = 5\text{Å}$ and $D = 1\text{Å}^2$. The corresponding truncated Lennard-Jones potential with cutoff length $l_c = 8.5\text{Å}$ is shown in Fig. 12. The blue line represents the potential and the dashed red line shows its harmonic approximation near the equilibrium.

3.4.2 *Thermal Fluctuations*

To study the stability of the breakable bonds, effects of thermal fluctuations can be considered. Although we disregard hydrodynamic interactions, thermal fluctuations can be modeled by including appropriate random forces into the dynamical equations, i.e. by writing them as

$$\gamma \dot{\mathbf{R}}_i = \mathbf{F}_i - \frac{\partial E_{\text{el}}}{\partial \mathbf{R}_i} + \boldsymbol{\xi}(t)\,. \tag{3.14}$$

Here, $\xi_i(t)$ is a Gaussian noise with the correlations

$$\begin{aligned} \langle \xi_i(t) \rangle &= 0 \\ \langle \xi_i(t)\xi_j(t') \rangle &= \sigma^2 \delta_{ij}\delta(t-t') \end{aligned}\,. \tag{3.15}$$

separately in each direction. The parameter σ specifies the noise intensity. It is related to the temperature as $\sigma^2 = 2\gamma k_B T$.

3.5 PROTEIN-PROTEIN INTERACTIONS

Within the framework of the EN approach, amino acids are stripped of all chemical details. Accordingly, additional information is needed to model protein-protein interactions. If the corresponding binding sites are however known, such interactions can be included in a suitable way. In the following, we show how to extend the EN accordingly.

3.5.1 *Electrostatic Interactions*

Side-chains of certain amino acids are charged [170]. Arginine and Lysine, for instance, are positively and Aspartic and Glutamic acid are negatively charged. The amino acid Histidine is charged in 10% of all cases. Accordingly, we assign to the corresponding residues charges of $q = 1$, $q = -1$ and $q = 0.1$, respectively.

The electrostatic interaction between two charged residues is

$$V_{\text{e.stat.}}(d_{ij}) = A\frac{q_i q_j}{\epsilon d_{ij}} \exp(-d_{ij}/l_D)\,. \tag{3.16}$$

The parameter ϵ corresponds to the dielectric constant and A is a prefactor. Furthermore, in the solvent charges are screened by interaction with water and ions. These are not explicitly included in the model, but effectively introduced by a decaying exponential term. Thus, the range of the electrostatic interaction is controlled by the Debye-Hückel length l_D [37]. Here, the value $l_D = 20\text{Å}$ is used and the parameters are chosen as $A/\epsilon = 2\text{Å}^3$, in agreement with Ref. [158].

Additional electrostatic interactions (3.16) are present between the residues of different molecules only. The reason for this assumption is that protein EN models are constructed based on the native state. It corresponds to the equilibrium conformation and the actual shape of the protein is a result of energy minimization, i.e. folding of the protein. Therefore, all intramolecular interactions, including electrostatic ones, are effectively considered in the EN approach.

Thus, electrostatic interactions introduce additional forces

$$\mathbf{F}_i^{\text{e.stat.}} = -\sum_{\textit{other proteins}} \sum_j \frac{\partial V_{\text{e.stat}}(d_{ij})}{\partial \mathbf{R}_i}\,, \tag{3.17}$$

the sum of Coulomb interactions with all other residues of different proteins. To speed up simulations, only residues closer than a cutoff distance $r_{\text{ele}} = 160\text{Å}$ are interacting via electrostatic interactions in our simulations.

3.5.2 *Soft sphere potentials*

A soft sphere potential is used if residues come close to each other. These short-ranged interactions lead to a repulsion of the proteins that prevent protrusion of different protein domains. To describe such a behavior, we use the high temperature limit of the Lennard-Jones model

$$V_{\text{sp}}(d_{ij}) = D\left(\frac{\sigma}{d_{ij}}\right)^{12} . \tag{3.18}$$

For the EN model, similar types of interactions have been previously considered by Takano et al. in Ref. [158]. For the soft sphere potentials, we use similar parameters. Here, the strength of the potential D is given as $D = 0.06\text{Å}^2$. The characteristic interaction distance is chosen as $\sigma = 5\text{Å}$.

Due to repulsive interactions between different residues, an additional force

$$\mathbf{F}_i^{\text{sp}} = -\sum_{\text{other proteins}} \sum_j \frac{\partial V_{\text{sp}}(d_{ij})}{\partial \mathbf{R}_i} \tag{3.19}$$

is introduced. The interaction is short range and, thus, we introduce a numerical cutoff distance of $r_c^{\text{sp}} = 10\text{Å}$. Note that the soft sphere potentials (3.18) even decay much earlier.

3.5.3 *Protein Binding*

A protein may attach to a different one and form stable bonds. Such bonds may be hydrogen bonds, salt bridges or other non-covalent bonds. Protein-protein complex can be very strong. Well-known examples are the actin filament, comprised out of many actin subunits, or the actin-myosin complex.

We model such interactions by Lennard-Jones type potentials

$$V_{\text{inter}}(d_{ij}) = C_{ij} D_e \left[\left(\frac{r_{ij}^{\text{eq}}}{d_{ij}}\right)^{12} - 2\left(\frac{r_{ij}^{\text{eq}}}{d_{ij}}\right)^{6}\right] \tag{3.20}$$

with a depth of the potential $D_e = 0.2$ Å^2. The matrix elements $C_{ij} = 1$ if the nodes i and j interact and $C_{ij} = 0$, otherwise. Missing information about the equilibrium distance r_{ij}^{eq} or the interaction matrix B_{ij} must be obtained from additional sources like experimental data or MD studies. For actin and myosin, details will be provided in Ch. 6.

Forces due to this protein-protein interaction are given as

$$\mathbf{F}_i^{\text{inter}} = -\sum_j \frac{\partial V_{\text{inter}}(d_{ij})}{\partial \mathbf{R}_i}\,. \tag{3.21}$$

Covalent and hydrogen bond lengths are relevant only on scale of several Å. This is also reflected by the fast decay of the Lennard-Jones type bonds. Here, we additionally introduce a cutoff of $r_c^{\text{pb}} = 20$Å to speed up the computation.

4 INTRAMOLECULAR MECHANICS OF G-ACTIN

A major open question in the field of actin research is the role of the nucleotide. How are the interactions with ATP and subsequent hydrolysis related to the functionality of the protein? It remains unclear, e.g., why ATP-bound actin is attached more stable to the filament than the ADP-bound monomer [42]. In this chapter, we will study free monomeric actin (G-actin) and investigate ligand-induced conformational changes.

Systematic numerical investigations of conformational motions in single actin molecules were performed by employing a simple EN model of this protein. We found that G-actin essentially behaves as a strain sensor, responding by well-defined domain motions to mechanical perturbations. Several sensitive residues within the NBP could be identified, such that the perturbation of any of them can induce characteristic flattening of actin molecules and closing of the cleft between their two mobile domains. Extending the EN model by introduction of a set of breakable links which become effective only when two domains approach one another, it was observed that G-actin can possess a metastable state corresponding to a closed conformation and that a transition to this state can be induced by appropriate perturbations in the NBP region. The ligands were roughly modeled as a single particle (ADP) or a dimer (ATP), which were placed inside the NBP and connected by elastic links to the neighbors. Our approximate analysis suggests that, when ATP is present, it stabilizes the closed conformation of actin. This may play an important role in the explanation why, in the presence of ATP, the polymerization process is highly accelerated.

4.1 G-ACTIN MODEL

As a reference state for the construction of the elastic network, the uncomplexed G-actin in the ADP-bound state (PDB ID: 1J6Z) was used [126]. For comparison, the elastic network of the F-actin model (PDB ID: 3MFP) [56], obtained by fitting to cryo-

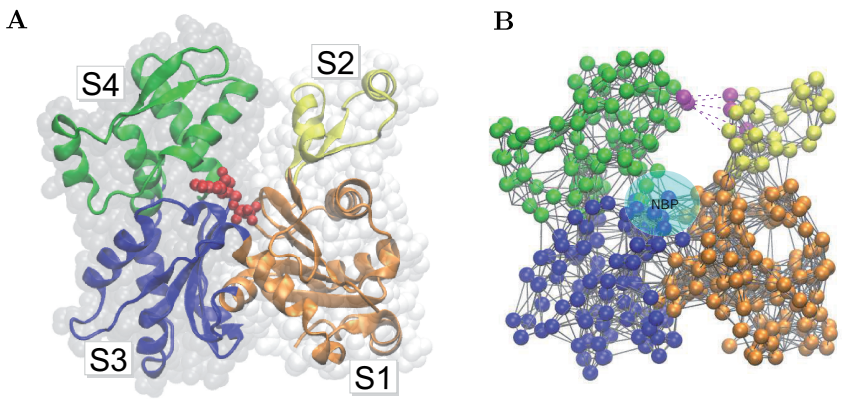

Figure 13: Actin and its elastic network: (A) G-actin in the ribbon representation, colored according to its subdomains S1 (orange), S2 (yellow), S3 (blue) and S4 (green). The bound ADP molecule (red) is shown. (B) The elastic network of G-actin, colored in the same way. Magenta dotted lines indicate Lennard-Jones bonds between some residues (also marked magenta) in the subdomains S2 and S4. The nucleotide-binding pocket (NBP) is schematically displayed.

electron microscopy data, was chosen. The G-actin data consists of 372 residues divided into two major domains, known as the outer and the inner domains. They are separated by a cleft in which the nucleotide binds. Traditionally, each of them is further divided into two subdomains [84]. The outer domain contains subdomains 1 (S1, residues 1–32, 70–144 and 338–372) and 2 (S2, residues 33–69). Part of S2 is the DB loop, playing an important role in inter-subunit binding. The inner domain consists of subdomains 3 (S3, residues 145–180 and 270–337) and 4 (S4, residues 181–269). Fig. 13 displays equilibrium structures of G- actin together with the elastic network of this protein with the cutoff length $l_0 = 8.5$Å. Furthermore, the subdomain structure of the actin monomer is shown in panel (a).

The distance L_{24} characterizes the scissor-like motion of the two mobile domains, while the angle θ provides a characterization of their scissor-like motion (see below). The three chosen order parameters show large variation when experimentally known conformations of G- and F-actin are compared. It should be noted that this order parameters agree with the dynamical variables employed in the coarse-grained four-domain description of the actin filament by Chu and Both [25].

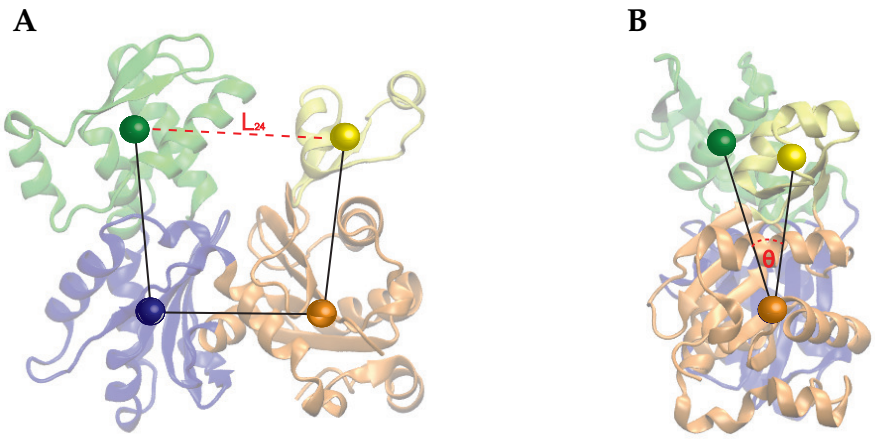

Figure 14: Subdomain distances and dihedral angle. (A) Center of masses of subdomains S1 (orange), S2 (yellow), S3 (blue) and S4 (green) are shown as beads. (B) The dihedral angle θ is defined as the angle between the two planes between the center of masses of S1, S2 and S3, and the center of masses of S2, S3 and S4, respectively.

In our simulations, positions of all residues have been determined at each integration step and, therefore, complete information about conformational motions was available. This full data has been used, e.g., when conformational snapshots were constructed or videos of characteristic conformational motions were generated. For concise characterization, we have additionally used a set of three order parameters traced in the simulations. Specifically, distances L_{13} and L_{24} between the centers of mass of S1 and S3 and the centers of mass of S2 and S4, respectively, were chosen. As the third order parameter, the dihedral angle θ, i.e. the angle between the plane defined by the mass centers of S1, S2 and S3 and the plane defined by the mass centers of S1, S3 and S4, was taken. Subdomain distances and dihedral angle are shown in Fig. 14.

4.2 DOMAIN MOTIONS AND METASTABLE STATES

Generally, application of a static force induces rigid translations and rotations of the entire protein. To eliminate such effects, additional balancing forces were computed at each inte-

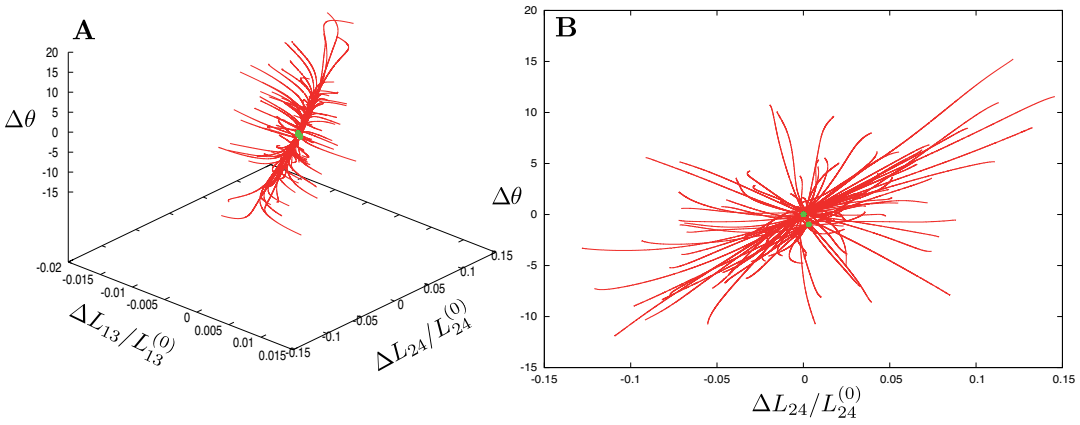

Figure 15: Responses to global perturbations. 100 relaxation trajectories (red curves) start from different initial conditions, generated by application of random, globally distributed static forces. Along the axes, relative changes $\Delta L_{13}/L_{13}^{(0)}$ and $\Delta L_{24}/L_{24}^{(0)}$ and absolute changes of the angle $\Delta\theta$ are varied.

gration step and applied to the network. They were chosen in such a way that only global translations and rotations could be caused - and thus compensated - by them, without any internal deformations arising. This immobilization is explained in depth in Ch. 3 where its detailed description can also be found. We have always used it in the presence of external forces in our current investigations.

To generate static forces, for each residue a direction was randomly chosen and the force magnitude was randomly selected from the interval between 0Å and 0.09Å. Such independently generated random forces were applied to all network nodes and a new stationary configuration of the network in the presence of the forces was determined by integrating for sufficiently long time the equations of motion (3.3), until a stationary state in the presence of forces was reached. Subsequently, the forces were lifted and a conformational relaxation process was followed by integrating the same equations.

Figure 15 displays results of such simulations for 100 different choices of random forces and, thus, for 100 different relaxation trajectories. The initial positions of the trajectories correspond to the stationary states of the network in the presence of random external forces. Hence, they characterize conformational responses of the network. As we see, the distance L_{24} between subdomains S2 and S4 can change considerably, i.e. up

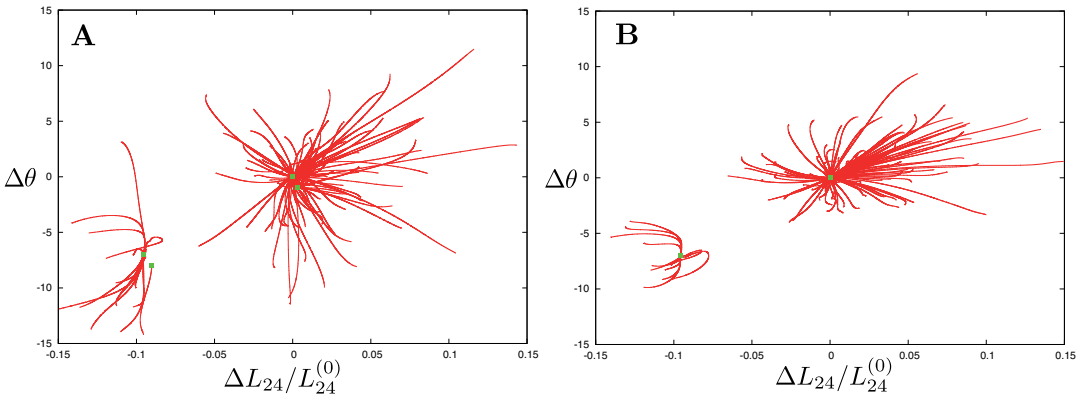

Figure 16: Responses to global perturbations (A) and to local pertubations of sensitive residues in the NBP region (B) are shown in the presence of breakable bonds. 100 relaxation trajectories (red curves) start from random initial conditions. Along the axes, relative changes of the distance L_{24} and absolute changes of the dihedral angle θ are varied.

to 15%, and the dihedral angle θ between the inner and outer domains can undergo variation up to 15 degrees. Significant changes in the distance L_{13} between the lower subdomains S1 and S3 were not found in our simulations. The experimentally observed difference of about 13% in the distance L_{13} in F-actin, as compared to the equilibrium state of G-actin, can be a consequence of the interactions between monomers in the actin filament.

When external forces were switched off, the network was undergoing relaxation back to its equilibrium conformation. The relaxation trajectories starting from different initial deformed states are displayed in Fig. 15. The end points of the trajectories (green dots) correspond to the finally reached states the farthest points of the trajectories represent the starting positions. There are only two such end points in Fig. 15. One of them lies in the origin of coordinates and thus corresponds to the equilibrium state of the elastic network. We have checked that the second state corresponds to a small buckling of a single residue within the flexible part of subdomain S4 and thus represents only a slight local modification of the equilibrium state. Even after relatively large deformations the network always returns to the equilibrium state or to its slight modification.

Thus, we see that the two principal mobile domains of actin are able to perform large-magnitude motions characterized by substantial changes of the distances between S2 and S4, as well

as of the dihedral angle between the two mobile domains. The displacements of residues, accompanying such motions, are large and the linearized description and the normal-mode analysis are not justified in this case (cf. the discussion in Refs. [46] and [164]). Nonetheless, such approximate descriptions can be still employed for qualitative understanding and interpretation of the observed motions.

We have computed the normal modes of G-actin in the framework of the EN approximation used in the present study (see Supplementary Movies in Ref. [45]). The slowest normal mode of the elastic network corresponds to the propeller-like twist of the two mobile domains, which can be well characterized by the dihedral angle (see Movie S1 in Ref. [45]). The second slowest normal mode represents the scissor-like opening or closing of the two domains, as seen in Movie S2 in Ref. [45]. These characteristic motions have been previously identified by Tirion and ben-Avraham [162] in the framework of a different normal-mode analysis, where all actin atoms were resolved and only angle variations of the bond angles were taken into account. It is remarkable that they are also reproduced in a much simpler EN model and, furthermore, are approximately retained on the much larger scales.

Our analysis based on full nonlinear equations of the elastic network has indicated that, for some large-amplitude motions, the cleft separating subdomains S2 and S4 almost disappeared, so that the residues belonging to opposite domains could come near one to another. In such situations, the EN model needs however to be modified, as explained below.

When an elastic network for a protein is constructed, distances between all pairs of residues in the equilibrium reference state are checked and elastic links are introduced whenever the distance between a pair is shorter than the cut-off length. Suppose now that some residues, well separated at equilibrium, come close when a perturbation is applied. If we want to follow the concept of the EN approximation, additional links connecting such residues would need to be introduced once they come close one to another. Such emergent (and breakable) links cannot be elastic, instead they should be described by a pair interaction potential which becomes flat as the distance between the particles increases. Hence, they would be effectively present only when the two particles are close one to another - and would disappear when the particles are far apart.

To allow such bonds to emerge, we add into the EN model a set of breakable links between those G-actin residues from opposite domains which are connected by elastic links in the EN model of F-actin. Thus, the original EN model of G-actin is extended by us through the introduction of five additional breakable links connecting residues 62–204, 63–203, 63–204, 66–203 and 67–203. The new links are described by truncated Lennard-Jones potential (3.11).

Comparing the experimentally known conformations of the globular G-actin and the filamentous F-actin [56, 126], one can notice that, under the cutoff length of $l_0 = 8.5$Å used in the EN model, there are eleven additional links between the subdomains S2 and S4 in the F-actin structure. Generally, breakable links may be introduced between all such eleven residue pairs. We have selected, however, only the five closest pairs of residues and introduced breakable links between them. We have chosen the same value of the equilibrium distance $r_{eq} = 5$Å for all additional links. With the choice of $D = 1$Å^2 the interaction potential (3.12) near the equilibrium distance was by a factor of 2.88 stronger than that of the regular elastic links. By choosing D in this way, we could approximately compensate for the smaller number of interacting pairs in our model as compared to the experimental F-actin structure.

Taking the expanded EN model, global mechanical responses of the elastic network were examined and its relaxation trajectories were explored using the same procedure as described above for the original network. The results are displayed in Fig. 16A. Not surprisingly, the relaxation behavior remains essentially the same in the neighborhood of the equilibrium reference state of G-actin, which defines the origin of coordinates. However, an important change is observed in the region corresponding to the closed actin conformations. Previously, such conformations could be easily visited in response to mechanical perturbations, but the network was always returning from them back to the equilibrium reference state (cf. Fig. 15). In contrast, the expanded EN model of G-actin possesses a new stationary closed state, stable with respect to sufficiently small perturbations. Its origin is clear: if the two mobile subdomains are brought close enough one to another, cross links connecting them are established and, thus, the closed actin conformation becomes locked.

Actually, not one, but two closed metastable states of actin can be discerned in Fig. 16A. A detailed examination of them

reveals that they differ only by local buckling in the flexible region of subdomain S4, involving just a single residue, whereas the global domain configuration is essentially the same in both of them. As can be seen in Fig. 16A, the metastable state is characterized by a closed cleft between subdomains S2 and S4 and a smaller dihedral angle θ, i.e. by a flattening of the molecule.

Summarizing the results of our investigations, we conclude that large-amplitude propeller and scissor motions of the principal mobile domains can take place in the elastic network of G-actin. These motions are generic and the protein responds by them when random globally distributed perturbations are applied. Moreover, we find that, in the expanded version of the EN model, the protein can also be found in the closed stationary conformation which represents its new metastable state. A transition from the equilibrium reference conformation to this metastable state can be induced by applying appropriate perturbations to the network nodes.

4.3 RESPONSES TO PERTURBATIONS IN THE NUCLEOTIDE-BINDING POCKET

When nucleotides (ATP or ADP) are bound to actin, this leads to local mechanical perturbations in the NBP. This pocket is located at the bottom of the cleft separating subdomains S2 and S4 (see Fig. 13). It includes a number of residues which are identified below. In the second part of our study, domain motions induced by application of static forces to individual residues in the NBP region were systematically probed.

Our attention was focused on the perturbations corresponding to the transition from the ADP- to the ATP-bound states of G-actin. The nucleotide-free state is less relevant in the context of actin polymerization and it was not analyzed here. As the reference conformation, the ADP-bound state (PDB ID: 1J6Z) was always taken. When ATP is instead bound, this means that the phosphate P_i is additionally present in the pocket. Hence, only the residues in the neighborhood of phosphate should be directly affected. They are residues 12-16 in the S-loop, residues 71-75 (with the methylated histidine at the position 73) in the H-loop, residues 155-160 in the G-loop, and residue 301 in the subdomain S3.

Our analysis was performed similar to the previous investigation for myosin-V [46]. To probe the responses, static forces

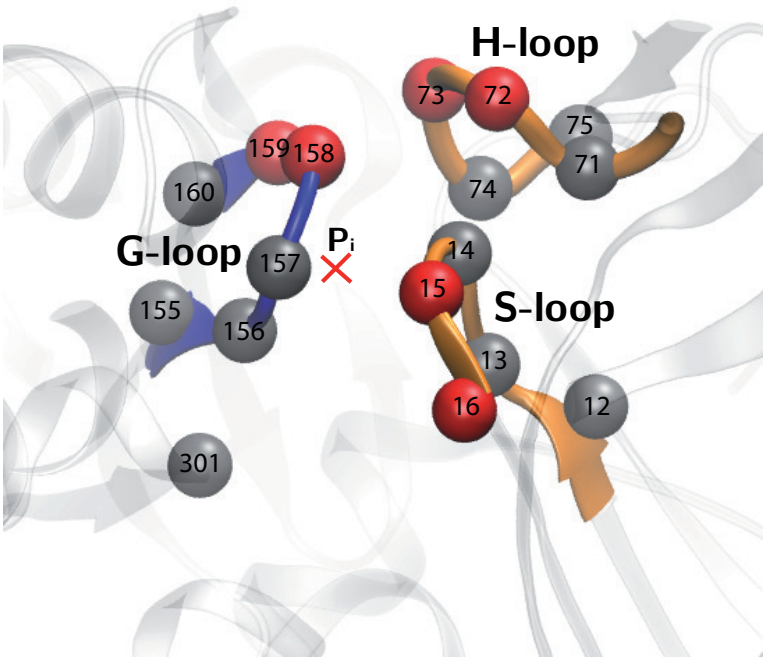

Figure 17: Residues in the neighborhood of the phosphate P_i (red cross) which belong to the three sensory loops G, H and S inside the NBP. Red beads indicate the sensitive residues.

with randomly generated orientations and a fixed magnitude were applied to an individual residue in the chosen set, equations of motion (3.3) were integrated and pair distances between the subdomains, as well as the dihedral angle, were determined in the new stationary state.

To probe mechanical sensitivity of each residue, 200 simulations have been performed for each probed residue. In each of these simulations, a static force with randomly generated orientations and the magnitude $f = 4$Å was generated and the subdomain distances L_{13}, L_{24} and the dihedral angle θ were determined in the resulting stationary state. For each residue the maximum response over the ensemble of 200 realizations was taken to characterize the sensitivity of this particular residue with respect to a certain distance or the dihedral angle.

The results of the sensitivity analysis are presented in Table 1. As we see, the maximal induced changes of the distance L_{13} between subdomains S1 and S3 were always small and not essential. In contrast, both the distance L_{24} and the dihedral angle θ could change substantially when perturbations to cer-

Table 1: Sensitivity of selected residues in the NBP region.

Residue ID	$\Delta\theta$	$\Delta L_{13}/L_{13}^{(0)}$	$\Delta L_{24}/L_{23}^{(0)}$
12	4.3	0.012	0.09
13	5.2	0.017	0.10
14	4.3	0.018	0.11
15	8.0	0.019	0.15
16	10.0	0.016	0.15
71	5.1	0.016	0.08
72	7.8	0.021	0.13
73	7.9	0.026	0.14
74	2.3	0.020	0.10
75	4.6	0.027	0.09
155	5.2	0.014	0.08
156	3.8	0.016	0.09
157	3.8	0.017	0.12
158	6.9	0.020	0.13
159	8.4	0.018	0.11
160	6.7	0.018	0.10
301	5.9	0.014	0.05

tain residues were applied. According to Table 1, the sensitive residues are 15, 16, 72, 73, 158 and 159. Applying forces of magnitude $f = 4$Å to such residues, dihedral angle changes of more than 6.9 degrees and relative domain distance L_{24} changes of more than 11% could be induced. The sensitive residues are additionally displayed in Fig. 17. Note that pairs of sensitive residues are located within each of the three important loops S, H and G.

In the above sensitivity analysis, the original EN model was employed. As we have shown in the previous section, this model can be, however, expanded by including a set of breakable links which become effective when subdomains S2 and S4 come close one to another. Domain motion responses to the application of forces to sensitive residues in the NBP region have been further analyzed in the framework of the expanded EN model.

For the detailed analysis, only one sensitive residue in each of the three loops was chosen. Similar behavior could be expected if its neighbor in the same loop was instead selected. Thus, we focused on the responses induced by application of perturbations to the group of three residues: 16 (in G-loop), 73

(in H-loop) and 159 (in G-loop). Static forces were applied, at the same time, to all three residues in the group. The magnitude of each force was randomly chosen between 0 and 2Å and its orientation was random. For every choice of forces, evolution equations (3.3) for the expanded EN model were integrated until a stationary state was reached. After that, the forces were lifted and the relaxation process was followed by integrating the same equations. The results are displayed for 100 different random perturbations in Fig. 16B.

Comparing Figs. 16A and 16B, it can be noticed that, although the forces were applied to only three NBP residues, essentially the same domain responses as for the application of globally distributed perturbations could be produced. The minor metastable states in Fig. 15, corresponding to single-residue buckling in the highly flexible region of subdomain S4 were absent because forces in that region were not applied. As we see, perturbations of the three sensitive residues already led to characteristic propeller- and scissor-like motions of the inner and outer domains. Furthermore, such local perturbations were sufficient to induce a transition to the metastable closed state of G-actin.

Thus, a small number of sensitive residues lying in the NBP region and belonging to three different loops could be identified. Applying appropriate static perturbations to a group of three such residues, each from a different group, a transition from the open to the closed state of G-actin could be reproduced. Remarkably, local deformations in the NBP region were able to spread over the elastic network and become transformed into large-amplitude global motions of mobile domains.

4.4 LIGAND-INDUCED CONFORMATIONAL CHANGES

Since EN models are coarse-grained and entire residues are replaced by point-like particles, the detailed atomic structure of ligands (ATP or ADP) cannot be resolved in this approach. In this section, the ligands are treated by picturing them as single particles. As it turns out, even this greatly simplified phenomenological description allows us to understand some important aspects of ligand-induced conformational changes.

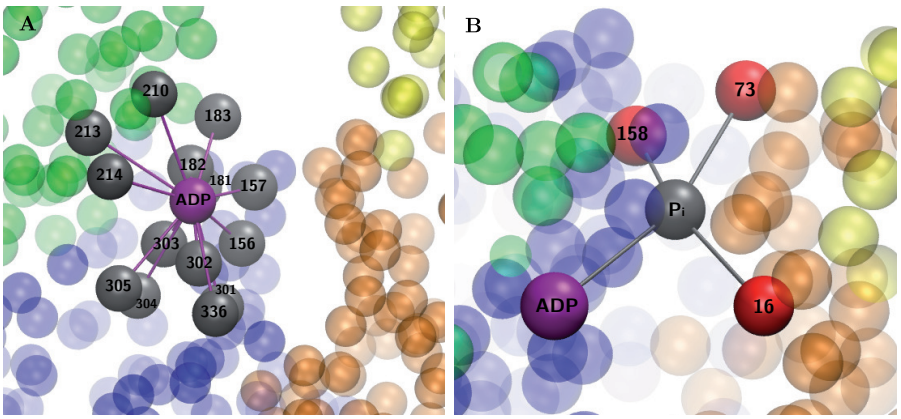

Figure 18: Simple modeling of ligands. (A) The ADP is modeled as an additional node (purple bead) added to the elastic network. It is connected to all its neighbors (grey beads) by elastic links. (B) The ATP is modeled as a dimer consisting of ADP (purple bead) and P_i (grey bead), connected by an elastic link. The ADP is elastically connected to its neighbors and the phosphate is elastically linked to the three sensitive nodes (red beads).

4.4.1 *Ligand Model*

The structure of G-actin with ADP is experimentally known and it was already used by us to construct its elastic network. Below, ADP is explicitly included into the EN description. We treat it as a single particle and put this particle into the equilibrium $C1'$ position, connecting it by elastic links to all residues within the cutoff distance l_0 (see Fig. 18A). The natural lengths of the links are chosen equal to the equilibrium distances between $C1'$ and the respective residues. Hence, by construction, the introduction of such a particle does not change the equilibrium conformation of the protein network. Because the particle is only connected to one of the subdomains (i.e. to S1), its introduction does not also significantly affect the dynamics of the mobile domains. The equilibrium state of the elastic-network of G-actin with the additional particle, modeling ADP, is shown in Fig. 19A.

When an ATP molecule is bound to actin, we model it as a dimer consisting of two particles (Fig. 18B). The first of them corresponds to the ADP part of ATP and the second of them imitates the P_i. The first particle is at the same position where ADP was located in the equilibrium conformation of G-actin. The second particle is placed in the center of mass of the residues

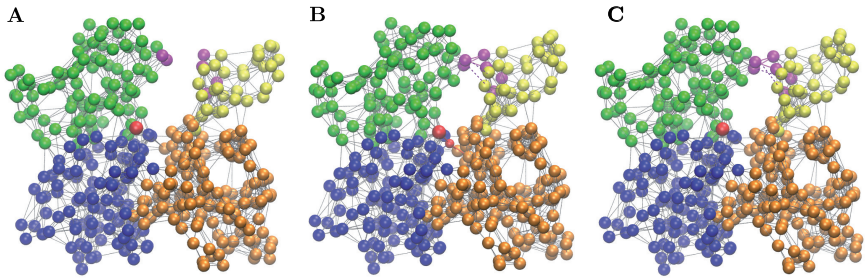

Figure 19: Snapshots of ligand-induced conformational motions. Additional bonds (magenta) are marked solid or dashed lines if they are established or broken, respectively. The ligand is colored red. (A) Equilibrium conformation of G-actin with ADP bound. (B) Model of the ATP-bound state. A transition to the closed conformation is observed. (C) In the closed state, the P_i is removed. The elastic network stays in a metastable closed conformation.

16, 73 and 159, and the ADP. It is connected by elastic links to these four particles (see Ch. 3 for the detailed description).

In contrast to ADP, residing entirely on one of the mobile domains, the phosphate interacts with the residues from different mobile domains (cf. Fig. 17) and, thus, its arrival may induce relative domain motions. Both the X-ray diffraction experiments [126] andMD simulations [128] reveal that, in the presence of ATP, the nucleotide binding pocket becomes contracted. To approximately account for this effect, we assume that the natural lengths of the elastic links, which connect the P_i ligand particle to its neighbors, are shorter than the distances between them and the P_i ligand when it is introduced. Namely, the natural lengths of the elastic links, connecting P_i to residues 16, 73 and 159, are chosen to be equal to 20% of the distances between these residues and the P_i position (i.e., the center of mass of these three residues) in the reference state which corresponds to the equilibrium conformation of G-actin with ADP bound. Thus, these links are initially stretched; they tend to contract the nucleotide-binding region.

Binding of the ATP, imitated in our simple phenomenological model through the introduction of an additional P_i ligand, leads to a shrinking of the NBP which translates into conformational motions of the inner and outer domains. The two do-

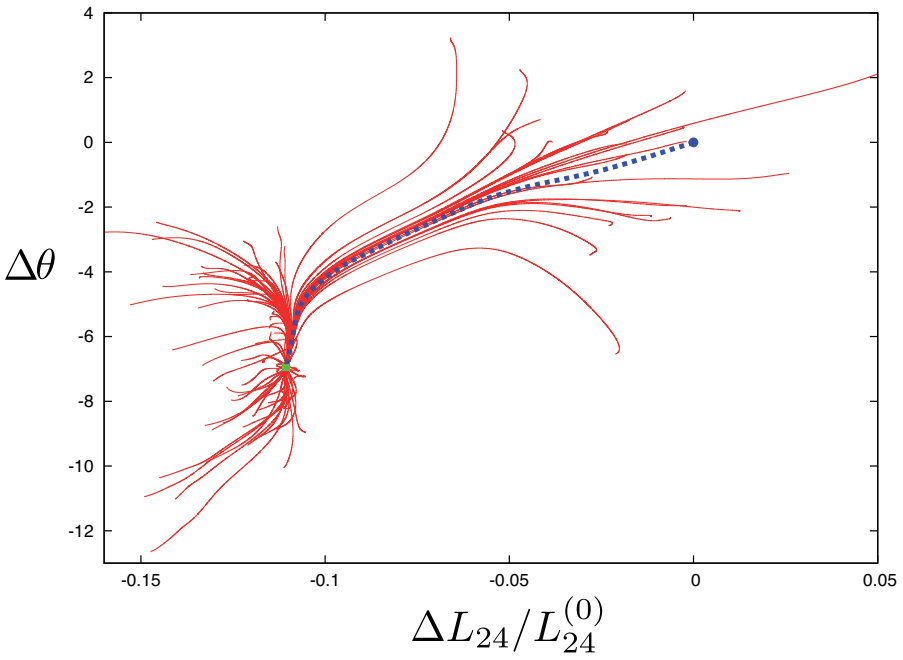

Figure 20: The pattern of relaxation trajectories for the ligand-network complex. The blue trajectory shows relaxation starting from the open equilibrium conformation of G-actin without the ligand. Other start from the perturbed conformations which were obtained by applying random static forces to the three sensitive residues in the NBP region. The open conformation does not correspond to a stationary state of the complex and all trajectories converge to the new equilibrium closed state indicated by the green dot.

mains approach one another, so that within the expanded EN model the additional links connecting them become effectively established and they lock the closed conformation of the protein. This process is illustrated in the first part of the supplementary Movie S3. The final closed conformation of G-actin, stabilized by binding of ATP, is displayed in Fig. 19B.

The hydrolysis reaction and the release of phosphate are roughly imitated in our model by cutting all links which connect the P_i ligand to its three neighbors and the ADP and by removing this particle from the pocket. When this takes place, the actin is in its closed conformation shown in Fig. 19B. The removal of P_i changes the interactions within the NBP and, as we observe in our numerical simulations (the second part of Movie S3), leads to a certain opening of the cleft between the two mobile domains. However, in absence of thermal fluctuations (see

below), the additional links between the two domains then do not break and, after the phosphate release, the actin is found in its metastable closed state (Fig. 19C).

Binding of the artificial ligand leads to a new, unique equilibrium position. 100 relaxation trajectories in the presence of the ligand are shown in Fig. 20. Initial deformations were prepared by applying static external forces with random directions and an amplitude drawn from the interval [0,2Å] to the three sensitive residues in the NBP. Starting from the equilibrium conformation of G-actin, the equations of motions (3.3) were integrated in the presence of the ligand until a stationary state was reached. Additionally, Fig. 20 shows the relaxation trajectory which starts from the original equilibrium state of G-actin in the absence of a ligand. As revealed by Fig. 20, binding of the ligand makes the open conformation unstable and stabilizes the closed actin conformation.

It should be noted that the choice of the interaction parameters still remained to some extent arbitrary. Indeed, it was also possible to choose other values of the lengths r_{eq} or to make such lengths dependent on a particular pair of residues. Moreover, the interaction strength D could also be somewhat varied. We have repeated some simulations with a smaller interaction strength of $D = 0.5\text{Å}^2$. In such simulations, we have found that the closed conformations could still be often visited as a result of perturbations, but the stationary closed conformation did not exist. When the ligand was introduced, the open conformation became unstable and the closed stable conformation emerged also in this case. Thus, the ligand-induced stabilization of the closed conformation of G-actin actin is a robust effect, which is not sensitive to possible parameter variations for the breakable links. The exact structural details of the closed conformational state may be sensitive to the specific choice of the parameters. In absence of direct experimental data, we have not however tried to optimize this choice.

So far, effects of thermal fluctuations have been excluded from our analysis. Such effects may become, however, important if metastable states are possible. If thermal fluctuations are strong enough, they can induce transitions between stable and metastable states, so that all of them can be visited by the system.

4.4.2 *Effects of Thermal Fluctuations*

The effects of thermal fluctuations can be taken into account by introducing additional random forces with appropriate intensities into the equations of motions. Such thermal fluctuations are described by equations (3.14). The noise parameter $\sigma = 2$Å has been chosen. We have checked that, with this choice of parameter, the experimentally known B-factors are reproduced by the orders of magnitude. Integrating such stochastic differential equations over sufficiently long time, data was gathered and statistical distributions for various order parameters in the presence of different ligands (ADP or ATP) were constructed.

Figure 21 displays statistical distributions of the distance L_{24} between the centers of mass of the mobile domains S2 and S4 in the ADP- or ATP-bound states, as described by our approximate model. In the ADP-bound state (black curve), the protein prefers to stay in the open conformation, with the distance between the domains approximately equal to 31.0Å. The closed conformation, representing a metastable state, is however also occasionally visited, as evidenced by the presence of a shoulder in the statistical distribution of the interdomain distances. Binding of ATP stabilizes the closed conformation, leading to the distance distribution shown by the red curve in Fig. 21. In the presence of ATP, spontaneous transitions to the open conformation are not possible (or very rare), as evidenced by the presence of a clear distribution maximum at the distance $L_{24} = 27.5$Å in this case. The width of the distance distributions characterizes the stiffness of the monomer. With ATP bound, the variance of the distance L_{24} is reduced to 0.45Å^2, as compared to the variance of 1.44Å^2 in the ADP-bound state. Thus, the presence of ATP in the NBP stiffens the monomer considerably.

Already the rough modeling employed in this section reveals some important effects of the nucleotides. Binding of ATP can directly lead to flattening of the protein and closing of the cleft between its inner and outer domains. While the ATP-free actin shows the tendency to switch between its two equilibrium states, the ligand can stabilize the closed conformation of actin and, furthermore, stiffen the macromolecule. Note that the structural details of the ligand-induced closed conformational state may depend on the parameters of interactions between the ligand particle and the NBP residues. Moreover, the dimer model of ATP used in the above simulations represents only a simple approximation for the actual ATP molecule. Therefore,

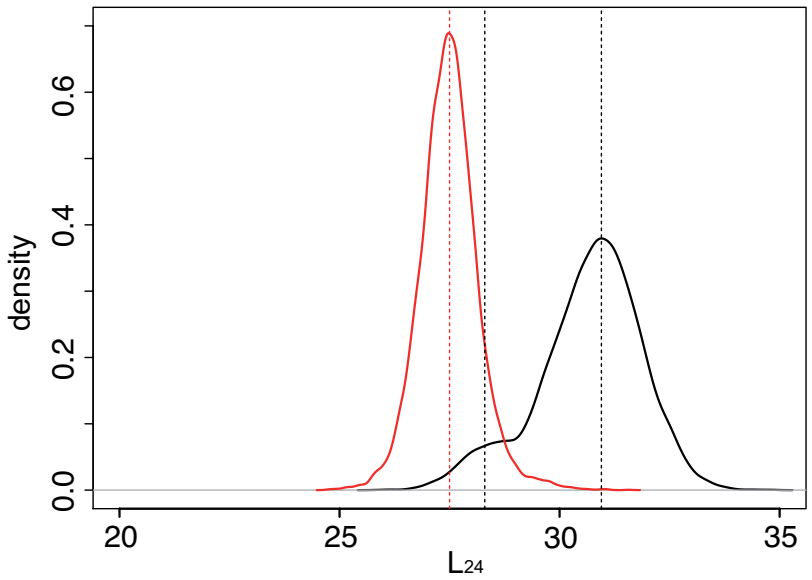

Figure 21: Statistical distributions of interdomain distance L_{24} in the presence of ADP (black) or ATP (red) ligands.

the results of our numerical investigations including the ligand should be viewed as only providing a demonstration that a transition to stable closed conformation can be induced by ATP binding. This model predictions need to be further confirmed in the experiments and in special MD simulations.

4.5 DISCUSSION

In our study, the attention was focused on purely mechanical aspects of actin dynamics. With this purpose, a greatly simplified dynamical model of this molecule was considered where all residues, independent of their chemical differences, were treated as identical particles connected by identical elastic links. In addition to the elastic links, the mechanical model also included a small number of breakable links, which become established when pairs of residues come sufficiently close and break down at large separations. The information about the chemical structure of G-actin was effectively encoded only in the architecture of the elastic network, determined by the experimentally known equilibrium conformation of the molecule.

Remarkably, already this greatly simplified model allowed us to understand many aspects of the intramolecular conforma-

tional motions in actin monomers. The model shows that the mobile inner and outer domains of actin are able to perform large-amplitude propeller twist and scissor-like motions, earlier revealed by the normal-mode analysis for small deviations from the equilibrium state [162]. While performing such motions, two upper subdomains (S2 and S4) can come so close one to another that attractive interactions between pair of residues from the opposite domains become present. Such emergent interactions lock the actin molecule in its closed conformation and thus lead to the formation of a metastable state.

We have found that, similar to myosin [46, 80, 123, 122], G-actin essentially behaves as a strain sensor, responding by well-defined domain motions to mechanical perturbations. In our study of actin, we identified a number of sensitive residues, such that small perturbations of these residues were translated into large-amplitude motions. Our investigations reveal three pairs of sensitive residues, belonging to different domain loops inside the NBP. Application of small perturbations to these particular residues can result in large-amplitude domain motions and in the transition to the metastable closed state. As we see, the internal mechanics of an actin macromolecule is highly organized and efficient communication between the NBP region and the mobile domains is present.

To demonstrate that ligand (i.e. ATP) binding can indeed induce large-scale conformational changes, we have imitated the ligand by a dimer; one of the particles, corresponding to phosphate, has attractive interactions with the sensitive residues inside the NBP. Previously, a similar ligand description was employed when cyclic operation of the molecular motor hepatitis C virus helicase was analyzed [53]. We have found that, under an appropriate choice of the interaction parameters, binding of ATP can induce a transition to the closed conformation and stabilize this metastable state.

In the hierarchy of coarse-grained models proposed to describe actin monomers and filaments (see, e.g., review [178]), the employed description is most closely resolving the structure of the individual proteins. Nonetheless, because of the simplifications involved in the formulation of the EN model and since some of the parameters, particularly referring to the interactions with ligands, remained arbitrary in the present study, quantitative agreement between the predictions based on the present coarse-grained description and the experimental data or the data of all-atom MD simulations should not be expected.

Nonetheless, the results of our approximate analysis can be used for better understanding of intramolecular dynamics of G-actin. They may provide helpful guidelines for further experimental investigations and act as motivation for MD studies.

The ATP-induced transition to the closed conformation of actin may play an important role in the explanation why, in the presence of ATP, the growth of actin filaments is strongly accelerated. The closed conformation of G-actin, stabilized under ATP binding, is not identical to that of the filamentous F-actin. However, in both of these conformations the cleft separating the upper mobile subdomains S2 and S4 is strongly reduced, so that a better fit and higher affinity to the actin filament may result. Another effect of binding of ATP observed in our model is the increased stiffness compared to the ADP state (see Fig. 20). This is in agreement with the experimental data showing that the presence of ATP-bound protomers leads to an increased stiffness of the filaments [82].

In recent experiments [96], metastable conformational states of single actin protomers in the filament could be already detected. The distribution of these states was sensitive to addition of myosin. Actin binding proteins (ABPs), including myosin, play crucial roles in the cell [132]. In the framework of our approach, interactions with actin binding protein (ABP)s can be interpreted as mechanical perturbations and can also be analyzed in future studies. It should also be possible to perform FRET measurements in single G-actin molecules under controlled conditions, thus elucidating conformational states involved in polymerization (G-F transitions), and specifically, the effects of ligands. The results of such experiments can be compared with the predictions based on the elastic-network models.

5 MYOSIN-V AS A MECHANICAL SENSOR

Even more than 50 years after Huxley proposed the first mechanism for muscle myosin force generation [76, 77], the details of how the molecular motor functions remain unclear. Is the chemical reaction with ATP used to perform mechanical work directly in form of a lever-arm swing or does it regulate a rectification of thermal noise in order to perform work?

In this chapter, we investigate the internal dynamics of a single myosin and identify ways in which myosin may control its machine cycle or bias thermal fluctuations. According to experiments [80, 122, 123], the molecular-motor myosin behaves like a strain sensor, exhibiting different functional responses when loads in opposite directions are applied to its tail. Within an EN model, we explore the sensitivity of the protein to the forces acting on the tail and find, in agreement with experiments, that such forces invoke conformational changes that should affect filament binding and ADP release. Furthermore, conformational responses of myosin to the application of forces to individual residues in its principal functional regions are systematically investigated and a detailed sensitivity map of myosin-V is thus obtained. The results suggest that the strain-sensor behavior is involved in the intrinsic operation of this molecular motor.

5.1 MYOSIN-V MODEL

The study is based on the elastic-network modeling of conformational dynamics in the presence of external forces. The EN model of myosin-V heavy chain is constructed by using as a reference state its post-rigor equilibrium conformation with Mg·ADP·BeFx, an ATP-analog, as yielded by X-ray diffraction analysis (Protein Data Bank ID: 1W7J, chain A) [31]. Myosin in this state does not attach strongly to the filament. The myosin-V experimental data and the corresponding EN with a cutoff of 10Å are shown in Fig. 22.

The entire elastic network of myosin-V includes 752 particles. For probing of mechanical responses, a subset of 82 particles

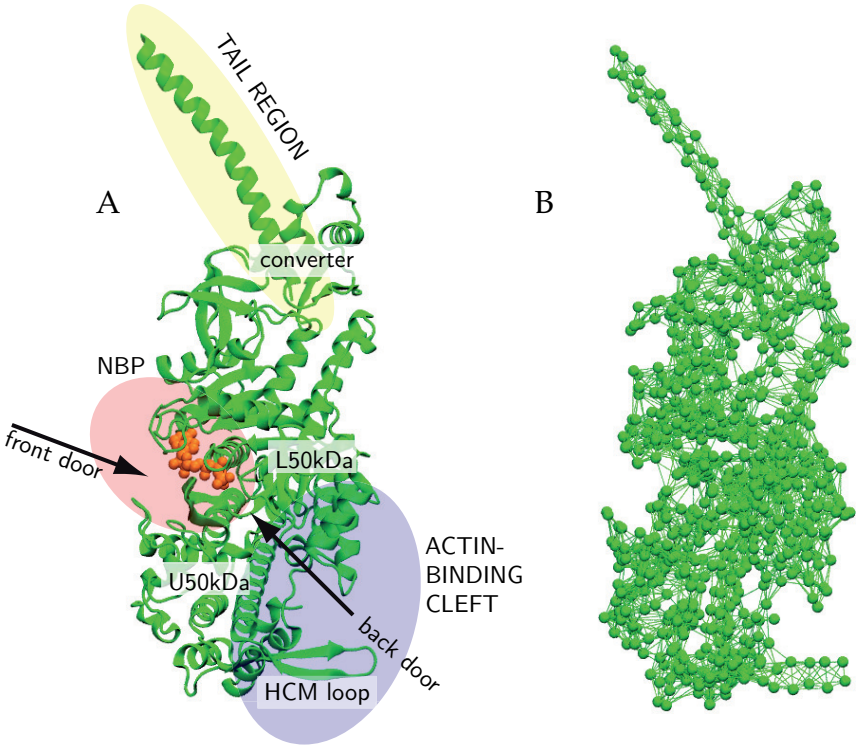

Figure 22: Myosin-V (A) and its elastic network (B). In panel (a), three principal functional regions of the protein are schematically shown; the ATP-analog is also displayed (orange). Moreover, some important structural elements, such as the front and the back doors and the HCM loop, are also indicated here. In panel (B), each particle corresponds to a residue, the links represent elastic interactions between them.

was selected (see Fig. 23A). These residues are found in the three important functional regions, the tail, the NBP and the actin-binding cleft. The residue 792 was located in the tail region and used to apply forces to the tail. The second group of residues from the NBP region is displayed in the first column in Table 3 in the Appendix. All residues in this group are ATP neighbors, i.e. they are adjacent to the ATP position. The third group (first column in Table 4 in the Appendix) included the residues located on the surface of the actin-binding cleft.

Although integration of equations (3.3) gave positions of all particles in the state with a force applied, this information was too detailed and to quantify induced deformations some measures (or "order parameters", cf. [127]) were needed. In our analysis, we chose a set of 10 particles as the labels and moni-

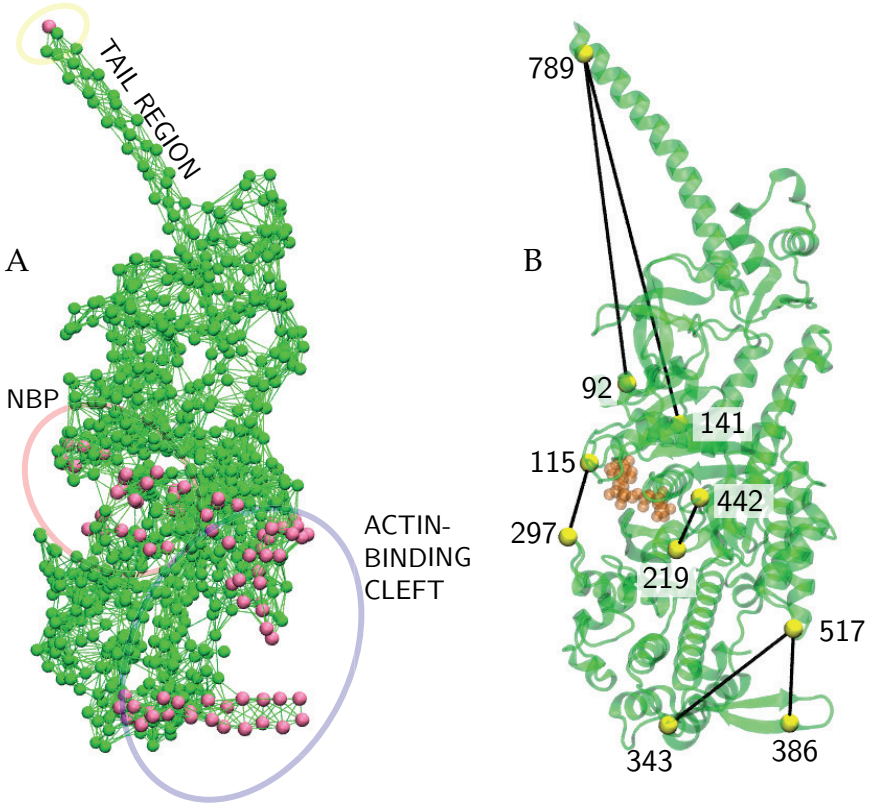

Figure 23: (A) The set of residues probed by application of static forces and (B) the labels and the distances between them, used to monitor conformational changes.

tored pair distances between them. The labels and the selected distances are shown in Fig. 23B.

The first three labels, corresponding to residues 789, 141, and 92, were selected to specify motion of the tail. Here, the first label is in the tail and the other two are attached to stiff parts of the protein.

Further, four labels were used to measure conformational changes in the NBP region. The labels, corresponding to residue 115 in the N-terminal subdomain and residue 297 in the upper 50kDa subdomain, were chosen to characterize the opening of the front door. They are in contact with the adenylate ring, gating the front door through which ATP enters and ADP leaves the reaction site [71]. The back-door opening and closing were characterized by the distance between residues 219 and 442 in switches 1 and 2 in the upper 50kDa subdomain, respectively. These two amino acids form a salt bridge which hinders the phosphate from leaving the NBP after hydrolysis [21, 100].

The last three residues belonged to the actin-binding region. Distances between residue 517 in the lower 50kDa and residues 343 and 386 in the upper 50kDa subdomain were monitored. These labels lie in the actin-binding site and characterize opening and closing of the cleft, as well as the motion of the HCM loop.

To examine responses of the network, static forces were applied to one of the chosen particles and, after integration of equations (3.3), changes of the distances between the labels with respect to their equilibrium values were determined. In such simulations, the immobilization procedure presented in Ch. 3 has always been used and, hence, only internal dynamics of the protein has been measured.

5.2 FORCES ACTING ON THE TAIL

In this section, we intend to computationally reproduce the experiments [80, 122, 123] where external forces were acting on the myosin tail. We apply forces to one residue in the tail and monitor the conformational responses in the nucleotide-binding pocket and in the actin-binding cleft, depending on the force orientation and amplitude.

Experimentally, forward and backward force directions are defined with respect to the direction of the proccessive motion of myosin along the actin filament. To determine filament orientation with respect to myosin in the considered model, a special analysis had to be performed. First, we have built a filament by using the structural data for F-actin (PDB ID: 2ZWH) [121]. Then, we needed to determine how the filament was positioned with respect to myosin in the actin-myosin complex. To do this, the results of the recent guided MD simulations [105], where several sites for binding of myosin to actin were identified, were used. By keeping the filament stiff, we anchored it to the myosin network by elastic links at these sites. After that, relaxation in the actomyosin system was followed by integration of dynamical equations and the final equilibrium configuration of the complex was determined. Thus, the relative filament direction, used in subsequent numerical investigations, could be identified. A more detailed description is given in the Appendix.

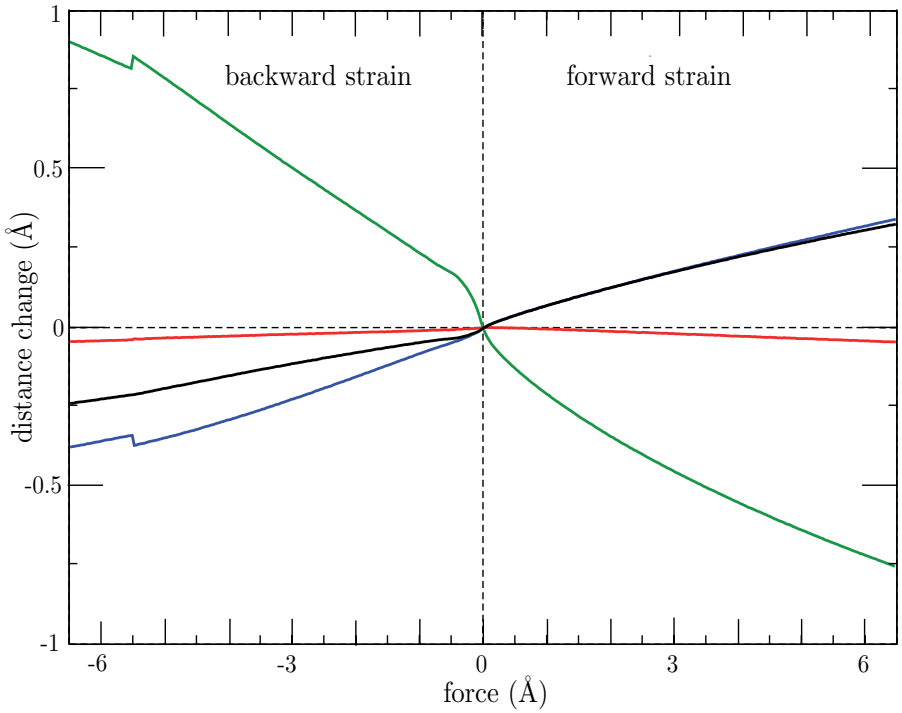

Figure 24: Responses of pair distances between the labels (black) 115 and 297, (red) 219 and 442, (blue) 343 and 517, and (green) 386 and 517, as functions of the amplitude of the force applied to the tail. Small abrupt changes observed at large negative forces are due to local buckling effects.

In the simulations, external forces have been always applied to the residue 792. Since the tail is a relatively stiff structure, the exact position of the force application point was not important. The forces were parallel to the filament direction, which has been previously identified. Their amplitudes were varied from 0 to 6.5Å and both forward and backward directions have been considered. For each force, equations (3.3) were numerically integrated until a stationary protein configuration was achieved.

The responses of the elastic network are displayed in Fig. 24. As we see, changes in the nucleotide-binding pocket are induced. The distance between residues 115 and 297, defining the opening of the front door, grows under forward strain and decreases if backward forces are applied. However, the change of the pair distance between residues 219 and 442, characterizing the salt bridge, remains smaller than 0.1Å. Hence, we conclude that, while the front door configuration is controlled by the force acting on the tail, the responses in the back door region of the NBP are negligible.

As evidenced by Fig. 24, external forces furthermore lead to conformational changes in the actin-binding region. When backward strain is applied, the actin cleft, characterized by the distance between residues 343 and 517, closes. At the same time, the distance between residues 386 and 517 increases and, thus, the HCM loop moves away from the lower 50kDa domain. The opposite conformational changes are observed when forward strain is applied.

The significance of the observed responses becomes clear if the operation mode of myosin is taken into account. ADP and P_i, the hydrolysis products, are exiting the nucleotide pocket in different directions, through the front and the back door, respectively. Therefore, closing of the front door, which, as we have found, is induced by backward strains, would hinder the ADP release and thus enhance the ADP affinity. This agrees with the experiments [122, 123]. In these experiments by Oguchi *et al.* the dependence of the ADP affinity on the force direction has been observed. Movie S1 in the Supporting Material of Ref. [46] displays the dynamical response of the network to an external force applied in the forward direction. The induced tail motion and the pronounced changes in the actin binding cleft region are clearly seen there. Changes in the front door, however, are weaker and less apparent.

The effects of strains on binding to the actin filament have been investigated in the experiments by Iwaki *et al.* [80]. They showed that backward strain increases the probability that myosin binds strongly to the filament. The original interpretation of these results in Ref. [80] was that such forces induce opening of the back door. This, in turn, would enhance P_i release that should precede strong binding. Thus, an indirect connection between binding affinity and strain to the tail. Our simulations, however, do not reveal any considerable sensitivity of the back door to the forces acting on the tail, so that this original interpretation is not supported. Nonetheless, the experimentally observed behavior can still be understood. For that, the responses induced in the actin binding cleft should be analyzed.

Conformational changes accompanying a transition to strong binding of myosin to the actin filament can de identified by comparing the structures in the post-rigor state with the filament detached and in the nucleotide-free (or rigor) state of the same myosin (PDB ID: 1OE9) [32] which corresponds to the conformation of myosin bound to the filament. Focusing on the changes in the actin binding cleft, one can notice that

the transition from the post-rigor to the rigor state is characterized by shortening of the distance between residues 343 and 517 and, at the same time, by an increase of the distance between the HCM loop and the lower 50kDa domain (characterized by residues 386 and 517). But these are exactly the changes which we found to be induced by the application of backward strain. Hence, the experimental data [80] is explained by conformational changes which are directly invoked in the actin binding cleft, rather than being mediated through hypothetical responses in the back-door region of the nucleotide pocket.

5.3 FORCES IN THE NUCLEOTIDE-BINDING POCKET

The nucleotide-binding pocket is an important functional region of myosin. Here, the chemical reaction takes place that fuels the myosin machine cycle. It is known that ATP enters the pocket from the front door and, after the hydrolysis, the ADP product leaves through the same opening. In contrast, the phosphate, representing the second product, leaves the NBP region through the back door. The processes taking place in the NBP affect, in turn, filament binding and tail motions.

Responses to perturbations localized in the NBP have earlier been investigated theoretically by using restrained targeted MD simulations [127], and by means of the normal mode analysis [184]. In these previous studies, it has been demonstrated that global conformational transitions from the nucleotide-free to the ATP-bound states could be reproduced by applying special forces to a group of residues inside the NBP, with the directions chosen to correspond to the experimentally known local changes between the two conformations.

The approach we pursued is different. Our aim was not to reproduce a particular known response, but, instead, to systematically test the global sensitivity of the protein to *arbitrary* forces applied to various single residues in the nucleotide-binding region. In this manner, we aimed to construct a map of the NBP in which residues responsible for particular functional behavior could be identified.

To probe mechanical responses, 27 residues adjacent to the ATP in the considered equilibrium conformation were selected (left column Table 3 and Fig. 23A). For every chosen residue, a series of 200 simulations was performed. In all simulations, the

magnitude of the applied force was the same ($f_0 = 1$ Å), but its orientations were randomly varied. The simulations were always continued until a stationary state was found. After that, changes in the monitored pair distances between the labels in different regions were determined. The induced distance changes were analyzed and, for each pair of labels, the maximum absolute distance change over 200 force orientations was evaluated. Such maximum distance change was then taken as the measure of the protein's sensitivity to forces applied to a particular residue. An example of the relaxation process leading to a new stationary state is shown in Movie S2 in Ref. [45]. Here, forces were applied to residue 115 in the front door and conformational changes, especially in the tail, are clearly visible.

The sensitivities of all 27 residues with respect to different pair distances are summarized in Table 3 in the Appendix and the directions of communication are schematically shown in Fig. 25.

As we have found, applying forces to the residues in the front-door region, a strong effect on the tail is produced (Fig. 25). However, the application of forces to residues near the back door or the P-loop only weakly affects the tail region. Thus, *the tail responds mainly to the perturbations applied at the entrance of the front door*.

Proceeding further, the sensitivity with respect to responses in the actin-binding cleft has been investigated. As we have observed (see Appendix), *the actin-binding region is mainly affected by the application of forces in the back-door region*. When the force is applied to residue 442 in the back door, this produces a strong response in the distance between residues 343 and 517, characterizing the cleft opening. Moreover, application of forces in the back door has a pronounced effect on the HCM loop to which residue 386 belongs. The HCM loop is known to come into contact with actin and may play an important role in myosin-actin interactions [32, 156, 171]. It should however be noted that some sensitivity of the actin-binding cleft to the perturbations in the front door has also been seen.

Thus, we have found that myosin behaves as a strain sensor not only with respect to the forces applied to its tail. The forces acting to some residues within the NBP are also producing well-defined conformational responses, which are functionally important.

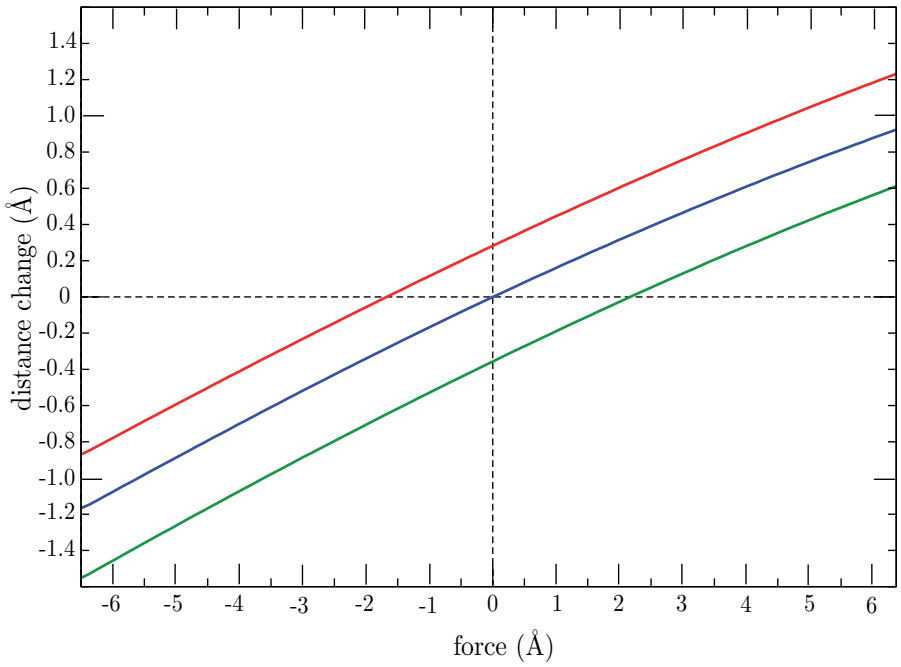

Figure 25: Sensitivity of residues in the NBP region. Directions of communication are indicated by colored arrows. The region of the nucleotide-binding pocket marked by a box is enlarged. Residues most sensitive with respect to the tail motion and to conformational changes in the actin cleft are colored red. The responses induced by the forces applied at the gray colored residues are weaker.

We have furthermore discovered that, in terms of the sensitivity of its residues, the NBP region is clearly divided into a front-door and a back-door domain (enlargement in Fig. 25). On the one hand, a pronounced effect on the actin cleft was observed when forces were applied to residues 219, 220 and 442 in the back-door region. Remarkably, it is exactly the salt bridge between the two sensitive residues 219 and 442 that hinders phosphate release after the hydrolysis. On the other hand, we have seen that the forces applied at the front door were primarily affecting the tail and could induce its motions. We have found that the forces applied to the residues of the P-loop region, lying in the middle between the front and the back doors, do not lead to significant conformational changes either in the tail or in the actin cleft.

Importantly, the response of the actin cleft to perturbations in the NBP can be controlled by the forces applied to the tail. Fig. 26 shows the change of the distance between the residues 343 and 517, characterizing the width of the actin cleft, as dependent on the force applied to residue 442 in the back door. The force was chosen in the direction that maximizes the absolute distance change and its amplitude was varied. Additionally, analogous dependences in the presence of forward and backward strain in the tail are shown in the figure. One can see that backward strain enhances the closing of the actin cleft, whereas forward strain tends to prevent it. Thus, while the forces applied at the tail do not directly affect phosphate release through the back door, they can nonetheless modulate the effects of phosphate release on the opening or closing of the actin cleft, which controls interactions of myosin with the filament.

5.4 FORCES IN THE ACTIN-CLEFT REGION

When myosin binds to an actin filament, this should lead to perturbations localized in the actin-binding cleft region. Such perturbations should have a specific form, determined by the organization of the actin-myosin interface and details of the myosin-actin interactions. As in the previous section, our aim is not to reproduce the responses to a particular local perturbation. Instead, we systematically investigate in this section the sensitivity of the protein to the application of forces with arbitrary orientations to individual residues in the actin-binding cleft region and look how strains in the cleft can affect the tail or the front and back doors.

High-resolution experimental data of myosin bound to the actin filament is currently not available. Based on cryo-EM experiments, models for the actomyosin interface were proposed [71, 73, 105]. Lorenz and Holmes [105] suggested possible electrostatic interactions and hydrogen bonds between myosin-II and actin. Using these results, we have identified a set of 54 residues which may come in contact with the filament (left column Table 4 and Fig. 23A). To probe sensitivities in the actin cleft, 200 independent simulations were performed for each single residue in the set. Forces with strength $f_0 = 1$ Å and randomly chosen orientation were applied to a given residue and

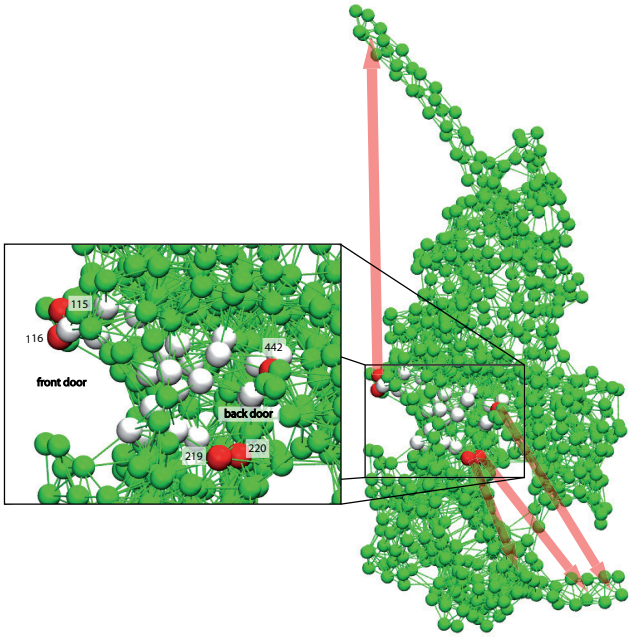

Figure 26: Changes in the distance between residues 343 and 517, characterizing opening of the actin-binding cleft, as functions of the force applied to the residue 442 in the back-door region. The red curve corresponds to the forward force of 5 Å applied to the tail. The green curve is for the force with the same strength applied in the backward direction. The blue curve corresponds to the absence of forces.

integration was continued until the system relaxed to a new equilibrium. After that, changes in the characteristic pair distances between the labels were determined. For each residue and the pair distance, the maximum response over the series of 200 simulations was recorded. The determined sensitivities are shown in Table 4 and systematically analyzed in the Appendix. The results are also schematically represented in Fig. 27 where arrows indicate the principal communication pathways. Strong responses of the tail were induced when forces were applied to the residues in the HCM loop (see, for example, Movie S3 in Ref. [46]). There is also some sensitivity of the tail to perturbations applied in the upper 50 kDa domain (residues 340 to 350). In contrast, the tail is not significantly sensitive to the forces acting in the lower 50 kDa domain. Examining responses

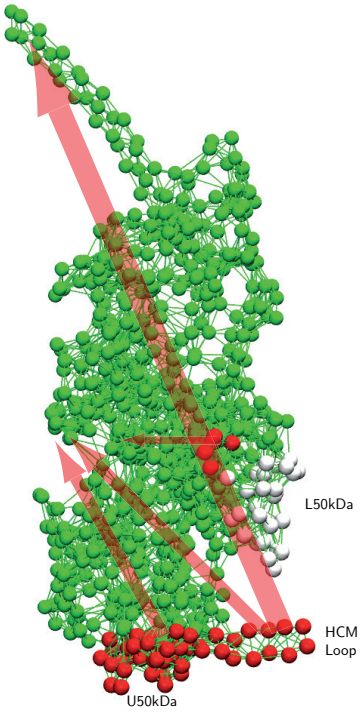

Figure 27: Responses induced by the application of forces to the residues in the actin binding cleft region: (red) residues 377 to 390 in the HCM loop, residues 340 to 350 in the upper 50 kDa subdomain, residues 540 to 544 in the lower 50 kDa subdomain, and (gray) less sensitive residues in the lower 50 kDa subdomain. Arrows schematically indicate the directions and strength of intramolecular communication.

in the NBP region, we observed that the front door is strongly sensitive to the forces applied in the upper 50 kDa domain and the HCM loop. The back door is sensitive to the perturbations acting in the lower 50 kDa domain.

5.5 DISCUSSION

Functional responses of myosin motors to the application of external forces have previously been experimentally investigated. Iwaki *et al.* [80] attached a bead to the tail of a myosin-VI monomer and dragged it along the actin filament in two opposite directions. It was found that the transition of myosin from weak to strong binding to the filament is affected by application

of a dragging force and strongly depends on the force direction. The probability of strong binding increases when forces are applied in the direction opposite to that of the intrinsic processive motion (i.e., the backward direction for this molecular motor). In other experiments, effects of external loads on the ADP release from myosin-V attached to the actin filament were studied [122, 123, 135, 169]. It has been found that the release is hindered when forces are applied in the backward direction, opposite to the direction of processive motion for this myosin [135, 169]. Oguchi *et al.* [122, 123] have measured the magnitudes of the force applied to the tail which are needed to unbind a myosin-V monomer from an actin filament for different force directions and ADP concentrations. These experiments indicated that ADP release is slowed down when a force is applied in the backward direction (see also [94, 144]).

Our study provides a theoretical explanation of these results. We have observed a direct effect of external forces on the front door, through which ADP leaves the protein. When backward strain is applied to the tail, this tends to close the front door and, accordingly, should make the ADP release less probable. Thus, external forces can regulate the ADP affinity through conformational changes in the front-door region. We have not found a direct effect of the strains on the back door, through which the phosphate leaves the protein leading to filament attachment. However, we have observed that strain directly influences the protein conformation in the actin-binding cleft region. Backward strains tend to favor closing of the actin cleft and to generate a movement of the HCM loop away from the lower 50 kDa domain, thus enhancing the effects of phosphate release through the back door (see Fig. 24) and making strong coupling more probable. In this way, an explanation of the experiments [80] is also provided.

The force-dependent release of ADP is important for the operation of the dimeric myosin-V, i.e. for its processive motion along the actin filament [113, 181]. Recent theoretical investigations using a reduced kinetic description of the cycles of the myosin-V dimer suggest that the transition rates of ATP and ADP binding to the leading head need to be load-dependent [14]. Thus, the strain-sensor behavior of myosin-V, revealed in the experiments with the application of external forces to its tail and explained in the present study, should play a profound role in natural functioning of this molecular motor.

Moreover, we have systematically analyzed conformational responses of myosin-V to the application of forces to individual residues in the nucleotide-binding pocket and on the surface of the actin-binding cleft. Thus, a detailed intrinsic sensitivity map of myosin has been constructed. As we have seen, by perturbing specific residues in the front- or back-door regions of the NBP, motions of the tail or opening and closure of the actin cleft can be induced. On the other hand, application of forces to residues in the actin-binding cleft can also invoke tail motions and have effects in the NBP region. In our numerical study, the responses have been induced by external forces. Under natural conditions, however, mechanical perturbations in the NBP and the actin-binding cleft can easily arise as a consequence of ligand binding and reaction events.

Remarkably, both the explanation of the experiments [80, 122, 123, 135, 169] with external loads and the identification of intrinsic communication pathways inside the protein could be already obtained in our study by using a greatly simplified elastic-network model. The model is stripped of chemical details, so that a protein is treated as a purely mechanical object, i.e. a network of particles connected by elastic strings. It turns out that generic elastic responses of such a network are sufficient to understand intramolecular communication responsible for the coordination of processes in different functional parts of the molecular motor. Our investigations have been performed in the framework of the full nonlinear elastic model, without the linearization and transition to a normal-mode description. We have checked (see Appendix) that nonlinear effects are indeed essential for the considered phenomena.

In the recent publication by Zheng [183], full nonlinear EN equations have been used and coordination between conformational changes in two coupled units in the myosin dimer, resulting from mechanical interactions through the common tail, have been considered. The analysis has however only been performed along a particular conformational pathway, connecting two experimentally known myosin states, and the responses have been considered at the level of entire protein domains, rather than for individual residues. In contrast, we have systematically analyzed the responses of the myosin molecule to the application of arbitrary forces with various directions to a large number of individual residues located in three principal functional regions. We have monitored how and to what ex-

tent such forces affected individual residues in other functional residues.

Our results suggest that conformational changes, induced in myosin-V by ATP binding, the hydrolysis reaction and the products release, should not be very sensitive to chemical details of the respective microscopic processes. Such changes can be invoked, as we have shown, by the application of forces to the network nodes corresponding to specific residues in the NBP region. We have also found that the tail and the NBP are sensitive to mechanical perturbations of single residues in the actin-binding cleft region, which may naturally arise when binding of myosin-V to the actin filament takes place. It should be noted that similar behavior, based on elastic responses of the macromolecule to mechanical perturbations in the ATP binding pocket, has recently been reported [53] for a different molecular motor, the hepatitis C virus helicase; within the EN model the entire operation cycle of this motor could be reproduced by applying forces to only a few residues.

Based on such observations, we conjecture that the strain-sensor behavior and the intramolecular communication relying on elastic deformations should be a general property of protein motors, essentially involved in the organization of their functional activity. It would be interesting to test this suggestion in further, specially designed experiments. In such experiments, forces can be applied to single selected residues (or small groups of them) and conformational responses can be monitored by using atomic force microscopy (AFM) or FRET techniques. Such kinds of experiments have been, e.g., performed to study partial unfolding of single proteins [38, 50]. Moreover, once specific residues, responsible for important conformational responses, have been identified, one can try to modify them by using protein engineering methods and thus verify their functional roles.

6 INTERACTIONS WITH THE FILAMENT

Many proteins bind to the actin filament. Two prominent examples are the molecular motor myosin and G-actin monomers. Myosin uses the filaments as tracks and moves processively along such actin polymers and actin monomers form the actual filament in a dynamic process called treadmilling. How is binding to the filament organized?

In this chapter, we model binding to the filament. At large distances, only long-ranged electrostatic interactions are important. If residues, however, come close to each other, short-ranged interactions become stronger and control the attachment to the filament. Apart from soft sphere potentials preventing protrusion of residues, strong bonds between specific binding sites form and lead to a stable attachment of ABPs. Such bonds may be hydrogen bonds, salt bridges or other non covalent bonds. Within our model, they are described by Lennard-Jones potentials. Secondly, we investigate the influence of the nucleotide ATP on the attachment of actin monomers at the growing end of the filament. We show that the ligand-induced conformational changes of the actin monomer, as modeled earlier in Chapter 3, indeed increase the binding affinity of actin to the filament. Specifically, binding of ATP stabilizes a conformation suitable to facilitate docking of free actin to the filament. To this end, a toy model is constructed based on which the effects of ligand binding can be directly quantified with respect to the filament.

6.1 ACTIN MONOMER AND FILAMENT MODELS

Monomeric actin is constructed as an elastic network based on specific conformational states. As already mentioned in Chapter 4, the protein is described in terms of its four subdomains (S1, residues 1–32, 70–144 and 338–372; S2, residues 33–69; S3, residues 145–180 and 270–337; S4, residues 181–269) [84]. In our investigation, two distinct states are used to model actin: globular G-actin and filamentous F-actin.

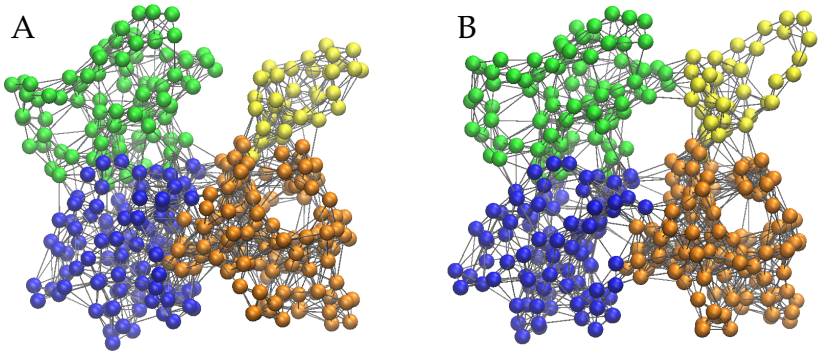

Figure 28: Elastic networks of two actin states colored according to its subdomains S1 (orange), S2 (yellow), S3 (blue) and S4 (green): (A) G-actin and (B) F-actin

In the absence of ATP, G-actins do not polymerize. They are characterized by a large dihedral angle and an open cleft between inner and outer domains. Moreover, in this structural state actin is known to have a low attachment probability at the growing end of the filament [132]. It is modeled using structural data of uncomplexed G-actin in the ADP-bound state (PDB ID: 1J6Z), which has been obtained via X-ray diffraction techniques [126]. The elastic network of G-actin is displayed in Fig. 28A.

Inside the filament, the actin monomer exhibits a different conformation. In this state, the monomer is called F-actin and differs considerably from the G-actin state. Most important conformational changes are a characteristic flattening and a closing of the cleft between the two mobile domains. We model this state using the experimental data of F-actin within the filament (PDB ID: 3MFP) [56]. The high-resolution data has been obtained by averaging over many cryo-electron microscopy images. The elastic network corresponding to this conformation is shown in Fig. 28B.

A further striking difference between the two structures in Fig. 28 is the conformation of the subdomain S2. It is here, where the highly mobile DNase-I binding loop (DB loop) is located. This loop is very flexible and in experimental monomer structures; it is either found in a stable α-helical conformation or in a disordered state. Up to now, spectroscopic methods have not been able to resolve the structure in a satisfying way.

In the G-actin experimental data, an α-helical conformation is found. This conformation, however, is thought to be an artifact of the crystallization methods used [150]. In F-actin, one sees

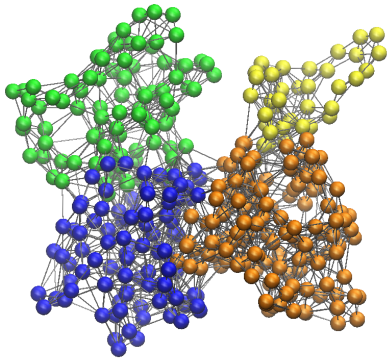

Figure 29: EN models of G-actin with F-actin conformation of DB loop colored according to its subdomains S1 (orange), S2 (yellow), S3 (blue) and S4 (green.

an open loop conformation. Note that the data for the F-actin monomer is obtained inside the filament and, hence, neighbors may stabilize the open loop conformation. The exact conformation of the DB loop, however, is critical for the ability of actin to attach to the filament. An α-helical conformation is seen to significantly weaken the interaction strength between actin subunits [25].

The description of the DB loop within the EN approximation is problematic. Generally, α-helical conformations, a common motif in protein structures, are densely packed and, hence, residues have many neighbors. In the standard EN approximation such α-helices are artificially stable, because breaking of elastic links is not allowed. To overcome such limits, hybrid models have been constructed. In G-actin, e.g., the DB loop may be exchanged by the the open loop conformation found in F-actin (see Fig. 29) [56, 121]. This approach is used by Splettstößer *et al.* [150] as a basis for MD studies of the actin filament. Also, Chu and Voth [26] have used double-well network models allowing switching between the two conformations which are both modeled as an elastic networks.

The conformation of the DB loop is nucleotide dependent [126, 128] and may regulate binding to the filament [185]. Fine details like the exact conformation of the DB loop may even be the final cause for a strong attachment. Our aim, however, is to identify collective domain motions that provide the overall basis for docking. Therefore, we abstain from expanding the model to suitably describe the DB loop with high accuracy.

Actin monomers cannot polymerize and form filaments in the absence of ATP. In Chapter 4, we suggested that ligand-binding induces a transition from the structural state of G-actin to the F-actin state. Later, we will directly monitor ligand-induced conformational changes of actin with respect to the filament and, in this way, explain the ATP-dependent attachment mechanism.

In this thesis, the interactions of proteins like actin and myosin with the actin filament are investigated. To study such systems from a theoretical point of view, a suitable filament model needs to be obtained. Here, we construct a filament out of its monomeric units modeled as elastic networks based on structures in specific conformational states. In experiments, a certain symmetry is found in the actin filaments. Subunits are translated by 27.50Å and rotated by 166.66° [56]. Using this information as a recipe, one can build actin filaments of arbitrary lengths.

An actin subunit in the filament is interacting with four neighboring proteins [121, 56]. We see in the experimental data that the F-actin conformation of the monomer inside the filament is stable. Thus, within the filament, the conformation does not depend so much on the actual nucleotide-state, which was of such important relevance when it came to attaching to the filament. One must thus assume that interaction with its four neighboring monomers stabilizes the F-actin conformation. Therefore, we will employ a filament model where the subunits are frozen, i.e. their conformation remains fixed at all times. To save computational time, only two or three subunits will represent the filament, depending on the situation.

6.2 ACTIN-ACTIN AND ACTIN-MYOSIN BINDING SITES

While intramolecular interactions are modeled by means of elastic links, it is necessary to develop a way of describing protein-protein interactions within the framework of the coarse-grained EN approximation to study the attachment of proteins to the actin filament. Since in the EN model, all chemical details are neglected, there is without further knowledge no way of deciding where stable bonds can be established. Hence, additional experimental data has to be used to identify protein specific binding sites.

Table 2: Links between myosin and actin monomers in the filament

myosin	1st actin monomer	2nd actin monomer
343	328	-
386	337	-
517	167	-
526	-	50
542	-	95

In the case of actin, high-resolution filament data is available [56]. The structure can provide clues that can be used to identify probable pairs of binding residues. Such residues can directly be extracted from the data in the following way:

- an EN is constructed on the basis of the filament data with a cutoff of $l_0 = 8.5$Å
- actin subunits are identified
- elastic links between different subunits are marked
- pairs of residues connected by such links are assumed to be actin-actin binding sites.

The corresponding actin-actin binding sites found by this procedure are listed in Sec. A.5 in the Appendix.

Identifying protein-protein binding sites for actomyosin is less straightforward. No high-resolution structures for the actin-myosin complex are currently available and we, therefore, cannot use the above method. Nonetheless, a recent MD study by Lorenz and Holmes [105] has investigated the actin-myosin-II interface. A low-resolution electron micrograph was used as constraint for MD simulations. In this set-up, myosin was fitted to the experimental data and residues that may form stable hydrogen bonds could be identified. Such bonds provide a mechanism for a strong interaction between myosin and the filament. Fortunately, the structures of myosin-II and myosin-V are very similar and, therefore, we could obtain a list of pairs of binding residues for myosin-V and the actin filament by analogy. Such pairs are given in Table 2.

Knowing probable pairs of binding residues between proteins, one can now expand the EN model of actin or myosin. Such residues can form breakable bonds described by Lennard-Jones potentials. More details can be found in Sec. 3.4.1 in Chapter 3. Note that such potentials account for the fact that specific protein-protein interactions are only short-ranged.

If residues come very close to each other, soft sphere potentials prevent protrusion of the residues (see Sec. 3.5.2). Such interactions are also short-ranged and become important for even smaller distances. Furthermore, a small number of amino acids carry a charge. They interact via Coulomb potentials. In a solvent, such interactions are screened and thus described according to the Debye-Hückel theory [37]. Electrostatic interactions are long-ranged and, hence, are the only important interactions of the expanded EN model at large distances. More details can be found in Sec. 3.5.1.

Thus, the interaction of myosin or actin with the actin filament is modeled in a coarse-grained way. For large distances, only electrostatic forces can be present. At shorter distances, stronger protein-specific interactions become more important and, thus, govern short-range behavior.

6.3 GUIDED BY ELECTROSTATIC INTERACTIONS

In this section, we focus on proteins interacting with the actin filament, i.e. we study how actin and myosin macromolecules approach it and subsequently form stable bonds. Electrostatic interactions, soft sphere potentials and bonds between protein specific binding sites are explicitly included.

A small group of amino acids carries a charge. The charge distributions of actin and myosin are displayed Fig. 30. Between these charges residues, electrostatic interactions are present.They are long-ranged and for distances larger than 20Å, only such interactions are present in our model. If proteins come close to each other, breakable bonds are formed between certain pairs of binding residues, as explained above. Furthermore, short-ranged soft sphere interactions prevent protruding of amino acids. A detailed discussion of all protein-protein interactions used in our modeling is given in Sec. 3.5.

In the following , we show how electrostatic interactions guide actin or myosin toward the filament, where specific protein-protein interactions lead to a stable attachment of those proteins.

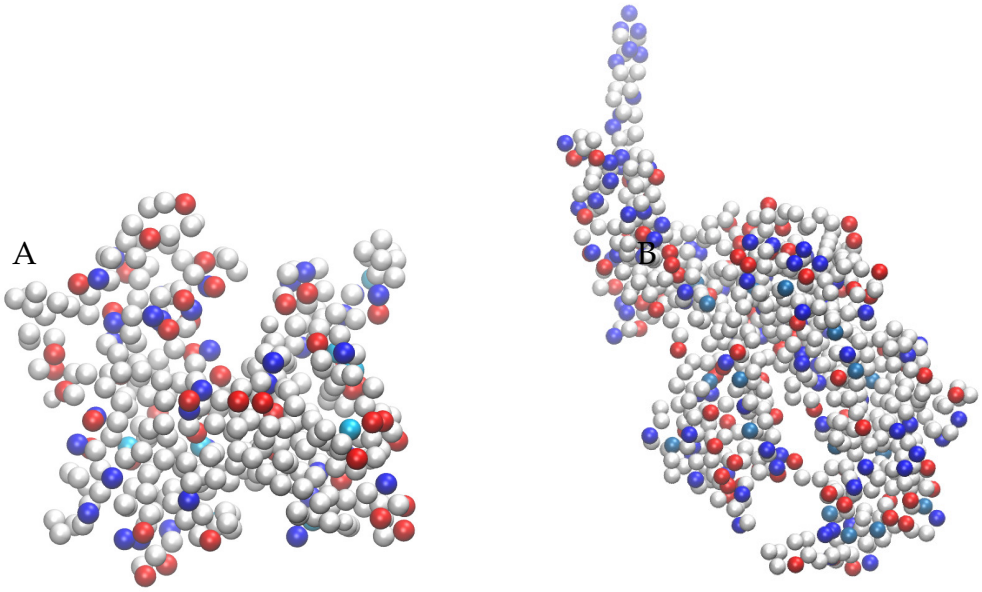

Figure 30: Charged residues of (A) actin and (B) myosin-V. Arginine and Lysine (blue) carry a positive charge, Aspartic and Glutamic acid carry (red) carry a negative one. Histidine (light blue) carries a positive charge in 10% of all cases.

6.3.1 *Interaction of Actin Monomer with the Filament*

The basis of our investigation are three actin monomers A1, A2 and A3. Actin subunits A1 and A2 are in the filament conformation and remain frozen. In this way, they provide a minimal model for the actin filament. In this part of our study, we are mainly interested in finding out how actin approaches the filament and we do not want to consider ligand-induced effects. Thus, we model the third monomer A3 as F-actin EN, i.e. its equilibrium is a closed and flat conformational state, suitable for docking to the filament.

If we position an actin monomer more than 20Å away from the closest filament residue, interactions between filament and protein can only be electrostatic. Thus, we start with such initial conditions and monitor the relaxation process. In our computer experiment, actin is shifted about 30Å away from the filament. The initial set-up is shown in Fig. 31A.

Due to electrostatic interactions, the filament and the monomer attract each other. Figure 31 shows the corresponding docking process in a range where only Coulomb interaction are present.

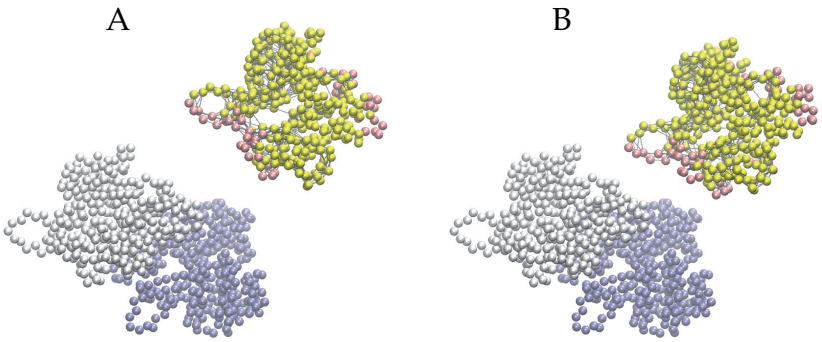

Figure 31: The filament is represent by two monomers (gray beads, iceblue beads) fixed in space. An actin monomer (yellow) approaches guided by electrostatic interactions. Starting from the initial position (A), the conformation of the actin trimer is shown after (B) 300 time steps in arbitrary units.

First, the actin subunit A3 mainly rotates to align its charges. Then, the monomer approaches the filament until it comes into a range of 20Å of the filament residues (Fig. 31B).

If the monomer has come this close to the filament, links between specific pairs of binding residues are established. The effect of such bonds is visualized in Fig. 32. Just as the electrostatic interactions have guided the protein toward the filament, this newly established bonds guide the molecule toward its equilibrium position bound to the filament (Fig. 32C). The short-ranged soft sphere potentials forces that become relevant if distances between residues are close to 5Å and prevent protrusion of protein domains.

Electrostatic interactions between charged residues and the specific actin-actin interactions provide a framework for a controlled binding of actin to the filament. Placed at a distance where only Coulomb interactions are present, the free actin protein first aligns its charges and then approaches the filament. The free monomer is guided towards its corresponding binding sites on the filament. If the monomers come close enough to such sites, strong bonds form between the specific pairs of binding residues of the actin monomer and the filament. Such strong bonds are necessary for a stable binding between protein subunits. Protrusion is prevented by soft sphere potentials. This provides the framework for controlled binding of actin to the filament.

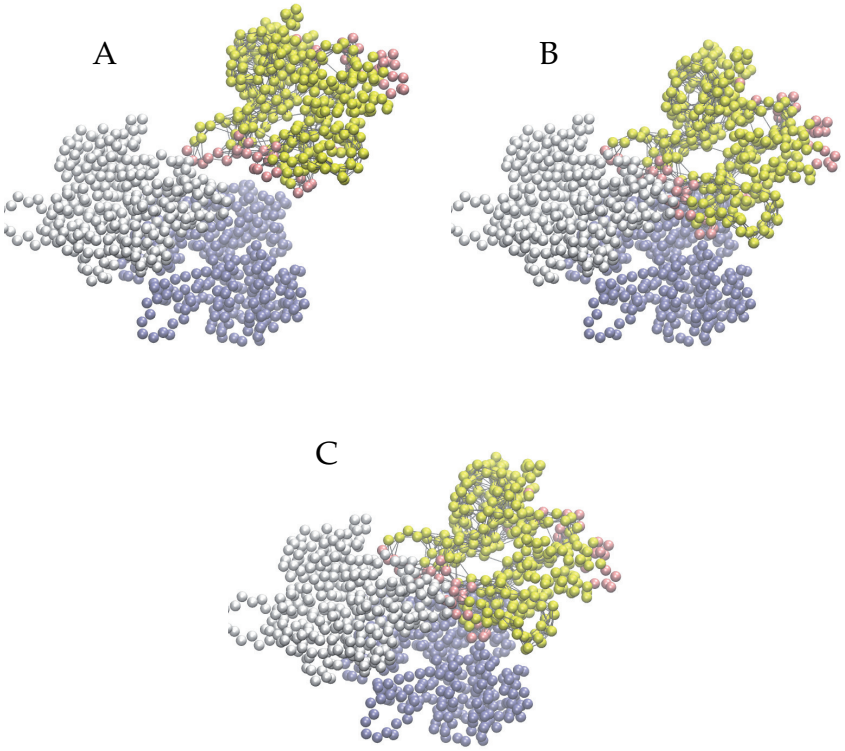

Figure 32: The filament is represent by two monomers (gray beads, iceblue beads) fixed in space. An actin monomer (yellow) approaches guided by electrostatic interactions. As soon as the actin monomer is close enough to the filament, bonds form between the binding sites between actin subunits (pink beads). Starting from position (A), the binding actin subunit interacts with the filament and quickly relaxes to an equilibrium position. (B) shows the relaxation 1 and (C) 2 timesteps in arbitrary units.

6.3.2 *Interaction of Myosin with the Filament*

We have seen how actin approaches the filament. In this part of the thesis, we will concentrate on the interactions between the actin filament and a myosin molecule. Again, the focus will be on how electrostatic interactions guide the proteins toward specific binding sites where strong bonds can be formed.

If a myosin protein attaches to the filament, it establishes connections to three monomers. Hence, the minimal filament model is a trimer of F-actin EN A1, A2 and A3 in the filament conformation. The conformations of the three subunits are fixed. Myosin is modeled as an EN on the basis of myosin-V experimental data in the post-rigor conformation (PDB ID:

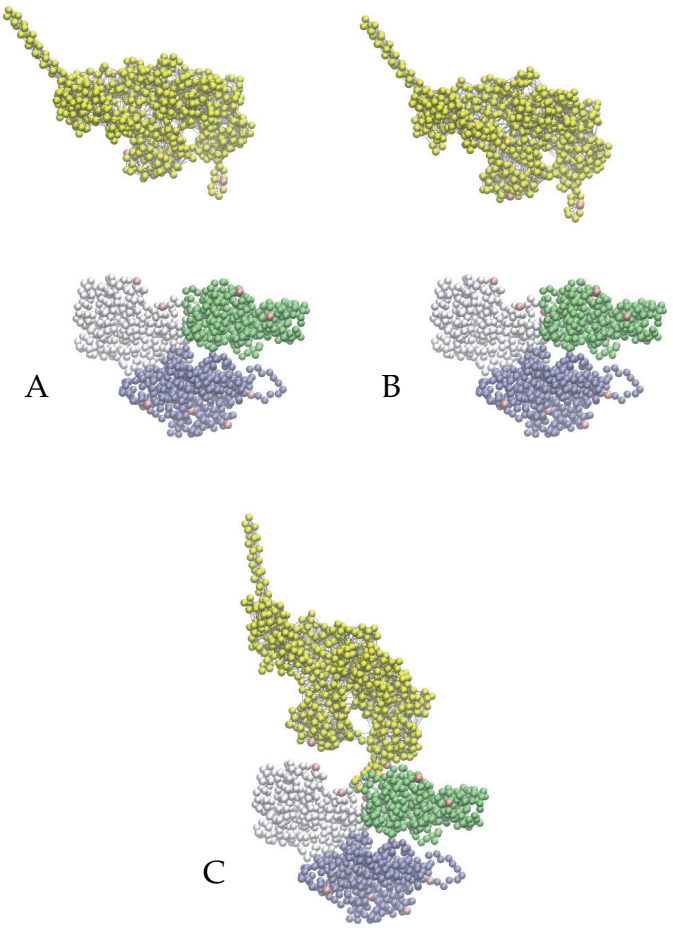

Figure 33: The filament is represent by three fixed actin monomers in their filament conformation (gray, iceblue, lime beads). A myosin monomer (yellow) approaches the filament guided by electrostatic interactions. Starting from the initial position (A), the conformation of the actin trimer is shown after (B) 80 and (C) 160 time steps in arbitrary units.

1W7J, cf. Ch. 5). It can interact with the filament via pairs of residues given in Tab. 2.

In the initial configuration, the myosin-V EN is shifted with respect to the trimer representing the filament (see Fig. 33A). The closest residues are approximately 63Å apart. It is clear that in our model actin and myosin can only communicate via electrostatic interactions. Qualitatively, we see the same behavior as in the previous section. The myosin aligns its charges (Fig. 33B) and then approaches the filament (Fig. 33C) until interacting residues come closer than 20Å to one another.

If the myosin comes close enough to the filament, the actin-myosin binding sites interact strongly. Such interactions lead

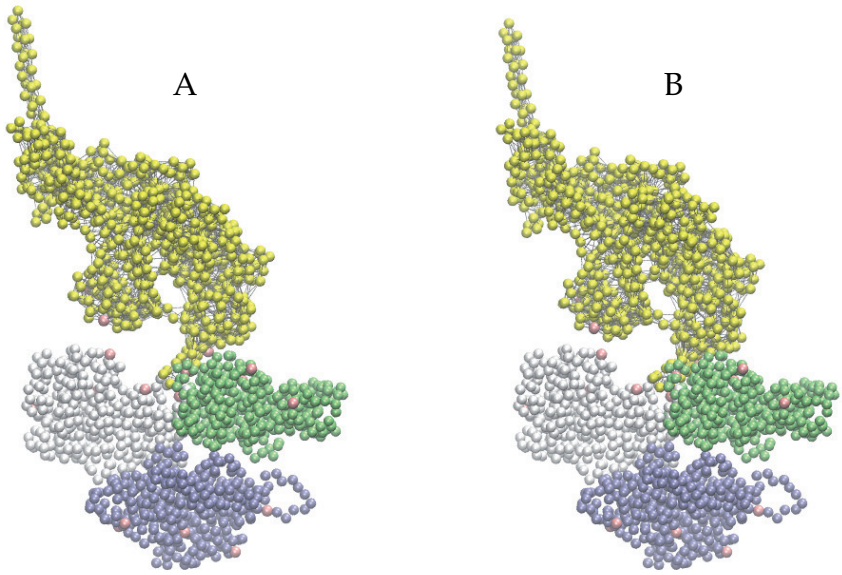

Figure 34: The filament is represent by three fixed actin monomers in their filament conformation (gray, iceblue, lime beads). A myosin monomer (yellow) attaches to the filament. After being guided by electrostatic interaction in a way that binding sites (pink beads) come close to each other (A), Lennard-Jones type bonds between such binding sites form. The equilibrium conformation is shown (B).

the protein to its final equilibrium position, which is displayed in Fig. 34. Again, soft sphere potentials prevent protrusion, if residues come too close to each other.

In Ch. 4 the HCM loop was suggested to play an important role for the force-generating mechanism. It was shown that forces on this region lead to a conformational change in the myosin tail region which may result in a so-called power stroke. Hence, it is noteworthy how well the HCM loop fits into a certain pocket in the actin filament. The role of the HCM loop, therefore, has to be further investigated.

In a nutshell, we identified the mechanism than enables the attachment of myosin to the filament. Placed at a large distance, short-ranged interactions like actin-myosin binding sites or soft sphere interactions do not play a role. In our model, only electrostatic interactions were present and guided the myosin toward its specific binding sites on the actin filament. Here, pair interactions between specific residues lead to a strong binding to the filament. Special attention should be paid to the role of

the HCM loop. We have seen in our simulations, that it is led to a specific pocket in the actin filament. Here, it fits almost perfectly and therefore the role of the HCM loop in the machine cycle of myosin should be further investigated.

6.4 LIGAND BINDING FACILITATES DOCKING

In Chapter 4 ligand binding has been modeled in the framework of an expanded EN description. A key result of this chapter was that binding of such an artificial ligand introduces conformational changes in G-actin. These conformational changes are found to describe the structural changes of the G- to F-actin transition, which have been found experimentally, quite well. Accordingly, it has been suggested that binding of a ligand facilitates docking of actin monomers to the filament. This means that ligand binding enhances the attachment affinity and, in this way, an ATP-dependent mechanism to regulate polymerization can be identified. In the following, we directly monitor the ligand-induced conformational changes and show that after nucleotide binding the actin monomer fits better to the filament. Thus, binding of ATP does indeed facilitate docking.

6.4.1 *Toy Model*

Our aim is to understand how ATP-induced conformational changes influence the probability of docking to the filament. The effect of nucleotide binding shall be understood independently of protein-protein interactions and, therefore, we will neglect soft sphere and electrostatic interactions at this point. Furthermore, actin-actin interactions are only used in a very specific way as explained below. It should be made clear that the toy model employed in this part of the thesis will not fully represent the interaction of an actin monomer with the actual filament, but will only focus on a small part of this process, the ligand-induced motions with respect to the filament.

First, we construct a toy system of an actin monomer interacting with the filament. If an actin protein attaches to the growing end of the filament, it establishes contacts with two filament subunits. These are modeled as a dimer of two F-actin elastic

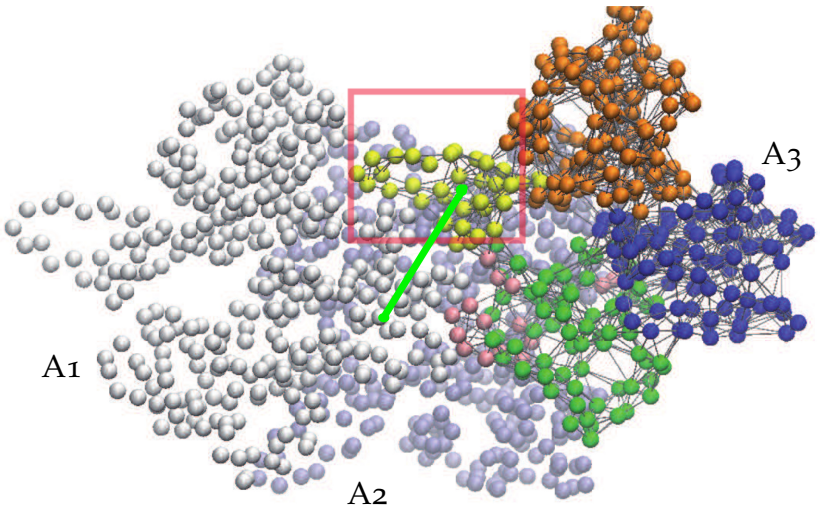

Figure 35: Actin trimer constructed out of F-actin. Static actin monomers A1 (gray) and A2 (iceblue) are connected to the subdomain S4 of the EN of actin subunit A3. Beads that interact with A1 and A2 are colored pink. The distance l between subdomain S2 of A3 and subdomain S3 of A1(light green) measures the distance of the DB loop to its corresponding binding sites in the neighboring actin subunit.

networks A1 and A2, fixed in space. A third actin monomer A3 is modeled as G-actin EN. It interacts with the filament via certain specific binding sites.

Natural motions of actin involve collective motions of the two mobile domains with respect to each other (cf. normal-mode analysis of G-actin in Chapter 3). If we only let the monomer interact with the filament via one of these domains, ligand-induced relative motions of them are not hindered. Accordingly, we allow only subdomain S4 of subunit A3 to interact with the filament. All other links between actin subunits are not present in this analysis. This corresponds to a situation where one mobile domain of a free actin monomer is anchored to the filament at its appropriate binding position while the other mobile domain can freely move with respect to its counterpart. The set-up is shown in Fig. 35. Pink residues in A3 represent the anchored binding sites.

It is obvious that such a set-up does not reflect real actin-actin interactions. Only ligand-induced conformational changes are monitored and compared to the filament while neglecting all other effects. The aim is to quantify the nucleotide-dependent actin dynamics with respect to the filament. We will do so by

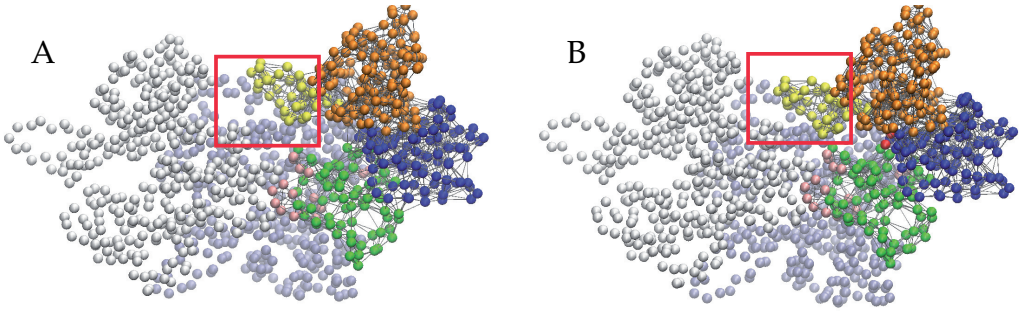

Figure 36: Actin trimer constructed out of F-actin. Static actin monomers A1 and A2 (grey beads) are connected to the subdomain S4 of the EN of actin subunit A3. Beads that interact with A1 and A2 are colored pink.

monitoring the distance l. In Fig. 35, l is displayed as the length of a light green line. It connects the centers of mass of subdomain S2 in actin subunit A3 and the center of subdomain S3 of actin subunit A1. It can be understood as a measure of how close the DB loop can approach its respective binding sites. Here one should remember that this loop plays a fundamental role in protein-protein interaction [25].

6.4.2 *Nucleotide-Dependent Dynamics*

We will follow the distance l to measure conformational changes of G-actin with respect to the filament. The starting conformation of A3 is the conformation of F-actin as it would be positioned in the filament (see Fig. 35). Thus, A3 is initially deformed. Accordingly, the system tends to relax to its equilibrium, i.e. the A3 monomer will open its cleft and unflatten. Ligand-binding in this state yet again leads to a flattened and closed state. Hence, following l over time we can quantify the transition from F-actin to G-actin and, subsequently, the transition from G-actin to ATP-G-actin. The respective equilibrium states are shown in Fig. 36.

Figure 37 displays the change of the distance l. The black line shows the initial relaxation from the distorted F-actin state to the G-actin equilibrium conformation. The distance l changes from $l = 24.0$Å in the F-actin conformation to $l = 32.7$Å in the relaxed state. This change in distance means that the DB loop of actin subunit A3 moves away from subdomain S4 in the neigh-

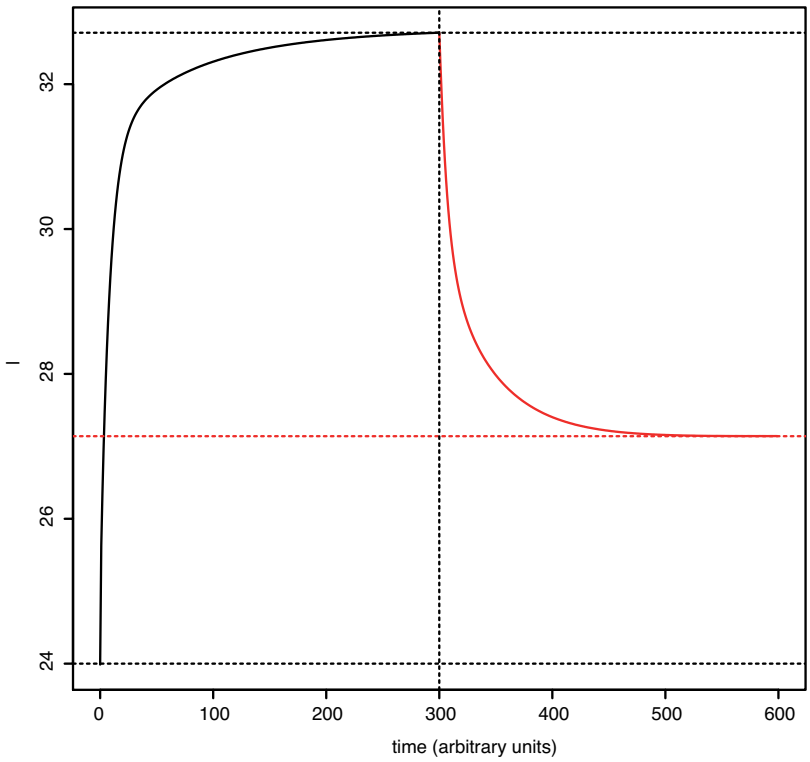

Figure 37: Distance between actin subdomain S4 and the filament. The distance between the center of mass of subdomain S3 of actin A1 and the subdomain S4 of actin A3 is plotted. From the starting conformation of F-actin, the G-actin EN relaxes to its equilibrium state (black line). Ligand binding leads to a decrease in the distance l (red line). Initial, maximum and final values are indicated by dashed lines.

boring subunit A1, i.e. the loop retreats from its corresponding binding position.

Next, we study the effect of ligand binding. The red line in Fig. 37 monitors the distance l after binding of ATP. The distance decreases by $\Delta l = 5.6$Å. This clearly means that the DB loop moves closer to its expected binding position. Now we see how ligand-binding facilitates docking: a closed conformation is stabilized that is more suitable for binding to the growing end of the actin filament.

Between the initial F-actin conformation and the ATP-induced conformation lies a difference of $\Delta l = 3.1$Å. Here, the structure of the loop mentioned above becomes important. In G-actin, the DB loop is found in its α-helical conformation. A mere conformational changes from α-helical to open loop conformation accounts for a distance change of approximately $\Delta l = 2.0$Å,

already, because the center of mass of subdomain S2 of A3 is shifted accordingly. Furthermore, we do not expect exact quantitative results due to the many approximations that were carried out.

We built a simple toy model to visualize ligand-induced effects with respect to the filament. By following the conformational changes, we see that the effect of ATP is to help the DB loop to approach its corresponding binding position. In this way, docking is regulated depending on the nucleotide.

6.5 DISCUSSION

In this chapter, we have investigated the interactions of actin and myosin with the actin filament. We have used EN approximations to model the two proteins. Furthermore, we have developed a minimal filament model comprised of two or three F-actin monomers, depending on the situation. These have been positioned according to the symmetry of the filament determined in experimental data. To take into account the effect of proteins in the filament stabilizing their conformation, on the one hand, and to save avoid high computational costs, on the other, filament monomers were fixed in space.

In general, we have introduced a framework to describe protein-protein interactions within the EN approximation. Short-ranged soft sphere potentials prevent unphysical protrusion of residues. Furthermore, charged residues interact via screened Coulomb potentials. Within the framework of the EN model, all chemical details are lost and, accordingly, we have used additional experimental data to identify specific binding sites where strong bonds could be established. In the case of actin, filament data was used to obtain such pairs of binding residues. Moreover, we could identify probable binding sites between actin and myosin by using the results of a recent MD study by Lorenz and Holmes [105].

How does a free actin monomer bind to the filament? It has been found that electrostatic interactions guide the protein towards its respective binding sites in the actin filament. We have placed an actin monomer at a large distance from the filament, so only Coulomb forces were present. After aligning its charges, the free monomer moved towards its respective binding site at the filament end. Here, links could be established which pulled

the protein into its correct position in the filament, which lead to a strong attachment.

Takano *et al.* [158] have found a ratchet-like behavior of myosin attached to the actin filament. Their discussion was entirely based on electrostatic interactions between charged and van der Waals interactions between all residues. Using results of a recent MD study of the actin-myosin interface [105], we have expanded their model by allowing strong bonds to form between specific binding sites.

On the basis of our model, we have in detail investigated the approach of myosin towards the filament guided by electrostatic forces. Placed at a large distance from the filament, the myosin protein was attracted to the filament by Coulomb forces and moved towards its respective binding sites. Thus, pairs of binding residues formed breakable Lennard-Jones-type bonds which enable a strong binding to the filament.

We therefore have found that the monomeric actin and the myosin motor protein independently have similar means of binding to the actin filament. Long-range electrostatic interactions guide the proteins towards a suitable binding position. Here, the macromolecules approach specific binding sites and establish bonds that lead to strong binding. This behavior seems to be a quite general mechanism allowing various actin-binding proteins to attach to the filament.

In a next step, we have studied the role of the ligand in the polymerization process. To this means, we have constructed a toy system. Our aim was to visualize the ligand-induced conformational changes of an actin monomer with respect to its neighbors. The filament has been modeled by two fixed F-actin monomers and a G-actin monomer has been anchored to the filament at its appropriate binding sites. An important aspect of the toy model was that it only has been attached with one of the two large mobile domains. Accordingly, relative motions of actin's main domains have not been hindered. Moreover, soft sphere and electrostatic interactions were neglected completely, because we were only interested in internal interactions of G-actin.

Studying the toy system, we could monitor conformational changes and relative motions of the two mobile domains of G-actin with respect to the filament. By using the coarse-grained ligand model of Ch. 4, we saw that binding of ATP induces a conformational change that lets the DB loop approach its corresponding binding sites in the neighboring actin subunit. Be-

cause we have seen that ATP-induced changes lead to a conformation more suitable for stable binding, we could substantiate our earlier hypothesis that ligand-induced conformational changes facilitate docking.

7

SUMMARY AND OUTLOOK

The main aim of this study was to understand the intrinsic machinery of two important molecules, the structural protein actin and the molecular motor myosin. An important question was, e.g., how binding of an ATP nucleotide regulates their machine cycles. Apart from intramolecular communication, we furthermore investigated interactions between different protein units. We discussed the polymerization of actin monomers into filaments and studied the interactions between actin and myosin.

Proteins were investigated from a theoretical point of view in the framework of an EN approximation. Such an approach has the advantage of allowing a high resolution description of biomolecules (up to one amino acid) while avoiding the high computational costs of all-atom approaches.

This thesis has been organized as follows. **Chapter 2** provided a background of the field of protein research. Here, general properties of proteins, e.g. their role in the cell and their construction principle, were presented. Furthermore, the biological functions of actin and myosin and their corresponding machine cycles were broadly explained. Additionally, a brief overview of scientific methods used in the study of proteins and biomolecules in general was presented. Throughout the last decades, a wide range of experimental techniques have been developed. In this chapter, methods relevant for the study of actin and myosin were introduced. Structural data with atomic resolution, e.g., can be obtained by X-ray crystallography, NMR or cryo-electron microscopy. Furthermore, optical tweezer may be used for manipulating single molecules and conformational changes can be dynamically followed by FRET measurements.

Moreover, theoretical approaches to investigate such macromolecules were reviewed in depth. The standard approach of MD simulations was presented and several ways to speed up its simulations, which suffer from high computational costs, were depicted. To overcome certain limitations of the MD simulation approach, coarse-grained approximations have been successfully applied. The main approximation method used in this thesis was the EN model.

The following **Chapter** 3 contains the detailed description of all mathematical tools used in our study. Slow conformational changes of proteins were investigated with the EN approach. Here, we presented the general model together with its linearization. If one applies external forces to elastic networks, rigid translations and rotations are induced. To study communication within proteins, however, only internal dynamics should be considered. Therefore, a method was established to immobilize such networks without pinning single residues.

If collective conformational motions are large, residues which are not neighbors in the EN framework may come close to each other. Following the logic of the model, they should, in this case, be connected by elastic links. To account for this behavior, the standard EN description was extended. Certain residues that could come close to each other were allowed to form breakable bonds. Additionally, we showed how to model protein-protein interactions within the coarse-grained EN approach.

In **Chapter** 4, the intramolecular communication of actin was investigated. Here, our aim was to understand the internal organization of the conformational mechanics of the protein. Within the EN approach, we found that there exist two large mobile domains which perform slow collective motions. We identified these natural motions as a propeller-like twist of the two large mobile domains with respect to each other and a scissor-like opening and closing of the cleft between them. Although our model is considerably simpler, the results of Tirion and ben Avraham could be reproduced [162].

Due to the large domain motions, residues inside the actin monomer, which were not connected in the EN model, were seen to approach each other. Accordingly, additional interactions should occur between them. We modeled this by introducing breakable bonds between residues that may come close. In this way, a metastable, closed state was generated.

Furthermore, we were interested in important residues in the NBP that are able to translate small local deformations into large-scale domain motions. To identify such residues, we studied the response to external forces applied to single residues in this region. We saw that, indeed, perturbations in the ATP-binding region of only a small group of residues could induce large collective domain motions. In actual biological systems, actin is activated by ATP binding and subsequent hydrolysis. The chemical reaction in the NBP can lead to large-magnitude conformational changes. Therefore, we introduced in **Chapter** 4

a coarse-grained model of the nucleotide on the basis of the previous sensitivity analysis within the nucleotide-binding region. We found that interaction with such a model ligand stabilized the closed state and could induce a transition from the open equilibrium conformation to closed state. Based on these results, we were able to understand the nucleotide-dependent binding affinity of the actin monomer to the filament. The actin monomer can be in an open or closed conformation. The closed conformation is seen to be more suitable for docking to the filament. If ATP is not present in the NBP, the monomer switches between those two states due to thermal noise. The open state, however, is much more probable and, hence, the binding affinity of actin to the filament is small. In the presence of ATP, however, the closed state is stabilized and, accordingly, the binding affinity of this state is much larger. Hence, the monomer tends to attach to the filament in the ATP state.

Chapter 5 dealt with the myosin motor. Inspired by recent experiments which used optical tweezers to exert forces to myosin [80], an EN model of myosin-V was used to study responses to external forces. The myosin molecule is built out of three functional regions: the tail, the NBP and the actin-binding cleft. Here, we studied communication between these regions by probing single residues in a specific region by external forces and measuring the effect in the respective other two. In this way, we constructed a map of intrinsic communication.

In our study, we found that the ATP-binding region is divided into two parts - the front and back doors. The front-door region interacts with the adenine ring of ATP or ADP, respectively. Perturbations in this region lead to a large conformational change in the tail. The back-door region, on the other hand, interacts with the γ-phosphate. Perturbations here induce conformational changes in the actin-binding cleft. On the basis of these results, we could assume that a chemical reaction with the adenine part of ATP/ADP may lead to a power stroke-like behavior, and interaction with the phosphate controls the binding affinity to the filament. We furthermore studied perturbations in the actin-binding site. It became clear that external forces applied to the HCM loop cause large conformational changes in the tail region. Because the HCM loop is known to strongly interact with actin, binding to the filament has in this way been identified to be a control mechanism for a possible power stroke.

Furthermore, the effect of forces in the tail region was investigated. We tried to reproduce the experiments by Iwaki *et al.* [80] and Oguchi *et al.* [123]. In these experiments, the effect of load on the filament and on the ligand binding affinities to myosin were studied. In our simulations, we saw communication of forces on the tail with the actin-binding region and the NBP. First of all, backward strain leads to a closing of the actin cleft and forward strain has the opposite effect. Comparing with the nucleotide-free state of myosin-V, thought to resemble the conformation of myosin bound to the filament, we concluded that backward strain directly leads to conformational changes in the actin-binding region that make it more suitable for binding to the filament. In this way, we could explain the results of Ref. [80]. Moreover, we saw that strain controls the opening of the so-called front door which explains the load-dependence of the nucleotide-binding affinity [123]. Thus, by means of the coarse-grained EN network approach we identified to a large extent the structural basis of the myosin motor mechanism.

In **Chapter** 6, we studied the interactions of unbound monomeric actin and the myosin motor protein with the filament. We investigated how long-ranged Coulomb interactions guide actin-binding proteins toward their specific binding sites. Both, a free actin monomer and the myosin macromolecule, approach the filament due to electrostatic interactions. Here, the proteins come close to their specific binding sites on the actin filament surface. Establishing bonds between pairs of residues enables the actin-binding proteins to strongly attach to the filament.

Furthermore, we elucidated in a toy model the conformational changes of actin due to binding of the artificial ligand which was modeled earlier in a coarse-grained way as a dimer of ADP and P_i nodes. We saw that induced conformational changes led to a movement of the DB loop towards a cleft in the neighboring actin subunit of the filament. Therefore, supporting the conclusion of Chapter 4, binding of the ligand leads to a conformational state that makes docking easier.

The EN approximation has been proven very useful to describe internal dynamics of proteins. This approximation, however, suffers from serious drawbacks mainly due to neglecting the chemical properties of single residues. Hence, chemical details are only included indirectly through the protein structure. Such details, however, are especially important during binding events, i.e. the binding of a ligand or the binding of myosin

to the actin filament. In the course of this thesis, we saw that additional information about pairs of binding residues is necessary and it remains difficult to model chemical interactions in a suitable way. However, using EN models as a guide for experiments or computationally costly MD simulations can be a powerful tool in the field of protein research. Two examples follow below.

A widespread method to monitor conformational changes on the scale of 1Å are FRET measurements [55, 130]. A combination of the EN modeling of proteins, approximating conformational dynamics, and such experimental methods could make it possible to follow tiny conformational changes dynamically. An example is the existence of certain metastable states in the actin filament [96]. An interesting application for EN approximation would be to study such conformations on a microscopic level.

Due to high computational costs of MD simulations, a wide range of acceleration methods have already been developed. To describe myosin-V, e.g., targeted molecular dynamics have recently been used [127]. In these simulations, a restraining potential was constructed based on structural data of myosin in different conformational states. A more general approach would be to investigate proteins within the EN approach and use these results as restraining potentials to understand the internal dynamics on an atomic level.

In this thesis, we introduced a coarse-grained framework to describe the interactions between the actin filament and actin or myosin. Our findings can be the basis for future studies of larger systems. One may think about modeling the actual myosin stepping along actin filaments, i.e. a complete actomyosin machine cycle. Such a model would be an extension of the Brownian stepping model presented by Takano *et al.* [158]. Furthermore, the actin monomer and its interaction with the ATP ligand have been approximated in the framework of the EN approach. The simple model introduced in this study should be extended to resolve the complete process of dynamic polymerization of actin into filaments.

A

APPENDIX

In the Appendix, additional information and details are provided. In Sec. A.1, the nucleotide model used for actin monomers is described in depth and, furthermore, residues interacting via truncated Lennard-Jones potentials are given. In the cell, myosin motors walk processively along actin filaments. The following Sec. A.2 describes how the direction of motion of myosin can be obtained by fitting the myosin elastic network to the actual filament. Then, in Sec. A.4 the difference between linearized equations of motions andx full-nonlinear equations is highlighted on the example of the myosin EN with external forces.. Finally, Sec. A.5 gives the binding sites of actin-actin interactions. Additionally, the Appendix contains Tab. 3 and Tab. 4, which where to large to place in the main part of the manuscript.

A.1 LIGAND MODEL FOR ACTIN MONOMER

The ADP is imitated by introducing an additional node in the network whose equilibrium coordinates are taken to be the $C1'$ position. This carbon connects the nucleotide's ribose with adenine and, therefore, is located in the central part of the molecule. The new node is connected to all neighboring residues within the cutoff distance l_c by elastic links of a stiffness κ. Note that the same stiffness also appears in equation (3.1) and, thus, ADP is treated as a regular node in the network and the conformation remains in the equilibrium. The neighbors of ADP are residues 156, 157, 181–181, 301–305, and 336 in subdomain S3 and residues 210, 213, and 214 in subdomain S4. The ADP model is shown in Fig. 18A. In this model, no links between the inner and outer domain are established. Therefore, the slow natural motions, i.e. collective motions of domains with respect to each other, remain unchanged.

Furthermore, P_i is modeled as a node connected to ADP and the three identified key residues 16, 73, 159. It is placed in the center of mass of these four nodes and connected by elastic

links, again with the same stiffness κ. The complete model of ATP interacting in the NBP is visualized in Fig. 18B. The presence of phosphate in this region leads to a shrinking of the NBP [128]. This fact is accounted for by shortening the equilibrium lengths of all links between P_i and its neighbors to 20% of their initial value. In this way, the phosphate is modeled as a particle in the NBP interacting attractively with its vicinity. It is a property of ATPases, that local changes upon ligand binding and release lead to conformation changes. Movie S3 in Ref. [45] shows the changes induced by this model of nucleotide binding.

A.2 MYOSIN DIRECTIONS

Myosin-V walks along the filament in the direction of the barbed end. In the experiments, the protein was dragged along the filament. The forward strain direction corresponded to the direction of processive motion, whereas the backward direction was opposite to it. If one wants to computationally reproduce the experimental situation, forward and backward directions for the elastic network of the protein must be identified. We have done this by including F-actin into the elastic network simulations and determining the equilibrium conformation of the myosin-actin complex.

Employing guided MD simulations, Lorenz and Holmes [73, 105] have recently identified several possible binding sites of myosin-II to actin. Comparing structures of myosin-II and myosin-V, analogous binding sites for myosin-V can be suggested. The myosin head binds to two distinct F-actin monomers in the filament (constructed from PDB ID: 2ZWH [121]) at the positions given in Table 2 in Ch. 5.

To determine the equilibrium position of myosin with respect to the actin filament, the following procedure has been employed: elastic links, connecting myosin to the actin filament, have been introduced with equilibrium lengths of 3.5 Å and stiffness $\kappa = 1$. After that, relaxation equations (3.3) of the myosin-actin complex were numerically integrated until a stationary state has been reached. In this way, we approximated the actomyosin structure as shown in Fig. 38.

Relaxation to the equilibrium state of the complex involved rotation of the myosin-V molecule. To quantify this rotation, we have chosen four residues (165, 195, 559, 691). These residues

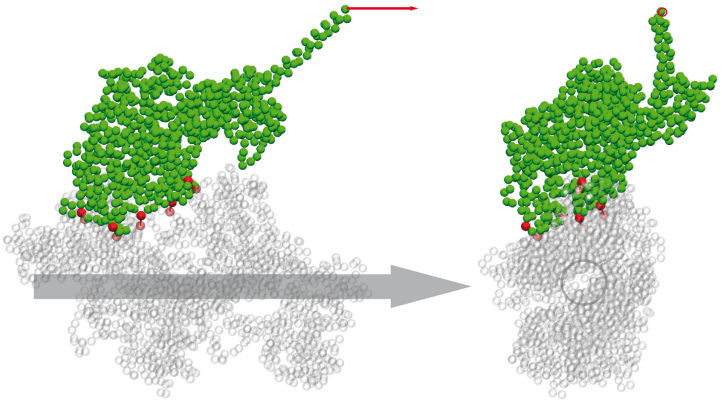

Figure 38: Myosin-V modeled on actin filament: the elastic network (green) is anchored to the actin at specific binding sites (red balls mark corresponding residues on myosin and actin, respectively). The direction of the processive motion is shown by the gray arrow and the force applied by the red arrow.

belong to the stiff core of the protein. With these residues, one can construct three linear independent vectors that define a coordinate system only in terms of the network structure. Thus, the forward direction $\mathbf{n}_{\parallel}$ can be approximated by transforming the filament axis to the coordinate frame of the reference state (PDB ID: 1W7J) [31] that is defined by the same residues. In this way, we found the forward direction to be approximately $\mathbf{n}_{\parallel} = (-0.254, -0.888, 0.383)$.

A.3 MYOSIN SENSITIVITY TABLES

Our aim is to examine the mechanical responses of the protein to forces with varying directions applied to individual residues in the nucleotide-binding pocket and actin-binding cleft. To probe mechanical responses, we select two sets of residues in the respective regions (see Fig. 23a). For every chosen residue, a series of 200 simulations was performed. In all simulations, the magnitude of the applied force was the same ($f_0 = 1$ Å), but its orientations were randomly varied. The simulations were continued until a stationary state was found. After that, changes in the monitored pair distances between the labels in different regions were determined. The induced distance changes were

analyzed and, for each pair of labels, the maximum absolute distance change of 200 force orientations was evaluated. In this way, we obtained the sensitivity to forces applied to a residue with respect to a particular pair distance.

The results are shown in Tables 3 and 4 and will be commented below. Note that absolute sensitivities for different pairs of labels cannot be compared. As a matter of fact, distance changes for the tail are always larger than for the actin-binding cleft. To show the variations of sensitivity, a color code was employed. In each column, the maximum and the minimum entries are taken and color gradations from dark blue for the minimum to dark red for the maximum are applied.

A.3.1 *Forces in the Nucleotide-Binding Region*

In the NBP, a set of 27 residues adjacent to the ATP in the considered equilibrium conformation was selected (left column Table 3 and Fig. 23a). The sensitivities of these residues with respect to different pair distances are shown in Table 3. The left column lists the residues and, in each of the other columns, the sensitivities with respect to the distance between a particular pair of labels (e.g., between residues 343 and 517) are given.

The last two columns of Table 3 show the sensitivity of the tail with respect to forces in the NBP. Applying forces to the residues 115 and 116 or their neighbors, a strong effect on the tail is induced. These two residues are located in the front-door region (Fig. 25). Remarkably, applying forces to residues in the back door (219, 220 and 438–442) or the P-loop (163–169) only weakly affects the tail region. Thus, the tail responds mainly to the perturbations applied at the entrance of the front door.

Moreover, sensitivity with respect to residues in the actin-binding cleft was investigated. The strongest response with respect to the distance 343-517 characterizing cleft opening is seen if forces are applied to the residue 442, which belongs to the back-door region. Additionally, perturbations near the front-door residues 115 and 116 show some effect. The distance between residues 386 and 517 describes cleft opening, but mostly reflects movement of the HCM loop to which residue 386 belongs. Here, large responses were observed when the forces were applied in the back-door region with the strongest sensitivity to the perturbations of residues 219 and 220. Only small

changes were seen if the forces were applied in the front-door area.

In terms of the sensitivity of its residues, the NBP region is clearly divided into a front-door and a back-door domain (Fig. 25). A pronounced effect on the actin cleft was observed when forces were applied to residues 219, 220 and 442 in the back-door region. Remarkably, it is exactly the salt bridge between residues 219 and 442 that hinders phosphate release after the hydrolysis. The P-loop region is seen to be relatively stiff and external forces here do not induce large conformational changes in the tail or the actin cleft. Perturbations in the front door affect the tail.

A.3.2 *Forces in the Actin-Cleft Region*

Using the results of Lorenz and Holmes [73, 105], we identified 54 residues which may come in contact with the filament (left column Table 4 and Fig. 23a). To study communication between the actin-binding region and the NBP or the tail, we repeat the simulation procedure described above and obtain the sensitivities shown in Table 4.

As can be seen from the results, application of forces to the HCM loop (residues 377 to 390) can induce strong responses of the tail. Moreover, there is some effect on the distance between residues 789 and 92 in the tail region to the forces applied at the residues from 340 to 350, which belong to the upper 50kDa subdomain, as well. Remarkably, the tail is only weakly affected by the forces applied to the residues in the lower 50kDa subdomain.

The front door (distance between residues 115 and 297) is strongly sensitive to the forces applied at the upper 50kDa subdomain, including the HCM loop. The back door (distance between residues 442 and 291) is mostly sensitive to the forces applied to residues 540 to 544 in the lower 50kDa subdomain; it should however be noted that these residues are located near the back door and, therefore, stronger sensitivity might have been expected.

A.4 COMPARISON TO THE LINEARIZED MODEL

The relaxation equations (3.3) of the elastic network are linear in terms of the distance changes between the particles. They are, however, still nonlinear in terms of the changes of the absolute coordinates of the particles $\mathbf{r}_i = \mathbf{R}_i - \mathbf{R}_i^{(0)}$, since the distance d_{ij} is a nonlinear function of the coordinates $\mathbf{R}_i$ and $\mathbf{R}_j$. Note that not the distance, but the particle coordinates are the dynamical variables in these equations. Hence, to proceed further to the linear (or harmonic) approximation, equations (3.3) need to be linearized with respect to the coordinate changes $\mathbf{r}_i$. After linearization, they take the form

$$\dot{\mathbf{r}}_i = \mathbf{F}_i - \sum_{j=1}^{N} \mathrm{A}_{ij} \frac{\mathbf{R}_i^{(0)} - \mathbf{R}_j^{(0)}}{\left(d_{ij}^{(0)}\right)^2} \left[\left(\mathbf{R}_i^{(0)} - \mathbf{R}_j^{(0)} \right) \cdot \left(\mathbf{r}_i - \mathbf{r}_j \right) \right] . \quad \text{(A.1)}$$

This system of linear equations can further be used to obtain the eigenvalues and the eigenvectors corresponding to various normal modes. It should be noted that, although the overdamped limit of relaxational dynamics is considered here, the resulting eigenvalues and eigenvectors are still the same as when the purely inertial (vibrational) dynamics is assumed.

The linearized equations (A.1) can be used as long as all coordinate changes $\mathbf{r}_i$ are much smaller than the (natural) lengths of the elastic links connecting neighbor particles. Therefore, to test the possible validity of the linear approximation, the observed coordinate changes should be compared with the typical natural lengths of the elastic links. By the construction of the EN model, natural lengths of all elastic links cannot exceed the cutoff length, which has been 10Å in the present study. The average natural length l_{av} of a link is smaller and, for a rough estimate, the value $l_{\mathrm{av}} = 5$Å can be chosen. Linearization holds if the coordinate changes $\mathbf{r}_i$ are much smaller than l_{av}, which requires that they should not exceed, e.g., 10% of l_{av}, that is they cannot be larger than 0.5Å.

When the effects of forward strain were considered, an external force with the magnitude $f = 6$Å was applied to the tail and, after a new equilibrium state was reached, conformational changes have been inspected and changes of the distances between the labels were analyzed. We have also checked what were the deviations in the absolute positions of some typical residues. As it turns out, when such a force is applied to the tail, the position of the characteristic residue 384 in the HCM loop

gets changed by $r_{384} = 7.4$Å. Moreover, the residue 792, which is located in the tail, moves by 12.2Å from its equilibrium position. Such displacements are comparable to the cutoff length and, thus, when responses in the actin cleft or in the tail are considered, the linear description cannot hold. On the other hand, the respective induced changes within the nucleotide binding pocket are much smaller. For example, residue 115 in the front door region shifts its position by only $r_{115} = 0.6$Å when the same force is applied to the tail. Such weaker changes in the nucleotide-binding region could probably have also been correctly reproduced within the local linear approximation for this protein region.

The limitations of the linearized normal-mode descriptions have been previously discussed for myosin-V and kinesin [164]. In the present study, we have decided to stay completely within the full nonlinear elastic description, so that such difficulties cannot arise. Because the linearized equations are only an approximation to the full set of nonlinear equations, considered here, their analysis, once performed within the validity region of the approximation, cannot obviously yield anything which is not already contained in the nonlinear model.

As an illustration of the difficulties encountered in the linearized description, Fig. 39 shows the behavior described by the linearized equations (A.1) as compared with the responses described by the full nonlinear equations (3.3). Here, a constant force $\mathbf{f} = (-1, 1, 1)/\sqrt{3}$ Å is applied to residue 384 in the HCM loop. The dynamical responses of the elastic network are determined by integration of equations (3.3) or (A.1), respectively. The absolute displacements r_{115} and r_{792} of the residues 115 and 792, located in the front-door region and the tail, respectively, are plotted here as functions of time for both descriptions. As we see, the full nonlinear equations yield the responses (solid curves) which saturate as the new equilibrium state of the network, under the constant applied force, is approached. In contrast to this expected behavior, integration of the linearized equations yields the displacements which indefinitely grow with time (dashed curves in Fig. 39).

Such unphysical behavior has been observed because the linearized equations have been used in the above example beyond their validity limit. Indeed, the final stationary displacements of the considered residues in the full nonlinear model are of the order of tens of in this case, strongly exceeding what is required for the validity of the linearized description. The ori-

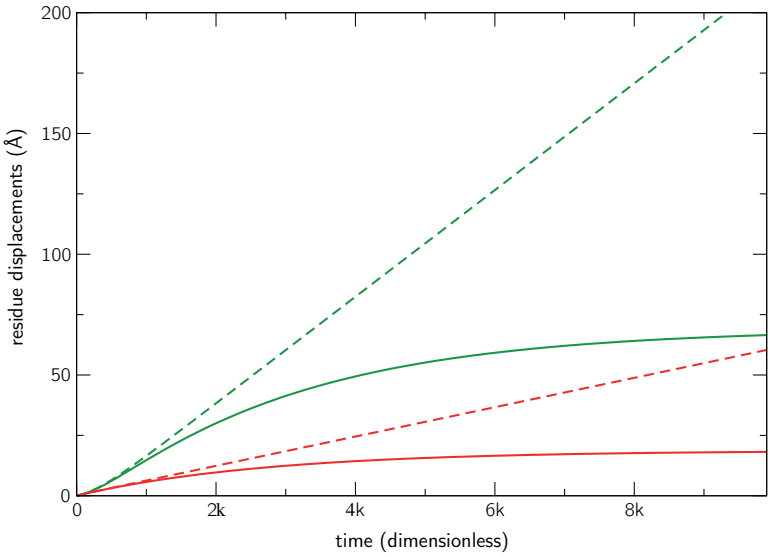

Figure 39: Comparison of the network responses to the application of a static force to the tail, as yielded by the full nonlinear and the linearized models. Constant force of amplitude $f = 0.5$ and direction $(-1, 1, 1)/\sqrt{3}$ is applied to residue 384 in the HCM loop. Time-dependent displacements r_{792} (green) and r_{115} (red) of residues 792 and 115 from their equilibrium positions are displayed, as yielded by the integration of the full nonlinear (3) (solid curves) and the linearized equations of motion (S5) (dashed curves) can be compared.

gin of the observed unphysical divergence lies in the fact that, after linearization, the energy of an elastic network does not depend on the displacement components of particles which are orthogonal to the directions of equilibrium links between them (cf. equations (A.1)). Therefore, such displacements may indeed grow indefinitely without increasing the energy of the linearized system. In the full nonlinear model, the energy is invariant, on the other hand, only under the displacements of particles which preserve distances between all of them, i.e the lengths of all elastic links. They correspond to rigid translations and rotations of the entire network, always eliminated in our simulations via the immobilization procedure.

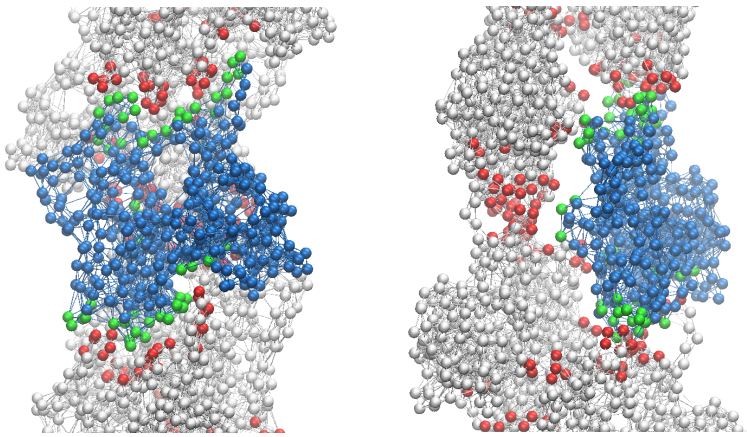

Figure 40: Actin-Actin-Binding Sites. Actin inside the filament (blue beads) is connected to its neighbors (gray beads). Its binding sites are colored green and the neighbor binding sites red, respectively. Green and red beads that are within the cutoff distance can form a bond.

A.5 ACTIN-ACTIN BINDING SITES

In Chap. 6, we model the actin filament with effective protein-protein interactions approximated as phenomenological Lennard-Jones bonds (3.20) between pairs of residues in different actin molecules. Fuji et al. could resolve the F-actin filament in atomic resolution by cryo-electron microscopy [56]. We are interested in the protein-protein interaction between single actin monomers in the filament. Thus, we construct an EN model of the actin filament with a cutoff distance of $l_0 = 8.5$Å. Links that connect different actin monomers in the filament are modeled as breakable Lennard-Jones potentials (3.20). Such pairs of residues are displayed in Fig. 40 and listed below:

39–270, 40–169, 40–171, 40–268, 41–169, 42–168, 42–169, 42–170, 42–171, 43–168, 43–169, 44–139, 44–143, 44–168, 44–169, 44–170, 45–143, 45–168, 45–346, 61–289, 62–286, 62–288, 62–289, 63–285, 63–286, 63–287, 63–288, 63–289, 64–166, 64–167, 110–194, 110–195, 110–196, 110–197, 111–195, 111–196, 111–197, 112–195, 112–196, 112–197, 172–268, 173–267, 173–268, 202–286, 204–286, 204–287, 204–288, 205–286, 205–287, 205–288, 208–288, 242–287, 242–288, 243–287, 243–288, 243–289, 243–290, 243–291, 244–283, 244–286, 244–287, 244–288, 244–289, 244–290, 244–291, 244–322, 244–325, 245–287, 245–290, 245–291, 245–321, 245–322, 245–323, 245–324, 245–325, 246–321, 246–322 and 247–322

The binding sites are shown in Fig. 40.

A.6 TABLES

Table 3: Maximal distance changes (Å) observed when forces are applied to different residues in the nucleotide-binding pocket

residue	343 to 517	386 to 517	789 to 141	789 to 92
111	0.126	0.069	7.199	6.346
112	0.134	0.078	8.275	7.231
113	0.148	0.067	8.029	7.222
114	0.146	0.104	9.112	8.065
115	0.171	0.140	9.517	8.533
116	0.167	0.138	9.825	8.476
163	0.124	0.167	4.304	3.719
164	0.137	0.186	4.131	3.746
165	0.140	0.203	4.001	3.869
166	0.131	0.157	4.897	4.817
167	0.123	0.126	5.439	4.827
168	0.121	0.117	5.768	5.114
169	0.114	0.156	4.859	4.279
170	0.107	0.188	5.171	4.494
171	0.109	0.148	6.395	5.468
214	0.075	0.244	4.953	5.040
215	0.048	0.305	5.523	5.615
216	0.066	0.282	5.362	5.299
217	0.068	0.292	4.168	4.303
218	0.090	0.307	3.580	3.669
219	0.087	0.336	2.644	2.983
220	0.125	0.333	2.310	2.359
438	0.106	0.255	2.364	2.159
439	0.135	0.250	2.274	2.203
440	0.134	0.229	2.852	2.722
441	0.144	0.272	3.004	2.682
442	0.228	0.286	2.956	2.470

Table 4: Maximal distance changes (Å) observed when forces are applied to different residues in the actin-binding pocket

residue	789 to 141	789 to 92	115 to 297	442 to 219
340	4.911	6.086	0.359	0.095
341	5.103	6.191	0.409	0.107
342	5.431	5.790	0.430	0.111
343	6.643	6.378	0.466	0.107
344	6.884	6.007	0.480	0.118
345	6.531	5.374	0.468	0.127
346	6.919	5.619	0.442	0.111
347	6.898	6.160	0.423	0.094
348	6.226	6.104	0.401	0.090
349	6.545	6.892	0.388	0.079
350	6.376	7.288	0.357	0.077
377	7.457	6.754	0.341	0.061
378	7.395	6.492	0.332	0.069
379	8.492	7.168	0.346	0.075
380	9.036	7.613	0.370	0.098
381	9.204	7.994	0.385	0.109
382	9.377	7.998	0.395	0.106
383	9.533	8.123	0.403	0.116
384	9.374	8.130	0.411	0.107
385	9.494	8.152	0.420	0.102
386	9.359	8.028	0.412	0.103
387	9.425	8.161	0.418	0.101
388	9.163	7.815	0.399	0.071
389	8.631	7.215	0.410	0.081
390	7.634	6.752	0.397	0.078
500	3.929	3.617	0.136	0.019
501	4.952	4.752	0.155	0.053
502	5.688	5.403	0.184	0.069
503	5.905	5.307	0.199	0.055
504	5.216	4.540	0.177	0.035
505	4.631	3.732	0.163	0.021
506	4.074	3.315	0.140	0.020
516	6.723	5.423	0.207	0.103
517	6.591	5.050	0.179	0.080
518	6.065	4.319	0.171	0.058
519	5.378	3.560	0.162	0.067
520	4.713	2.870	0.163	0.075
521	5.584	3.334	0.202	0.072
522	6.114	4.012	0.207	0.038
523	5.386	3.621	0.191	0.033
524	5.261	3.627	0.208	0.064
525	6.319	4.426	0.236	0.060
526	6.227	4.830	0.228	0.037
527	5.616	4.385	0.218	0.056
528	6.419	5.106	0.252	0.089
529	6.908	5.667	0.272	0.088
530	6.689	5.728	0.249	0.086
540	6.058	4.730	0.260	0.145
541	5.986	4.442	0.267	0.172
542	6.953	4.672	0.292	0.199
543	7.004	4.175	0.287	0.197
544	5.939	3.638	0.262	0.160
545	5.990	3.735	0.253	0.125
634	4.464	3.959	0.100	0.117

BIBLIOGRAPHY

1. R. Ait-Haddou and W. Herzog, *Brownian ratchet models of molecular motors.*, Cell Biochemistry and Biophysics, 38 (2003), pp. 191–214.

2. B. Alberts, A. Johnson, J. Lewis, M. Raff, K. Roberts, and P. And Walter, *Molecular Biology of the Cell*, vol. 54, Garland Press, 2008.

3. B. J. Alder and T. E. Wainwright, *Phase Transition for a Hard Sphere System*, The Journal of Chemical Physics, 27 (1957), p. 1208.

4. B. J. ALDER and T. E. WAINWRIGHT, *Studies in molecular dynamics. I. General method*, The Journal of Chemical Physics, (1959).

5. R. D. Astumian, *Thermodynamics and Kinetics of a Brownian Motor*, Science, 276 (1997), pp. 917–922.

6. R. D. Astumian, *Thermodynamics and Kinetics of Molecular Motors*, Biophysical Journal, 98 (2010), pp. 2401–2409.

7. A. R. Atilgan, S. R. Durell, R. L. Jernigan, M. C. Demirel, O. Keskin, and I. Bahar, *Anisotropy of fluctuation dynamics of proteins with an elastic network model.*, Biophysical Journal, 80 (2001), pp. 505–15.

8. C. Atilgan, Z. N. Gerek, S. B. Ozkan, and A. R. Atilgan, *Manipulation of Conformational Change in Proteins by Single-Residue Perturbations*, Biophysical Journal, 99 (2010), pp. 933–943.

9. I. Bahar, A. R. Atilgan, and B. Erman, *Direct evaluation of thermal fluctuations in proteins using a single-parameter harmonic potential.*, Folding & Design, 2 (1997), pp. 173–81.

10. D. Baker, *A surprising simplicity to protein folding.*, Nature, 405 (2000), pp. 39–42.

11. R. L. Baldwin, *The search for folding intermediates and the mechanism of protein folding.*, Annual Review of Biophysics, 37 (2008), pp. 1–21.

12. M. Bárány, *ATPase activity of myosin correlated with speed of muscle shortening.*, The Journal of General Physiology, 50 (1967), pp. 197–218.

13. J. M. Berg, L. Stryer, and J. L. Tymoczko, *Biochemistry*, W H Freeman, New York, fifth ed., 2002.

14. V. Bierbaum and R. Lipowsky, *Chemomechanical coupling and motor cycles of myosin V.*, Biophysical Journal, 100 (2011), pp. 1747–1755.

15. B. R. Brooks, R. E. Bruccoleri, B. D. Olafson, D. J. States, S. Swaminathan, and M. Karplus, *CHARMM: A program for macromolecular energy, minimization, and dynamics calculations*, Journal of Computational Chemistry, 4 (1983), pp. 187–217.

16. C. Brooks, M. Karplus, and B. Pettitt, *Advances in Chemical Physics, Proteins: A Theoretical Perspective of Dynamics, Structure, and Thermodynamics*, John Wiley & Sons, Inc., 1990.

17. R. Brown, *A brief account of microscopical observations made in the months of June, July and August, 1827, on the particles contained in the pollen of plants; and on the general existence of active molecules in organic and inorganic bodies*, Philosophical Magazine, 4 (1828), pp. 161–173.

18. A. Brünger, *Crystallographic R factor refinement by molecular dynamics*, Science, (1987).

19. M.-F. Carlier, C. Le Clainche, S. Wiesner, and D. Pantaloni, *Actin-based motility: from molecules to movement.*, BioEssays News and Reviews in Molecular Cellular and Developmental Biology, 25 (2003), pp. 336–345.

20. J. Cavanagh, W. J. Fairbrother, A. G. Palmer, M. Rance, and N. J. Skelton, *Protein NMR spectroscopy: principles and practice*, Elsevier Academic Press, Burlington, second edi ed., 2007.

21. M. Cecchini, Y. Alexeev, and M. Karplus, *Pi release from myosin: a simulation analysis of possible pathways.*, Structure, 18 (2010), pp. 458–70.

22. M. Cecchini, A. Houdusse, and M. Karplus, *Allosteric Communication in Myosin V: From Small Conformational Changes to Large Directed Movements*, PLoS Computational Biology, 4 (2008), p. 19.

23. M. Cecchini, F. Rao, M. Seeber, and A. Caflisch, *Replica exchange molecular dynamics simulations of amyloid peptide aggregation.*, The Journal of Chemical Physics, 121 (2004), pp. 10748–10756.

24. C. Chennubhotla, A. J. Rader, L.-W. Yang, and I. Bahar, *Elastic network models for understanding biomolecular machinery: from enzymes to supramolecular assemblies.*, Physical Biology, 2 (2005), pp. S173–S180.

25. J.-W. Chu and G. a. Voth, *Coarse-grained modeling of the actin filament derived from atomistic-scale simulations.*, Biophysical Journal, 90 (2006), pp. 1572–82.

26. J.-W. Chu and G. A. Voth, *Coarse-Grained Free Energy Functions for Studying Protein Conformational Changes: A Double-Well Network Model*, Biophysical Journal, 93 (2007), pp. 3860–3871.

27. M. Cieplak, T. X. Hoang, and M. O. Robbins, *Thermal effects in stretching of Go-like models of titin and secondary structures*, Proteins, 56 (2003), pp. 285–297.

28. M. Clarke, *Sighting of the swinging lever arm of muscle.*, Nature, 395 (1998), p. 443.

29. R. Cooke and W. Bialek, *Contraction of glycerinated muscle fibers as a function of the ATP concentration.*, Biophysical journal, 28 (1979), pp. 241–258.

30. Cooper Geoffrey M. and R. E. Hausman, *The Cell: A Molecular Approach*, Sinauer Associates, Inc., fifth ed., 2009.

31. P.-D. Coureux, H. L. Sweeney, and A. Houdusse, *Three myosin V structures delineate essential features of chemomechanical transduction.*, The EMBO journal, 23 (2004), pp. 4527–37.

32. P.-D. Coureux, A. L. Wells, J. Ménétrey, C. M. Yengo, C. A. Morris, H. L. Sweeney, and A. Houdusse, *A structural state of the myosin V motor without bound nucleotide.*, Nature, 425 (2003), pp. 419–423.

33. T. E. Creighton, *Protein Folding*, W. H. Freeman, 2001.

34. A. Cressman, Y. Togashi, A. S. Mikhailov, and R. Kapral, *Mesoscale modeling of molecular machines: cyclic dynamics and hydrodynamical fluctuations.*, Physical Review E, 77 (2008), p. 050901.

35. R. A. Cross, J. C. M. Gebhardt, A. E. M. Clemen, J. Jaud, and M. Rief, *Myosin-V is a mechanical ratchet*, Proceedings of the National Academy of Sciences of the United States of America, 103 (2006), pp. 8680–8685.

36. Q. Cui and I. Bahar, eds., *Normal Mode Analysis: Theory and Applications to Biological and Chemical Systems*, vol. 8, Chapman & Hall/CRC, 2006.

37. P. Debye and E. Hückel, *Zur Theorie der Elektrolyte. I. Gefrierpunktserniedrigung und verwandte Erscheinungen*, Physikalische Zeitschrift, 24 (1923), pp. 185–206.

38. H. Dietz, F. Berkemeier, M. Bertz, and M. Rief, *Anisotropic deformation response of single protein molecules*, Proceedings of the National Academy of Sciences of the United States of America, 103 (2006), pp. 12724–12728.

39. K. A. Dill and H. S. Chan, *From Levinthal to pathways to funnels*, Nature Structural Biology, 4 (1997), pp. 10–19.

40. C. M. Dobson, *Protein folding and misfolding.*, Nature, 426 (2003), pp. 884–890.

41. R. Dominguez, *Actin-binding proteins–a unifying hypothesis.*, Trends in Biochemical Sciences, 29 (2004), pp. 572–578.

42. R. Dominguez and K. C. Holmes, *Actin Structure and Function*, Annual Review Biophysics, (2011), pp. 169 – 186.

43. P. Doruker, A. R. Atilgan, and I. Bahar, *Dynamics of proteins predicted by molecular dynamics simulations and analytical approaches: application to alpha-amylase inhibitor.*, Proteins, 40 (2000), pp. 512–24.

44. J. Drenth, *Principles of Protein X-ray Crystallography*, Springer, 1994.

45. M. Düttmann, M. Mittnenzweig, Y. Togashi, T. Yanagida, and A. S. Mikhailov, *Complex Intramolecular Mechanics of G-actin - an Elastic Network Study*, PLoS ONE, (2012), p. e45859.

46. M. Düttmann, Y. Togashi, T. Yanagida, and A. S. Mikhailov, *Myosin - V as a Mechanical Sensor : An Elastic Network Study*, Biophysical Journal, 102 (2012), pp. 542–551.

47. C. Echeverria, Y. Togashi, A. S. Mikhailov, and R. Kapral, *A mesoscopic model for protein enzymatic dynamics in solution.*, Physical Chemistry Chemical Physics, 13 (2011), pp. 10527–10537.

48. A. Einstein, *Eine neue Bestimmung der Moleküldimensionen*, Annalen der Physik, 324 (1906), pp. 289–306.

49. S. Esaki, Y. Ishii, and T. Yanagida, *Model describing the biased Brownian movement of myosin*, Proceedings of the Japan Academy Series B Physical and Biological Sciences, 79 (2003), pp. 9–14.

50. E. Eyal and I. Bahar, *Toward a Molecular Understanding of the Anisotropic Response of Proteins to External Forces: Insights from Elastic Network Models*, Biophysical Journal, 94 (2008), pp. 3424–3435.

51. R. P. Feynman, R. B. Leighton, and M. L. Sands, *The Feynman Lectures on Physics*, vol. 1 of The Feynman Lectures on Physics, Addison-Wesley, 1963.

52. R. Fine, G. Dimmler, and C. Levinthal, *FASTRUN: a special purpose, hardwired computer for molecular simulation.*, Proteins, 11 (1991), pp. 242–253.

53. H. Flechsig and A. S. Mikhailov, *Tracing entire operation cycles of molecular motor hepatitis C virus helicase in structurally resolved dynamical simulations.*, Proceedings of the National Academy of Sciences of the United States of America, 107 (2010), pp. 20875–20880.

54. H. Flechsig, D. Popp, and A. S. Mikhailov, *In Silico Investigation of Conformational Motions in Superfamily 2 Helicase Proteins*, PLoS ONE, 6 (2011), p. e21809.

55. T. Förster, *Zwischenmolekulare Energiewanderung und Fluoreszenz*, Annalen der Physik, 437 (1948), pp. 55–75.

56. T. Fujii, A. H. Iwane, T. Yanagida, and K. Namba, *Direct visualization of secondary structures of F-actin by electron cryomicroscopy.*, Nature, 467 (2010), pp. 724–728.

57. T. Furusawa, S. Ikawa, N. Yanai, and M. Obinata, *Isolation of a novel PDZ-containing myosin from hematopoietic supportive bone marrow stromal cell lines.*, Biochemical and Biophysical Research Communications, 270 (2000), pp. 67–75.

58. M. A. Geeves and K. C. Holmes, *Structural mechanism of muscle contraction.*, Annual Review of Biochemistry, 68 (1999), pp. 687–728.

59. M. A. Geeves and K. C. Holmes, *The molecular mechanism of muscle contraction.*, Advances in Protein Chemistry, 71 (2005), pp. 161–193.

60. N. Go, *Theoretical studies of protein folding*, Annual Review of Biophysics and Bioengineering, 12 (1983), pp. 183–210.

61. M. Gruebele, *Protein folding: the free energy surface.*, Current Opinion in Structural Biology, 12 (2002), pp. 161–168.

62. T. Ha, T. Enderle, D. F. Ogletree, D. S. Chemla, P. R. Selvin, and S. Weiss, *Probing the interaction between two single molecules: fluorescence resonance energy transfer between a single donor and a single acceptor.*, Proceedings of the National Academy of Sciences of the United States of America, 93 (1996), pp. 6264–8.

63. T. Haliloglu, I. Bahar, and B. Erman, *Gaussian Dynamics of Folded Proteins*, Physical Review Letters, 79 (1997), pp. 3090–3093.

64. C. Hardin, Z. Luthey-Schulten, and P. G. Wolynes, *Backbone dynamics, fast folding, and secondary structure formation in helical proteins and peptides.*, Proteins, 34 (1999), pp. 281–294.

65. K. Hayashi and M. Takano, *Violation of the fluctuation-dissipation theorem in a protein system.*, Biophysical Journal, 93 (2007), pp. 895–901.

66. K. A. Henzler-Wildman, M. Lei, V. Thai, S. J. Kerns, M. Karplus, and D. Kern, *A hierarchy of timescales in protein dynamics is linked to enzyme catalysis*, Nature, 450 (2007), pp. 913–916.

67. J. Higo and H. Umeyama, *Protein dynamics determined by backbone conformation and atom packing.*, Protein Engineering, 10 (1997), pp. 373–380.

68. R. D. Hills and C. L. Brooks, *Insights from Coarse-Grained Go Models for Protein Folding and Dynamics*, International Journal of Molecular Sciences, 10 (2009), pp. 889–905.

69. K. Hinsen, *Analysis of domain motions by approximate normal mode calculations*, Proteins, 33 (1998), pp. 417–429.

70. T. Hodge, M. Jamie, and T. Cope, *A myosin family tree*, Journal of Cell Science, (2000).

71. K. Holmes, I. Angert, F. Kull, and W. Jahn, *Electron cryo-microscopy shows how strong binding of myosin to actin releases nucleotide*, Nature, 425 (2003), pp. 423–427.

72. K. C. Holmes, *The swinging lever-arm hypothesis of muscle contraction.*, Current Biology, 7 (1997), pp. R112–R118.

73. K. C. Holmes, R. R. Schröder, H. L. Sweeney, and A. Houdusse, *The structure of the rigor complex and its implications for the power stroke.*, Philosophical Transactions of the Royal Society of London - Series B: Biological Sciences, 359 (2004), pp. 1819–1828.

74. W. Humphrey, A. Dalke, and K. Schulten, *VMD: visual molecular dynamics*, Journal of Molecular Graphics, 14 (1996), pp. 33–38.

75. A. F. Huxley, *Muscle. Support for the lever arm.*, 1998.

76. H. Huxley, *The mechanism of muscular contraction*, Science, 164 (1969), pp. 1356–1366.

77. H. E. Huxley, *Muscular contraction.*, Annual Review of Physiology, 50 (1988), pp. 1–16.

78. A. Inoue, H. Takenaka, T. Arata, and Y. Tonomura, *Functional implications of the two-headed structure of myosin.*, Advances in Biophysics, 13 (1979), pp. 1–194.

79. B. Isralewitz, J. Baudry, J. Gullingsrud, D. Kosztin, and K. Schulten, *Steered molecular dynamics investigations of protein function.*, Journal of Molecular Graphics Modelling, 19 (2001), pp. 13–25.

80. M. Iwaki, A. H. Iwane, T. Shimokawa, R. Cooke, and T. Yanagida, *Brownian search-and-catch mechanism for myosin-VI steps*, Nature Chemical Biology, 5 (2009), pp. 403–405.

81. S. Izrailev, S. Stepaniants, M. Balsera, Y. Oono, and K. Schulten, *Molecular dynamics study of unbinding of the avidin-biotin complex.*, Biophysical Journal, 72 (1997), pp. 1568–1581.

82. P. A. Janmey, S. Hvidt, G. F. Oster, J. Lamb, T. P. Stossel, and J. H. Hartwig, *Effect of ATP on actin filament stiffness*, Nature, 347 (1990), pp. 95–99.

83. E. A. Jares-Erijman and T. M. Jovin, *FRET imaging*, Nature Biotechnology, 21 (2003), pp. 1387–1395.

84. W. Kabsch, H. G. Mannherz, D. Suck, E. F. Pai, and K. C. Holmes, *Atomic structure of the actin: DNase I complex*, Nature, 347 (1990), pp. 37–44.

85. J. Karanicolas and C. L. Brooks III, *Improved Go-like Models Demonstrate the Robustness of Protein Folding Mechanisms Towards Non-native Interactions*, Journal of Molecular Biology, 334 (2003), pp. 309–325.

86. M. Karplus, *The Levinthal paradox: yesterday and today*, Folding Design, 2 (1997).

87. M. Karplus and J. A. McCammon, *Molecular dynamics simulations of biomolecules.*, Nature Structural Biology, 35 (2002), pp. 321–323.

88. M. Karplus and G. Petsko, *Molecular dynamics simulations in biology*, Nature, (1990).

89. J. C. Kendrew, G. Bodo, H. M. Dintzis, R. G. Parrish, H. Wyckoff, and D. C. Phillips, *A three-dimensional model of the myoglobin molecule obtained by x-ray analysis.*, Nature, 181 (1958), pp. 662–666.

90. J. C. Kendrew and M. F. Perutz, *X-ray studies of compounds of biological interest.*, Annual Review of Biochemistry, 26 (1957), pp. 327–372.

91. M. K. Kim, G. S. Chirikjian, and R. L. Jernigan, *Elastic models of conformational transitions in macromolecules.*, Journal of Molecular Graphics Modelling, 21 (2002), pp. 151–160.

92. A. Kitao, F. Hirata, and N. Go, *The effects of solvent on the conformation and the collective motions of protein: Normal mode analysis and molecular dynamics simulations of melittin in water and in vacuum*, Chemical Physics, 158 (1991), pp. 447–472.

93. N. Koga and S. Takada, *Roles of native topology and chain-length scaling in protein folding: a simulation study with a Go-like model.*, Journal of Molecular Biology, 313 (2001), pp. 171–80.

94. T. Komori, S. Nishikawa, T. Ariga, A. H. Iwane, and T. Yanagida, *Simultaneous measurement of nucleotide occupancy and mechanical displacement in myosin-V, a processive molecular motor.*, Biophysical Journal, 96 (2009), pp. L4–L6.

95. E. D. Korn, M. F. Carlier, and D. Pantaloni, *Actin polymerization and ATP hydrolysis.*, Science New York NY, 238 (1987), pp. 638–44.

96. J. Kozuka, H. Yokota, Y. Arai, Y. Ishii, and T. Yanagida, *Dynamic polymorphism of single actin molecules in the actin filament.*, Nature Chemical Biology, 2 (2006), pp. 83–6.

97. J. Kubelka, J. Hofrichter, and W. A. Eaton, *The protein folding speed limit*, Current Opinion in Structural Biology, 14 (2004), pp. 76–88.

98. A. Kumar, G. Wagner, R. R. Ernst, and K. Wuethrich, *Buildup rates of the nuclear Overhauser effect measured by two-dimensional proton magnetic resonance spectroscopy: implications for studies of protein conformation*, Journal of the American Chemical Society, 103 (1981), pp. 3654–3658.

99. E. E. Lattman and P. J. Loll, *Protein Crystallography - A Concise Guide*, vol. 65, John Hopkins University Press, Baltimore, 2009.

100. J. D. Lawson, E. Pate, I. Rayment, and R. G. Yount, *Molecular dynamics analysis of structural factors influencing back door pi release in myosin.*, Biophysical Journal, 86 (2004), pp. 3794–3803.

101. C. Levinthal, *Are there pathways for protein folding?*, Journal of Medical Ethics, 65 (1968), pp. 44–45.

102. J.-L. Liao and D. N. Beratan, *How does protein architecture facilitate the transduction of ATP chemical-bond energy into mechanical work? The cases of nitrogenase and ATP binding-cassette proteins.*, Biophysical Journal, 87 (2004), pp. 1369–1377.

103. E. Lindahl, B. Hess, and D. Van Der Spoel, *GROMACS 3.0: a package for molecular simulation and trajectory analysis*, Journal of Molecular Modeling, 7 (2001), pp. 306–317.

104. H. F. Lodish, A. Berk, S. L. Zipursky, P. Matsudaira, D. Baltimore, and D. James, *Molecular Cell Biology*, vol. 5, W. H. Freeman, 4 ed., 2008.

105. M. Lorenz and K. C. Holmes, *The actin-myosin interface.*, Proceedings of the National Academy of Sciences of the United States of America, 107 (2010), pp. 12529–34.

106. M. Lorenz, D. Popp, and K. C. Holmes, *Refinement of the F-actin model against X-ray fiber diffraction data by the use of a directed mutation algorithm.*, Journal of Molecular Biology, 234 (1993), pp. 826–836.

107. H. Lu and K. Schulten, *Steered Molecular Dynamics Simulations of Force-Induced Protein Domain Unfolding*, ProteinsStructure Function and Genetics, 463 (1999), pp. 453–463.

108. R. W. Lymn and E. W. Taylor, *Mechanism of adenosine triphosphate hydrolysis by actomyosin.*, Biochemistry, 10 (1971), pp. 4617–4624.

109. M. W. MacArthur, R. A. Laskowski, and J. M. Thornton, *Knowledge-based validation of protein structure coordinates derived by X-ray crystallography and NMR spectroscopy*, Current Opinion in Structural Biology, 4 (1994), pp. 731–737.

110. P. Maragakis and M. Karplus, *Large amplitude conformational change in proteins explored with a plastic network model: adenylate kinase.*, Journal of Molecular Biology, 352 (2005), pp. 807–822.

111. L. Marcucci and T. Yanagida, *From Single Molecule Fluctuations to Muscle Contraction: A Brownian Model of AF Huxley's Hypotheses*, PloS ONE, (2012).

112. J. A. McCammon, B. R. Gelin, and M. Karplus, *Dynamics of folded proteins.*, Nature, 267 (1977), pp. 585–590.

113. a. D. Mehta, R. S. Rock, M. Rief, J. a. Spudich, M. S. Mooseker, and R. E. Cheney, *Myosin-V is a processive actin-based motor.*, Nature, 400 (1999), pp. 590–3.

114. L. Michaelis and M. L. Menten, *Die Kinetik der Invertinwirkung*, Biochemische Zeitschrift, 49 (1913), pp. 333–369.

115. A. S. Mikhailov and V. Calenbuhr, *From Cells to Societies: Models of Complex Coherent Action (Springer Series in Synergetics)*, Springer, 2nd ed., 2002.

116. T. J. Mitchison and L. P. Cramer, *Actin-based cell motility and cell locomotion*, Cell, 84 (1996), pp. 371–379.

117. O. Miyashita, J. N. Onuchic, and P. G. Wolynes, *Nonlinear elasticity, proteinquakes, and the energy landscapes of functional transitions in proteins*, Proceedings of the National Academy of Sciences of the United States of America, 100 (2003), pp. 12570–12575.

118. D. M. Monack and J. A. Theriot, *Actin-based motility is sufficient for bacterial membrane protrusion formation and host cell uptake.*, Cellular Microbiology, 3 (2001), pp. 633–647.

119. V. Muñoz and W. A. Eaton, *A simple model for calculating the kinetics of protein folding from three-dimensional structures.*, Proceedings of the National Academy of

Sciences of the United States of America, 96 (1999), pp. 11311–11316.

120. T. Narumi, M. Taiji, M. Ikei, Y. Ohno, N. Okimoto, T. Koishi, A. Suenaga, N. Futatsugi, R. Yanai, R. Himeno, and S. Fujikawa, *A 55 TFLOPS simulation of amyloid-forming peptides from yeast prion Sup35 with the special-purpose computer system MDGRAPE-3*, Proceedings of the 2006 ACMIEEE conference on Supercomputing, (2006).

121. T. Oda, M. Iwasa, and T. Aihara, *The nature of the globular-to fibrous-actin transition*, Nature, 457 (2009), pp. 441–446.

122. Y. Oguchi, S. V. Mikhailenko, T. Ohki, A. O. Olivares, E. M. De La Cruz, and S. Ishiwata, *Load-dependent ADP binding to myosins V and VI: implications for subunit coordination and function.*, Proceedings of the National Academy of Sciences of the United States of America, 105 (2008), pp. 7714–7719.

123. Y. Oguchi, S. V. Mikhailenko, T. Ohki, A. O. Olivares, E. M. De La Cruz, and S. Ishiwata, *Robust processivity of myosin V under off-axis loads*, Nature Chemical Biology, 6 (2010), pp. 300–305.

124. K.-i. Okazaki, N. Koga, S. Takada, J. N. Onuchic, and P. G. Wolynes, *Multiple-basin energy landscapes for large-amplitude conformational motions of proteins: Structure-based molecular dynamics simulations*, Proceedings of the National Academy of Sciences of the United States of America, 103 (2006), pp. 11844–11849.

125. H. Oschkinat, C. Griesinger, P. J. Kraulis, O. W. Sø rensen, R. R. Ernst, A. M. Gronenborn, and G. M. Clore, *Three-dimensional NMR spectroscopy of a protein in solution.*, Nature, 332 (1988), pp. 374–376.

126. L. R. Otterbein, P. Graceffa, and R. Dominguez, *The crystal structure of uncomplexed actin in the ADP state.*, Science, 293 (2001), pp. 708–11.

127. V. Ovchinnikov, B. L. Trout, and M. Karplus, *Mechanical coupling in myosin V: a simulation study.*, Journal of Molecular Biology, 395 (2010), pp. 815–33.

128. J. Pfaendtner, D. Branduardi, M. Parrinello, T. D. Pollard, and G. A. Voth, *Nucleotide-dependent conformational states of actin*, Proceedings of the National Academy of Sciences of the United States of America, 106 (2009), pp. 12723–12728.

129. F. Piazza, P. De Los Rios, and Y. H. Sanejouand, *Slow Energy Relaxation of Macromolecules and Nanoclusters in Solution*, Physical Review Letters, 94 (2005), p. 145502.

130. D. W. Piston and G.-J. Kremers, *Fluorescent protein FRET: the good, the bad and the ugly.*, Trends in Biochemical Sciences, 32 (2007), pp. 407–414.

131. T. D. Pollard, *Rate constants for the reactions of ATP- and ADP-actin with the ends of actin filaments.*, The Journal of Cell Biology, 103 (1986), pp. 2747–54.

132. T. D. Pollard and G. G. Borisy, *Cellular motility driven by assembly and disassembly of actin filaments*, Cell, 112 (2003), pp. 453–465.

133. T. D. Pollard and J. A. Cooper, *Actin and actin-binding proteins. A critical evaluation of mechanisms and functions*, Annual Review of Biochemistry, (1986), pp. 987–1035.

134. T. J. Purcell, C. Morris, J. A. Spudich, and H. L. Sweeney, *Role of the lever arm in the processive stepping of myosin V*, Proceedings of the National Academy of Sciences of the United States of America, 99 (2002), pp. 14159–14164.

135. T. J. Purcell, H. L. Sweeney, and J. A. Spudich, *A force-dependent state controls the coordination of processive myosin V.*, Proceedings of the National Academy of Sciences of the United States of America, 102 (2005), pp. 13873–13878.

136. A. J. Rader, C. Chennubhotla, L.-w. Yang, and I. Bahar, *The Gaussian Network Model: Theory and Applications*, Normal Mode Analysis Theory and Applications to Biological and Chemical Systems, 36 (2005), pp. 41–64.

137. A. Rahman, *Correlations in the motion of atoms in liquid argon*, Physical Review, (1964).

138. F. Rao and A. Caflisch, *Replica exchange molecular dynamics simulations of reversible folding*, The Journal of Chemical Physics, 119 (2003), pp. 4035–4042.

139. I. Rayment, H. M. Holden, M. Whittaker, C. B. Yohn, M. Lorenz, K. C. Holmes, and R. a. Milligan, *Structure of the actin-myosin complex and its implications for muscle contraction.*, Science, 261 (1993), pp. 58–65.

140. I. Rayment, C. Smith, and R. G. Yount, *The active site of myosin.*, Annual Review of Physiology, 58 (1996), pp. 671–702.

141. S. L. Reck-Peterson, D. W. Provance, M. S. Mooseker, and J. A. Mercer, *Class V myosins.*, Biochimica et Biophysica Acta, 1496 (2000), pp. 36–51.

142. C. Revenu, R. Athman, S. Robine, and D. Louvard, *The co-workers of actin filaments: from cell structures to signals.*, Nature Reviews Molecular Cell Biology, 5 (2004), pp. 635–646.

143. G. S. Rule and T. K. Hitchens, *Fundamentals of protein NMR spectrosopy*, Springer, Dordrecht, 2006.

144. T. Sakamoto, M. R. Webb, E. Forgacs, H. D. White, and J. R. Sellers, *Direct observation of the mechanochemical coupling in myosin Va during processive movement.*, Nature, 455 (2008), pp. 128–132.

145. J. Sellers, *Myosins*, Oxford University Press, New York, 2 ed., 1999.

146. J. R. Sellers, *Myosins: a diverse superfamily.*, Biochimica et Biophysica Acta, 1496 (2000), pp. 3–22.

147. D. E. Shaw, P. Maragakis, K. Lindorff-Larsen, S. Piana, R. O. Dror, M. P. Eastwood, J. a. Bank, J. M. Jumper, J. K. Salmon, Y. Shan, and W. Wriggers, *Atomic-level characterization of the structural dynamics of proteins.*, Science, 330 (2010), pp. 341–6.

148. K. Shiroguchi and K. Kinosita Jr., *Myosin V walks by lever action and Brownian motion*, Science, 316 (2007), pp. 1208–1212.

149. M. Smoluchowski, *Zur kinetischen Theorie der Brownschen Molekularbewegung und der Suspensionen*, Annalen der Physik, 326 (1906), pp. 756–780.

150. T. Splettstoesser, K. C. Holmes, F. Noé, and J. C. Smith, *Structural modeling and molecular dynamics simulation of the actin filament.*, Proteins, 79 (2011), pp. 2033–43.

151. J. A. Spudich and S. Sivaramakrishnan, *Myosin VI: an innovative motor that challenged the swinging lever arm hypothesis.*, Nature Reviews Molecular Cell Biology, 11 (2010), pp. 128–137.

152. F. H. Stillinger and A. Rahman, *Improved simulation of liquid water by molecular dynamics*, The Journal of Chemical Physics, 60 (1974), p. 1545.

153. J. I. Sulkowska and M. Cieplak, *Selection of Optimal Variants of Go-Like Models of Proteins through Studies of Stretching*, Biophysical Journal, 95 (2008), pp. 3174–3191.

154. T. M. Svitkina, A. B. Verkhovsky, K. M. McQuade, and G. G. Borisy, *Analysis of the actin-myosin II system in fish epidermal keratocytes: mechanism of cell body translocation.*, The Journal of Cell Biology, 139 (1997), pp. 397–415.

155. H. L. Sweeney and A. Houdusse, *Structural and functional insights into the Myosin motor mechanism.*, Annual Review of Biophysics, 39 (2010), pp. 539–557.

156. H. L. Sweeney, A. J. Straceski, L. A. Leinwand, B. A. Tikunov, and L. Faust, *Heterologous expression of a cardiomyopathic myosin that is defective in its actin interaction.*, The Journal of Biological Chemistry, 269 (1994), pp. 1603–1605.

157. S. Takada, *Go-ing for the prediction of protein folding mechanisms*, Proceedings of the National Academy of Sciences of the United States of America, 96 (1999), pp. 11698–11700.

158. M. Takano, T. P. Terada, and M. Sasai, *Unidirectional Brownian motion observed in an in silico single molecule experiment of an actomyosin motor.*, Proceedings of the National Academy of Sciences of the United States of America, 107 (2010), pp. 7769–74.

159. F. Tama and Y. H. Sanejouand, *Conformational change of proteins arising from normal mode calculations.*, Protein Engineering, 14 (2001), pp. 1–6.

160. J. A. Theriot and T. J. Mitchison, *Actin microfilament dynamics in locomoting cells.*, Nature, 352 (1991), pp. 126–131.

161. M. Tirion, *Large Amplitude Elastic Motions in Proteins from a Single-Parameter, Atomic Analysis.*, Physical Review Letters, 77 (1996), pp. 1905–1908.

162. M. M. Tirion and D. Ben-Avraham, *Normal mode analysis of G-actin.*, Journal of Molecular Biology, 230 (1993), pp. 186–195.

163. Y. Togashi and A. S. Mikhailov, *Nonlinear Relaxation Dynamics in Elastic Networks and Design Principles of Molecular Machines*, Proceedings of the National Academy of Sciences of the United States of America, 104 (2007), pp. 8697–8702.

164. Y. Togashi, T. Yanagida, and A. S. Mikhailov, *Nonlinearity of Mechanochemical Motions in Motor Proteins*, PLoS Computational Biology, 6 (2010), p. e1000814.

165. V. Tozzini, *Coarse-grained models for proteins.*, Current Opinion in Structural Biology, 15 (2005), pp. 144–50.

166. K. M. Trybus, *Myosin V from head to tail*, Cellular and Molecular Life Sciences, 65 (2008), pp. 233–42.

167. V. M. Unger, *Electron cryomicroscopy methods.*, Current Opinion in Structural Biology, 11 (2001), pp. 548–554.

168. R. D. Vale, *Myosin V motor proteins: marching stepwise towards a mechanism.*, The Journal of Cell Biology, 163 (2003), pp. 445–450.

169. C. Veigel, S. Schmitz, F. Wang, and J. R. Sellers, *Load-dependent kinetics of myosin-V can explain its high processivity.*, Nature Cell Biology, 7 (2005), pp. 861–869.

170. D. Voet and J. G. Voet, *Biochemistry*, John Wiley & Sons, New Jersey, 3. ed., 2004.

171. N. Volkmann, H. Lui, L. Hazelwood, K. M. Trybus, S. Lowey, and D. Hanein, *The R403Q Myosin Mutation Implicated in Familial Hypertrophic Cardiomyopathy Causes Disorder at the Actomyosin Interface*, PLoS ONE, 2 (2007), p. 8.

172. M. Wanger, T. Keiser, J. M. Neuhaus, and A. Wegner, *The actin treadmill.*, Canadian Journal of Biochemistry and Cell Biology, 63 (1985), pp. 414–421.

173. A. Wegner and G. Isenberg, *12-fold difference between the critical monomer concentrations of the two ends of actin filaments in physiological salt conditions.*, Proceedings of the National Academy of Sciences of the United States of America, 80 (1983), pp. 4922–4925.

174. P. Wolynes, Z. Luthey-Schulten, and J. Onuchic, *Fast-folding experiments and the topography of protein folding energy landscapes.*, Chemistry & Biology, 3 (1996), pp. 425–432.

175. C.-H. Wong and G. M. Whitesides, *Enzymes in synthetic organic chemistry*, Academic Press, Oxford, 1st ed., 1994.

176. K. Wüthrich, *Protein structure determination in solution by NMR spectroscopy.*, The Journal of Biological Chemistry, 265 (1990), pp. 22059–22062.

177. K. Wüthrich, *The way to NMR structures of proteins*, Journal of Molecular Biology, 8 (2001), pp. 923–925.

178. H. Yamaoka, S. Matsushita, Y. Shimada, and T. Adachi, *Multiscale modeling and mechanics of filamentous actin cytoskeleton.*, Biomechanics and Modeling in Mechanobiology, 11 (2011), pp. 291–302.

179. T. Yanagida, M. Ueda, T. Murata, S. Esaki, and Y. Ishii, *Brownian motion, fluctuation and life.*, Bio Systems, 88 (2007), pp. 228–242.

180. L. Yang, G. Song, and R. L. Jernigan, *How Well Can We Understand Large-Scale Protein Motions Using Normal Modes of Elastic Network Models?*, Biophysical Journal, 93 (2007), pp. 920–929.

181. A. Yildiz, J. N. Forkey, S. A. McKinney, T. Ha, Y. E. Goldman, and P. R. Selvin, *Myosin V walks hand-over-hand: single fluorophore imaging with 1.5-nm localization.*, Science, 300 (2003), pp. 2061–5.

182. K. Yonekura, S. Maki-Yonekura, and K. Namba, *Complete atomic model of the bacterial flagellar filament by electron cryomicroscopy.*, Nature, 424 (2003), pp. 643–650.

183. W. Zheng, *Coarse-grained modeling of conformational transitions underlying the processive stepping of myosin V dimer along filamentous actin.*, Proteins, 79 (2011), pp. 2291–305.

184. W. Zheng and B. R. Brooks, *Probing the local dynamics of nucleotide-binding pocket coupled to the global dynamics: myosin versus kinesin.*, Biophysical Journal, 89 (2005), pp. 167–178.

185. X. Zheng and K. Diraviyam, *Nucleotide effects on the structure and dynamics of actin*, Biophysical Journal, 93 (2007), pp. 1277–1283.

EIDESSTATTLICHE ERKLÄRUNG

Ich erkläre hiermit, dass ich diese Dissertation selbstständig ohne Hilfe Dritter und ohne Benutzung anderer als der angegebenen Quellen und Hilfsmittel verfasst habe. Alle den benutzten Quellen wörtlich oder sinngemäßentnommenen Stellen sind als solche einzeln kenntlich gemacht.

Berlin , September 2012

Markus Düttmann